Effects of Piston Design and Lubricant Selection on Reciprocating Engine Friction

by

Luke Moughon

B.S., Mechanical Engineering
Georgia Institute of Technology, 2004

Submitted to the Department of Mechanical Engineering in Partial Fulfillment of the Requirements of the Degree of

Masters of Science in Mechanical Engineering

at the

MASSACHUSETTS INSTITUTE OF TECHNOLOGY

June 2006

Signature of Author: _____
Department of Mechanical Engineering
May 12, 2006

Certified by: _____
Dr. Victor W. Wong
Lecturer, Department of Mechanical Engineering
Thesis Supervisor

Accepted by: _____
Professor Lallit Anand
Chairman, Department Committee on Graduate Studies
Department of Mechanical Engineering

Effects of Piston Design and Lubricant Selection on Reciprocating Engine Friction

by

Luke Moughon

Submitted to the Department of Mechanical Engineering in Partial Fulfillment of the Requirements of the Degree of Masters of Science in Mechanical Engineering

Abstract

The interaction between the piston and the liner in a reciprocating engine is of much interest because it affects reliability, noise, and efficiency. This study evaluated various changes to the piston skirt with the specific goal of minimizing friction. An analytical model of the piston, previously developed at MIT, was used to perform parametric studies of various designs in order to predict the effect of each on engine efficiency. The model incorporated hydrodynamic, boundary, and mixed lubrication modes, and it allowed for either fully-flooded or partially-flooded skirts. It also considered the effects of skirt deformation in response to applied loads.

A dominant factor influencing net friction between the skirt and liner was the distribution between hydrodynamic lubrication (support by the oil film) and boundary lubrication (direct metal-to-metal contact). Design changes that shifted support from the high-friction boundary lubrication regime toward the hydrodynamic regime generally reduced net friction. For example, the model predicted that if a piston is originally supported largely by boundary contact, increasing the viscosity of the oil can reduce friction by enabling the oil film to sustain a greater load. If, however, the load is already supported primarily hydrodynamically, decreasing the viscosity reduces hydrodynamic drag and may reduce net friction. Moreover, increasing oil supply (i.e., increasing effective oil film thickness) tends to decrease net friction by promoting hydrodynamic lubrication.

Changes to piston geometry were shown to have significant effects on friction. In order to maximize hydrodynamic support, the pressure must be distributed evenly across the piston skirt; this can be achieved by making the skirt-liner clearance as even and smooth as possible. The model confirmed that skirt profiles with gentle slopes tend to reduce net friction, as do skirt ovality values that closely approximate the shape of the liner. Moreover, the grooves machined into the skirt surface were shown to have a deleterious effect on friction if their amplitude was large relative to the thickness of the oil film. Using relatively small-amplitude grooves facilitates oil movement and retention without leading to direct contact with the liner. After piston geometry has been optimized to promote hydrodynamic lubrication, further refinements, such as reducing oil viscosity, are possible.

Thesis Supervisor:
Dr. Victor W. Wong (Lecturer, Department of Mechanical Engineering)

(This page was intentionally left blank)

Acknowledgements

First and foremost, I would like to thank my advisor, Dr. Victor Wong, for his assistance and advice throughout my program. He exposed to me a breadth of knowledge of various aspects of engine modeling and provided a strong foundation for a career in the engine design field. Dr. Wong encouraged and facilitated my internship at Waukesha Engine, which was enormously helpful. He also gave me the opportunity to publish a paper documenting various friction reduction strategies.

In association with my research at MIT, I had the privilege of completing an internship at Waukesha Engine Dresser, Inc. in the fall semester of 2005. My supervisor was Rick Donahue, who was an outstanding mentor. He—along with his colleagues Andy May, Jim Zurlo, Ed Reinbold, and others—gave me valuable perspective on the methods and challenges inherent in designing and manufacturing pistons in a real-world environment. Rick has been designing pistons for engines of various sizes for multiple applications over the past several years, and he was intimately knowledgeable of what factors affected real-world performance and reliability.

Numerous others have contributed to my educational development. Jeff Jocsak helped me get settled into the lab, provided background in understanding the models, and helped me learn Fortran. Fiona McClure offered much valuable perspective on modeling the piston and liner. Other students in the Sloan Automotive Lab enhanced my understanding of various aspects of the engine, both in casual conversation and in the weekly seminars at the Lab. Rudy Stanglmaier and his students at Colorado State University offered useful input and advice on the experimental aspect of engine research. Finally, Leslie Regan has been extremely helpful, both in assisting me in finding a research position and guiding me throughout my time at MIT.

Finally, I would like to thank my wonderful family and my friends, both at MIT and elsewhere, for their support.

(This page was intentionally left blank)

Table of Contents

(This page was intentionally left blank)

List of Figures

(This page was intentionally left blank)

List of Tables

(This page was intentionally left blank)

1 Introduction

1.1 Sources of friction

In a typical reciprocating engine, about 10% of the chemical energy of the fuel is lost to mechanical friction (Figure 1.1 shows an estimated distribution). This friction loss derives from three primary sources: power cylinder, crankshaft/gear train, and water pumps.[1-2] The power cylinder contributes about 30-40% of the net friction (Fig. 1.2), and this friction is developed by the piston skirt, rings, and rods in roughly equal proportions (Fig. 1.3). Previous studies[3-11] have investigated how the rings affect friction, and this study extends the analysis to the piston skirt. A reduction in piston friction ultimately leads to improvement in fuel economy and reduction in emissions.

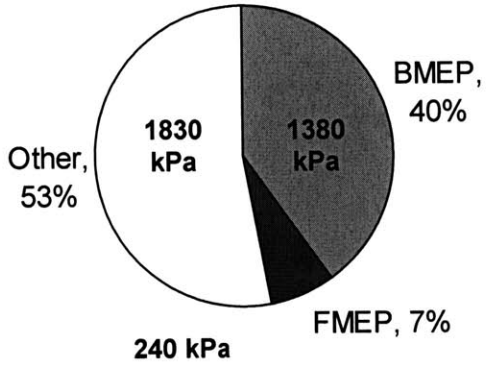

Figure 1.1: Distribution of energy in reciprocating engine; estimated values for Waukesha engine shown

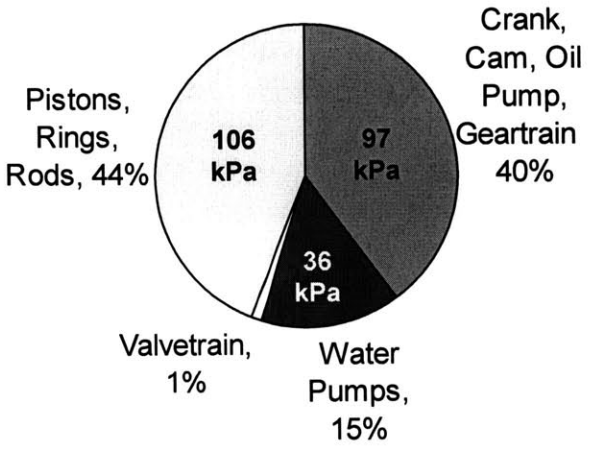

Figure 1.2: Sources of FMEP; estimated values for Waukesha engine shown

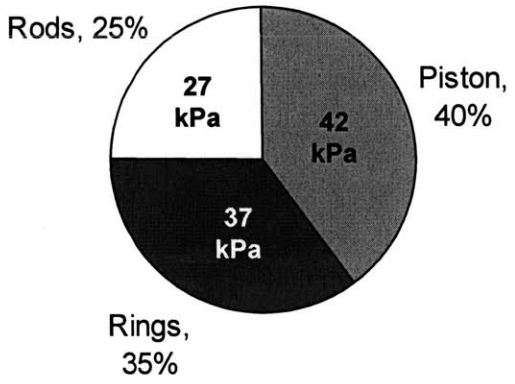

Figure 1.3: Relative contribution of FMEP from piston, rings, and rods; estimates for Waukesha engine shown

1.2 Description of power cylinder system

A schematic of the power cylinder system is shown in Figure 1.4. The piston skirt is the area on the piston below the ring-pack, and it is the target of this study. The skirt is designed to counter the lateral force from the connecting rod and guide the piston within the liner. In contrast to the rings, which are exposed to a very thin oil layer, the piston skirt typically has a much thicker oil film because it remains under the oil control ring.

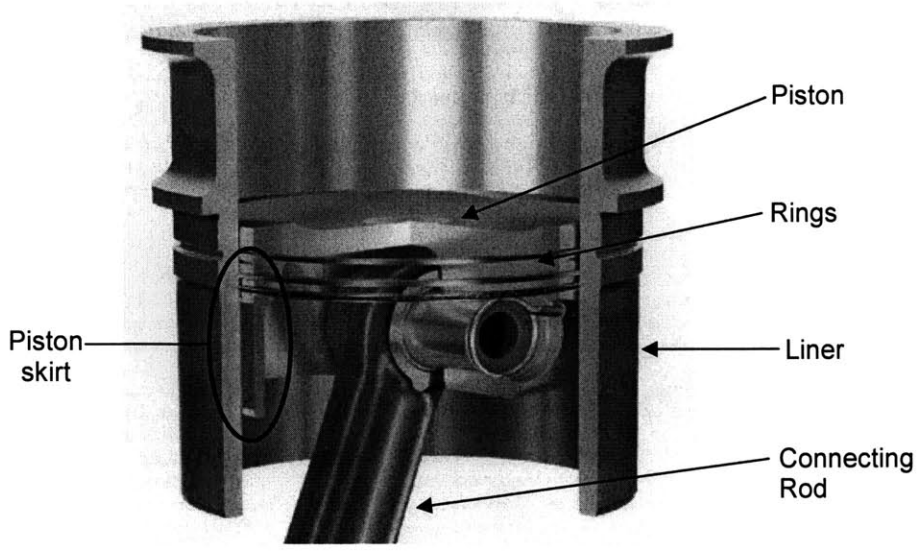

Figure 1.4: Schematic of power-cylinder system, showing piston skirt

2 Friction Analysis

Friction is the resistive force that arises from contact between two surfaces in relative motion. In an engine, a design goal is to minimize friction, with its concomitant efficiency loss, in order to improve fuel economy. In order to understand friction, the methods of lubrication must be investigated. In general, there are three major lubrication regimes: hydrodynamic, boundary, and mixed. Figure 2.1 illustrates the three modes, which are described in the following sections.

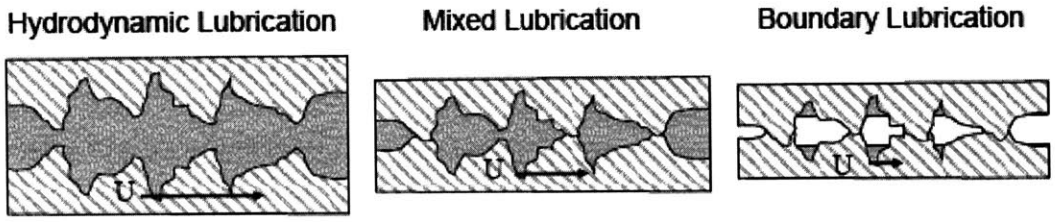

Figure 2.1: Modes of lubrication, shown in context of surfaces microstructure

2.1 Hydrodynamic lubrication

Hydrodynamic lubrication is the support of a surface by oil pressure alone without any direct surface contact. A schematic of the skirt-liner system under hydrodynamic lubrication is shown in Figure 2.2, where h_i is the inlet oil film height, h_e is the exit oil film height, $h(x)$ is the film height at a distance x from the entrance, and h_∞ is the original film height. If $h(x)$ drops below a critical value, the piston and liner surfaces enter boundary lubrication, discussed in Section 2.2.

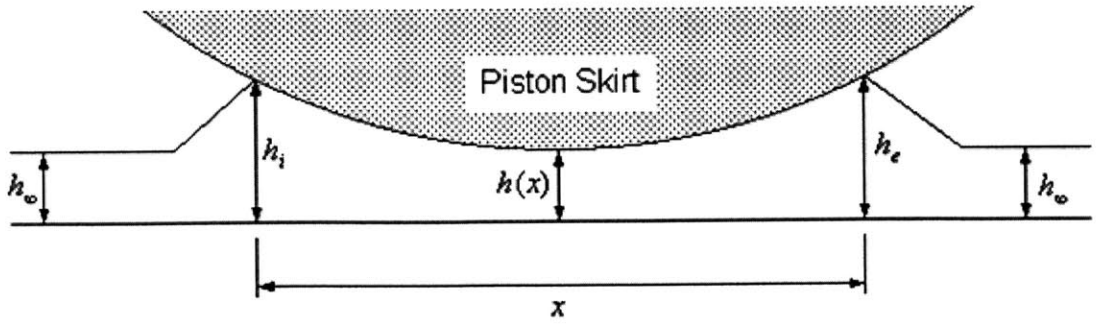

Figure 2.2: Schematic diagram of skirt-liner system

The first step in finding hydrodynamic pressure is calculating volumetric flow of oil, which can be determined by applying the conservation of mass and conservation of momentum equations (in the form of the Navier-Stokes equations). By making the following six assumptions, the full Navier-Stokes equations can be reduced to a much simpler system[12-13]. The volumetric flow rate, shown in Eq. 2.1, is derived in detail in Appendix A.1.

1. Height of fluid film $y << x, z$ (film curvature can be ignored)
2. Negligible pressure variation across fluid film $\Rightarrow \frac{\partial p}{\partial y} = 0$
3. Laminar flow
4. No external forces act on fluid film $\Rightarrow X = Y = Z = 0$
5. Fluid inertia is small compared to viscous shear $\Rightarrow$ LHS terms in Eq. (A.2) neglected
6. All velocity gradients are negligible compared to $\frac{\partial u}{\partial y}, \frac{\partial w}{\partial y}$.

$$Q(x) = -\frac{h^3}{12\mu}\frac{dp}{dx} + \frac{Uh}{2} \qquad \text{Eq. 2.1}$$

The pressure distribution over the piston can be calculated by applying the conservation of mass and conservation of momentum equations to a fluid element under the skirt surface[12-13]. By using appropriate boundary conditions and assuming that the oil is incompressible, the system reduces to the 2-D Reynold's Equation, shown in Eq. 2.2. This equation is the central equation used in numerical models of the piston, and it is derived in detail in Appendix A.2. The Reynold's equation relates the pressure (p) to the oil film thickness (h) using parameters such as piston speed (U) and viscosity (μ).

$$\frac{\partial}{\partial x}\left(\frac{h^3}{\mu}\frac{\partial p}{\partial x}\right) + \frac{\partial}{\partial z}\left(\frac{h^3}{\mu}\frac{\partial p}{\partial z}\right) = 6U\frac{\partial h}{\partial x} + 12\frac{\partial h}{\partial t} \qquad \text{Eq. 2.2}$$

2.2 Boundary lubrication

The piston can be supported by direct surface contact with the liner surface, a phenomenon called boundary lubrication. On a microscopic level, boundary lubrication is caused by asperity contact. Boundary lubrication arises from contact between many asperities of various shapes, and it is treated stochastically because the distribution of asperity heights is essentially random.

Several models, exhibiting various levels of sophistication and accuracy, are available in the literature. A commonly used model is the one proposed by Greenwood and Tripp[15], which treats the asperities as a statistical distribution. The Greenwood and Tripp formulation begins with an expression for the contact pressure:

$$P_c\left(\frac{d}{\sigma}\right) = K' E' \int_{d/\sigma}^{\infty} \left(z - \frac{d}{\sigma}\right)^{2.5} \phi(z) dz \qquad \text{Eq. 2.2}$$

where

$$K' = \frac{8\sqrt{2}\pi}{15} (\eta\beta\sigma)^2 \sqrt{\frac{\sigma}{\beta}} \qquad \text{Eq. 2.2}$$

In the equations above, P_c is the nominal contact pressure between the surfaces, d is the mean separation of the two surfaces (i.e., piston skirt and liner), η is the asperity density per unit area, β is the asperity peak radius of curvature, $\varphi(z)$ is the probability distribution of asperity heights, and z is the offset between asperity height mean and surface height mean. Moreover, the Young's modulus (E') and standard deviation of asperity heights (σ) are taken to be composite values, where E_1, E_2 and σ_1 σ_2 represent the respective values for Young's modulus and asperity standard deviation for each surface:

$$E' = \frac{2}{\frac{1-\nu_1^2}{E_1} + \frac{1-\nu_2^2}{E_2}} \qquad \text{Eq. 3.1}$$

$$\sigma = \sqrt{\sigma_1^2 + \sigma_2^2} \qquad \text{Eq. 3.3}$$

2.3 Mixed lubrication

As the name implies, mixed lubrication involves support by both hydrodynamic and boundary lubrication. It is the transition region between hydrodynamic and boundary lubrication, in which there is significant pressure applied by the fluid, but not enough to eliminate asperity contact. In many cases, the lowest friction value is achieved when the surface is in mixed lubrication (see Stribeck curve in next section), since this provides the optimum tradeoff between hydrodynamic and boundary support. In operation, as the piston moves between the ends of the stroke (low velocity, boundary lubrication) and the middle of the stroke (high velocity, hydrodynamic lubrication), it passes through the mixed lubrication regime many times.

2.4 Stribeck curve

The relationship between the three lubrication regimes is given by the Stribeck curve, shown schematically in Fig. 2.3. It illustrates how boundary friction decreases with sliding speed, while hydrodynamic friction increases with sliding speed; consequently, there is an optimum sliding speed for minimum friction, assuming a given set of viscosity and surface parameters.

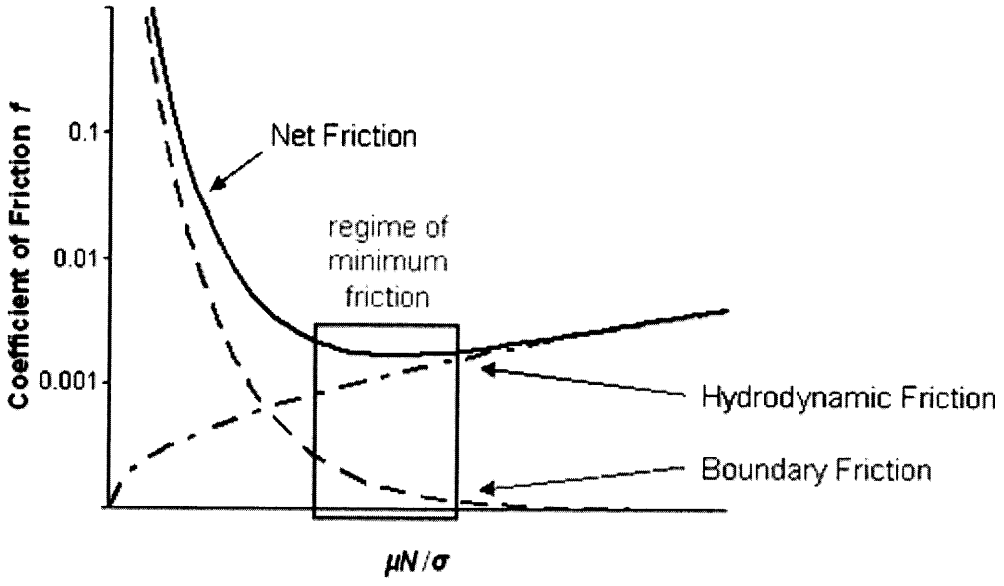

Figure 2.3: Stribeck curve, showing friction coefficient as a function of duty parameter, where μ is dynamic viscosity, N is speed, and σ is the loading force per unit area

3 Modeling Approach

A numerical model of the piston skirt, previously developed by Wong et al., was used to perform parametric studies of the power cylinder system.[16-20]

3.1 Overview of model

The model of the piston combines the equations of motion, the Reynold's equations of hydrodynamic lubrication, the stiffness matrix of the piston, and various other correlations to predict how the piston will deform and interact with the liner under operational conditions. It calculates the oil film thickness, friction work loss, etc., and uses them to predict how a change in a single parameter will affect friction. This model includes the following three important features:

1. Mixed lubrication: rather than simply assuming a dry skirt (exclusively boundary lubrication) or a thick oil film (exclusively hydrodynamic lubrication), this model allows for any combination of contact, hydrodynamic, and mixed lubrication.
2. Oil film thickness: some other models assume a fully-flooded skirt, which is somewhat unrealistic. In this model, an oil film thickness can be specified, and the model assumes atmospheric pressure if the skirt-liner separation is greater than the oil film thickness.
3. Flexible skirt: rather than assuming that the piston is infinitely rigid, a stiffness matrix describing deformation characteristics of the piston is included in the model. The pressure from hydrodynamic and boundary lubrication interacts with the deformation of the skirt to produce a net oil film thickness, which is used in lubrication calculations.

3.2 Equations of motion

The piston is evaluated in a free-body diagram, illustrated in Figure 3.1. The equations of static equilibrium are given by Equations 3.1-3.3. This system is described in more detail by Wong, et al., in *A Numerical Model of Piston Secondary Motion and Piston Slap in Partially Flooded Elastohydrodynamic Skirt Lubrication*, 1994.[16]

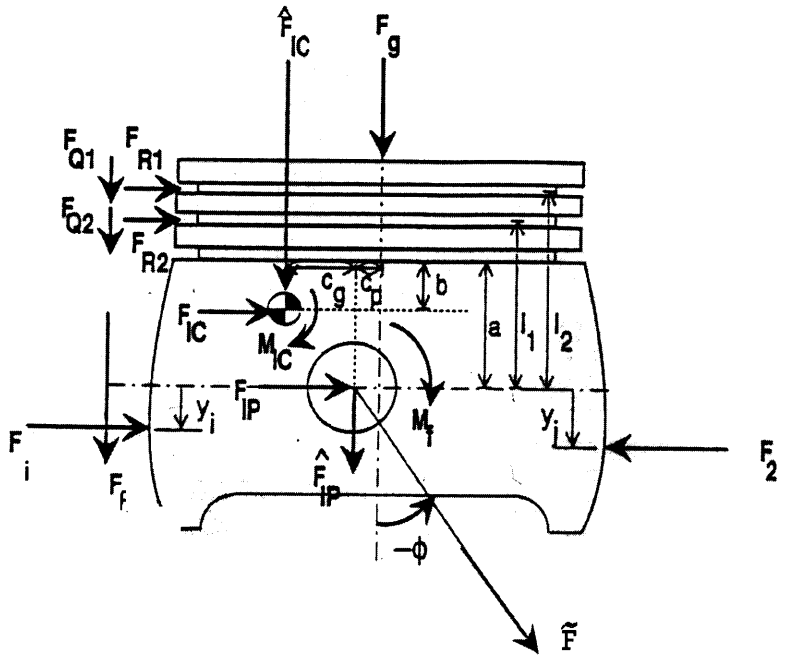

Figure 3.1: Free-body diagram of piston, showing forces and moments acting upon it

$$\Sigma F_y : F_g + \hat{F}_{IP} + \hat{F}_{IC} + \tilde{F}\cos\varphi + \Sigma F_{qj} + F_f = 0 \qquad \text{Eq. 3.1}$$

$$\Sigma F_x : \Sigma F_s \delta_s + F_{IP} + F_{IC} - \tilde{F}\sin\varphi + \Sigma F_{rj} = 0 \qquad \text{Eq. 3.2}$$

$$\Sigma M_p : -\Sigma F_s y_s \delta_s + M_{IP} + M_{IC} + M_{pp} + F_{IC}(a-b) - \hat{F}_{IC} C_g + F_g C_p + M_f + C_p \Sigma F_{qj} + \Sigma F_{rj} l_j = 0 \qquad \text{Eq. 3.3}$$

All the lubrication equations, such as the Reynold's equation and the contact pressure terms, produce pressure terms that are integrated to yield the force terms in the free-body diagram in Figure 3.1. After some algebraic manipulations, the equations of motion can be reduced to two equations of eccentricity, which describe how the top (e_t) and bottom (e_b) of the piston deviate from the bore centerline (shown in Figure 3.2); these form the constitutive equations for the system:

$$\ddot{e}_t = F_\sigma(t) + G_1\left(e_t, \dot{e}_t, e_b, \dot{e}_b, t\right) \qquad \text{Eq. 3.4}$$

$$\ddot{e}_b = M_s(t) + G_2\left(e_t, \dot{e}_t, e_b, \dot{e}_b, t\right) \qquad \text{Eq. 3.5}$$

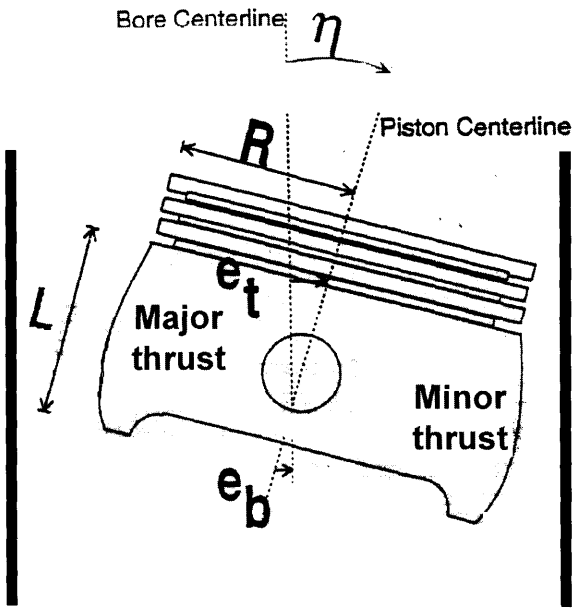

Figure 3.2: Schematic diagram of piston, showing eccentricities at top (e_t) and bottom (e_b)

3.3 Finite-difference solution to Reynold's equation (rigid skirt)

In order to simulate how the piston skirt is supported by the oil film, the Reynold's equation, a second-order differential equation, is solved by means of a second-difference method. The Reynold's equation is shown in simplified 1-D form in Equation 3.6. The terms μ and U are constants. The array of oil film thickness values h is initially treated as a known independent variable, and the system is solved for the map of dependent pressure variables p.

$$\frac{\partial}{\partial x}\left(h^3 \frac{\partial p}{\partial x}\right) = -6\mu U \frac{\partial h}{\partial x} + 12\mu \frac{\partial h}{\partial t} \qquad \text{Eq. 3.6}$$

3.3.1 First-difference approximation of first derivative

The Reynold's equation is first discreetized by dividing the skirt area into small segments (nodes), shown schematically in Fig. 3.3. The first derivative is approximated as the slope of each of these linear segments, and it can be defined in three different ways. The first, the forward difference, measures the slope based on the following node. The second method, the backward

difference, calculates on the basis of the previous point. The third method computes the slope by taking an average of the other two, and it is generally more accurate because it considers more information. The three techniques are expressed in Eq. 3.7-9.

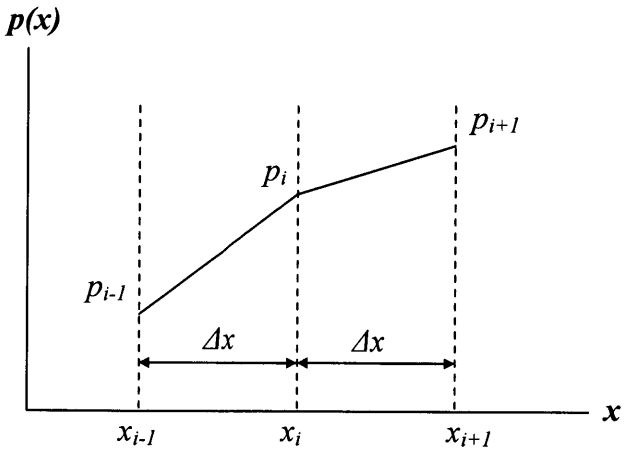

Figure 3.3: Discreetization of a function. The forward difference determines the slope on the right, the backward difference determines the slope on the left, and the centered difference finds their average

Forward difference: $$\frac{\partial p}{\partial x} \approx \frac{p_{i+1} - p_i}{\Delta x} \qquad \text{Eq. 3.7}$$

Backward difference: $$\frac{\partial p}{\partial x} \approx \frac{p_i - p_{i-1}}{\Delta x} \qquad \text{Eq. 3.8}$$

Centered difference: $$\frac{\partial p}{\partial x} \approx \frac{p_{i+1} - p_{i-1}}{2 \cdot \Delta x} \qquad \text{Eq. 3.9}$$

3.3.2 Second-difference approximation of second derivative

The second derivative is approximated by taking the difference of two adjacent first differences and dividing by the distance between their centers, as shown in Eq. 3.10. This is known as the second-difference approximation.

$$\frac{\partial^2 p}{\partial x^2} = \frac{\left(\frac{p_{i+1} - p_i}{\Delta x}\right) - \left(\frac{p_i - p_{i-1}}{\Delta x}\right)}{\Delta x} = \frac{p_{i+1} - 2p_i + p_{i-1}}{(\Delta x)^2} \qquad \text{Eq. 3.10}$$

However, in the actual Reynold's equation (Eq. 3.6), the oil film thickness (h) term is included inside the second-derivative, so a more intricate formulation is warranted. In Eq. 3.11, the intermediate h values are included in each first derivative to produce the most accurate second difference; Fig. 3.4 provides a schematic of the approximation.

$$\frac{\partial}{\partial x}\left(h^3\frac{\partial p}{\partial x}\right) \approx \frac{\left(h_{i+1/2}^3\frac{p_{i+1}-p_i}{\Delta x}\right)-\left(h_{i-1/2}^3\frac{p_i-p_{i-1}}{\Delta x}\right)}{\Delta x} = \frac{h_{i+1/2}^3 p_{i+1}-\left(h_{i+1/2}^3+h_{i-1/2}^3\right)p_i+h_{i-1/2}^3 p_{i-1}}{(\Delta x)^2} \quad \text{Eq. 3.11}$$

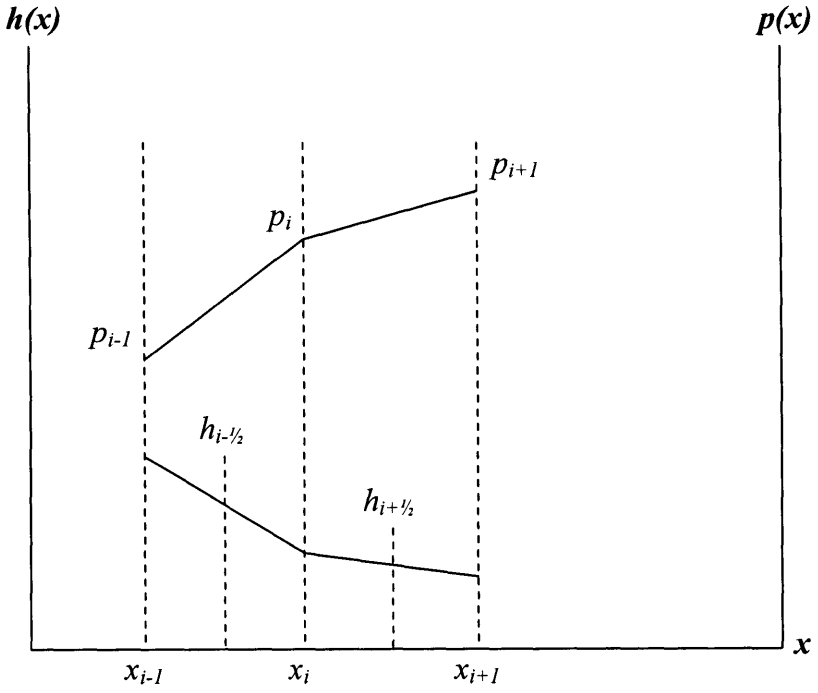

Figure 3.4: Schematic of second-difference method, with intermediate $h_{i+1/2}$ and $h_{i-1/2}$ values at each slope

It is difficult to work with variables that are located at non-integer node points. Since the first difference terms are linear, however, the $h_{i+1/2}$ and $h_{i-1/2}$ terms can be expressed as the averages of their neighbors, h_{i-1}, h_i, and h_{i+1}. These expressions are shown in Eq. 3.12-14.

$$h_{i+1/2} = \frac{h_i + h_{i+1}}{2} \quad \text{Eq. 3.12}$$

$$h_{i-1/2} = \frac{h_i + h_{i-1}}{2} \quad \text{Eq. 3.13}$$

$$\frac{\partial}{\partial x}\left(h^3\frac{\partial p}{\partial x}\right)\approx\frac{\left(\frac{h_i+h_{i+1}}{2}\right)^3\cdot\frac{p_{i+1}-p_i}{\Delta x}-\left(\frac{h_i+h_{i-1}}{2}\right)^3\cdot\frac{p_i-p_{i-1}}{\Delta x}}{\Delta x} \qquad \text{Eq. 3.14}$$

The complete discreetized 1-D Reynold's equation is summarized in Eq. 3.15. Note that the first spatial derivative on the right-hand side is a centered difference for accuracy, and the time derivative is a backward difference (in the model, the previous time step is known, so it is straightforward to use a backward difference).

$$\frac{\partial}{\partial x}\left(h^3\frac{\partial p}{\partial x}\right)=-6\mu U\frac{\partial h}{\partial x}+12\mu\frac{\partial h}{\partial t}\rightarrow$$

$$\frac{\left(\frac{h_i+h_{i+1}}{2}\right)^3\cdot\frac{p_{i+1}-p_i}{\Delta x}-\left(\frac{h_i+h_{i-1}}{2}\right)^3\cdot\frac{p_i-p_{i-1}}{\Delta x}}{\Delta x}=-6\mu U\frac{h_{i+1}-h_{i-1}}{2\Delta x}+12\mu\frac{h_j-h_{j-1}}{\Delta t} \qquad \text{Eq. 3.15}$$

The discreetized Reynold's equation is applied to each node in the oil film mesh, using the local oil film thickness values for the h term. These individual equations are solved simultaneously by a matrix, as shown in Eq. 3.16. Since the h terms are assumed to be known and constant, the p terms can be solved directly by any of a variety of matrix solution methods. An example of a simplified solution matrix (1-D, no time dependence) is provided in Fig. 3.16.

$$\begin{bmatrix} 1 & & & & & & \\ h_2^3-\frac{3}{4}h_2^2(h_3-h_1) & -2h_2^3 & h_2^3+\frac{3}{4}h_2^2(h_3-h_1) & & & & \\ & h_3^3-\frac{3}{4}h_3^2(h_4-h_2) & -2h_3^3 & h_3^3+\frac{3}{4}h_3^2(h_4-h_2) & & & \\ & & \ddots & \ddots & \ddots & & \\ & & & h_n^3-\frac{3}{4}h_n^2(h_{n+1}-h_{n-1}) & -2h_n^3 & h_n^3+\frac{3}{4}h_n^2(h_{n+1}-h_{n-1}) & \\ & & & & & 1 & \end{bmatrix}\begin{bmatrix} p_1 \\ p_2 \\ p_3 \\ \vdots \\ p_n \\ p_{n+1} \end{bmatrix}=$$

$$=\begin{bmatrix} 1 \\ -3\mu U(\Delta x)(h_3-h_1) \\ -3\mu U(\Delta x)(h_4-h_2) \\ \vdots \\ -3\mu U(\Delta x)(h_{n+1}-h_{n-1}) \\ 1 \end{bmatrix} \qquad \text{Eq. 3.16}$$

3.4 Friction factors

The Reynold's equation assumes that surfaces are perfectly smooth. The actual piston and liner surfaces have natural surface roughness (asperities) and waviness (machined grooves), but analytical determinations of hydrodynamic pressure for rough surfaces are not practicable. Patir and Cheng[21-22] proposed a system of friction factors which evaluate the piston surface stochastically and introduce constants into the Reynold's equation to reflect the overall effects of roughness (Eq. 3.17). The piston model used for this study generates the appropriate flow factors based on input data and integrates them into its calculations; in this way, the model includes the effects of surface roughness and waviness.

$$\frac{\partial}{\partial x}\left(\Phi_x h^3 \frac{\partial p_h}{\partial x}\right)+\frac{\partial}{\partial y}\left(\Phi_y h^3 \frac{\partial p_h}{\partial y}\right)=-6\mu U\left(\frac{\partial h}{\partial y}+\Omega\frac{\partial \Phi_s}{\partial y}\right)+12\mu\frac{\partial h}{\partial t} \qquad \text{Eq. 3.17}$$

In Eq. 3.17, Φ_x and Φ_y are pressure flow factors that adjust the pressure according to the roughness characteristics of the surfaces. The shear flow factors Φ_s and Ω indicate how the shear stress developed in the oil film is modified by surface roughness. A drawback of the Patir and Cheng flow factors is that they assume the surfaces are Gaussian, but the actual piston skirt surface contains anisotropic (directional) honing grooves whose troughs are much deeper than their peaks (i.e., the surface has negative skewness). However, the flow factor formulation furnishes a useful way to approximate an otherwise intractable system.

3.5 Compliance of piston

When modeling piston dynamics, approximating the skirt as a rigid structure is not accurate. Typical oil film thicknesses are on the order or 10-50 microns, and the total deformation of the skirt is one the same order of magnitude. Moreover, the hydrodynamic pressure (p) is very sensitive to changes in the film thickness (h) because p depends on the cube of h (see Reynold's equation, Eq. 2.2). Since piston deformation significantly changes the value of h (potentially doubling it, in some situations), deformation must be included in the model.

The deformation of the piston in response to applied loads is described by a stiffness matrix, as shown in Eq. 3.18. The stiffness matrix is based on the specific geometry of the piston, and it indicates how each point on the piston deforms (Δh_i) in response to applied loads (p_i).

$$\begin{bmatrix} & & \\ & K & \\ & & \end{bmatrix} \begin{bmatrix} \Delta h_1 \\ \Delta h_2 \\ \vdots \\ \Delta h_n \\ \Delta h_{n+1} \end{bmatrix} = \begin{bmatrix} p_1 \\ p_2 \\ \vdots \\ p_n \\ p_{n+1} \end{bmatrix} \qquad \text{Eq. 3.18}$$

The algorithm follows an iterative process, in which the pressure terms from the rigid-skirt solution (section 3.3) are input into the stiffness matrix (Eq. 3.17), which calculates associated deformations. Then the h_i values from the rigid-skirt solution are adjusted by the Δh_i deformation terms, and the rigid-skirt solution is solved again. The stiffness matrix and Reynold's equation are solved alternately until they converge on common p_i and h_i values.

3.6 Additional phenomena

3.6.1 Oil film thickness

The stipulation that oil film thickness not exceed a given value requires that the film thickness values (h) be discontinuous. For instance, if the film thickness is given to be 50 microns, any region on the skirt surface that is more than 50 microns away from the liner must have its pressure value artificially set to zero, since that region is not in contact with oil and cannot sustain any pressure. The inlet condition for the Reynold's equation is described in Appendix C.

3.6.2 Cavitation

If the Reynold's equation is solved without regard to the physical constraints of the system, it will calculate many regions with substantial negative pressures, particularly at the trailing edge of the contact patch (see Figure 3.5). In an actual system, the oil cannot sustain negative

pressure; the film will simply peel away from the piston surface, exposing the piston surface to atmospheric pressure; this process is called cavitation. The model treats cavitation by setting all pressures less than 1 bar to crankcase pressure (typically 1 bar); this introduces a second discontinuity to the pressure map. The Reynold's exit condition is explained in Appendix D.

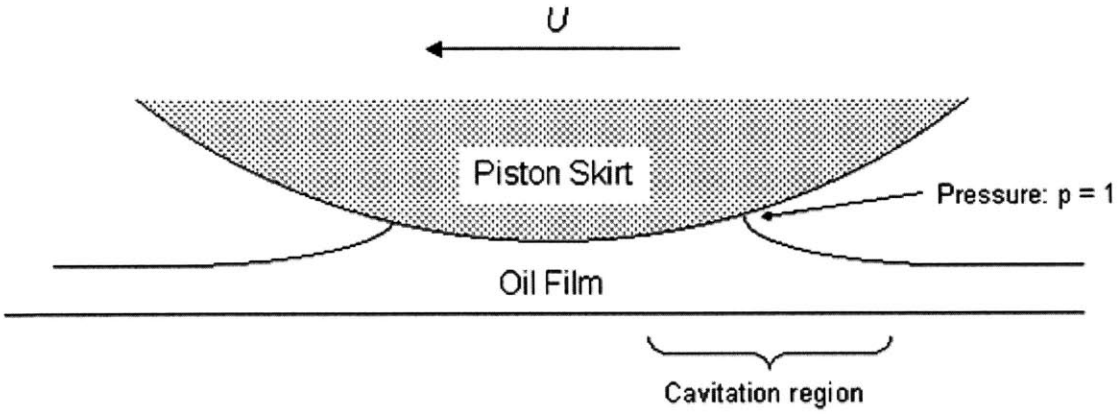

Figure 3.5: Schematic of piston skirt and oil film, showing cavitation at the trailing edge of the contact patch

3.6.3 Asperity contact

When the effective separation between skirt and liner drops below a critical value, the asperities on the surface begin to contact each other, and boundary contact replaces hydrodynamic lubrication. The simulation program uses the waviness parameters to determine when asperity contact occurs; that is, when the skirt-liner separation distance drops below the waviness value, the surfaces begin to touch, and the model switches to boundary lubrication mode. This is another discontinuous phenomenon that complicates solution of the second-difference Reynold's equation.

For simplicity, the correlations in Eq. 3.19-20 are used for boundary contact pressure[23-24]. In Eq. 3.19, the quantity x_i is calculated as a function of wave height (Ω) and amplitude (L_w). Then Eq. 3.20 predicts the contact pressure p_w as a function of x_i, L_w, and the Young's modulus E'.

$$\delta(x,y) = x_i\left[-0.635\ln\left(x_i L_w / 4\Omega\right)+1.0556\right] \qquad \text{Eq. 3.19}$$

$$p_w = x_i E' / L_w \qquad \text{Eq. 3.20}$$

3.7 Application to Waukesha engine

This investigation was conducted as part of a Department of Energy project to increase the efficiency of large, stationary, natural-gas engines. An essential component of the overall program was experimental verification of model predictions on an actual engine. The project was conducted in collaboration with Waukesha Engine Dresser and Colorado State University, which operated a Waukesha VGF-18 in their laboratory. The Waukesha VGF in-line 6 engine configuration (155 mm bore x 165 mm stroke) is turbocharged, aftercooled, with modern combustion chamber design. It has a four-ring pack and an aluminum piston. The piston skirt model was exercised with geometric and operating parameters from this engine; the specifications are summarized in Table 1.

Engines in this class are often destined for continuous duty, so they are designed for long-term operation, with typical time between overhauls in the tens of thousands of hours. Consequently, small improvements in friction and other efficiency-related factors can yield substantial fuel savings over the life of the engine. Relative to other engine classes (such as automotive), the pistons in large stationary engines justify significant manufacturing resources, so engineers have more latitude when designing them.

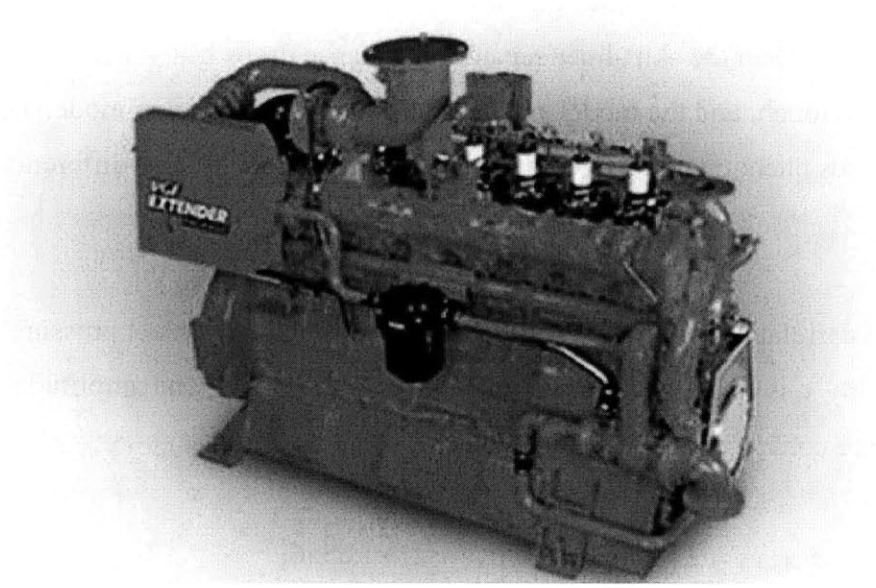

Figure 3.6: Waukesha VGF-18 six-cylinder, 18-liter stationary natural-gas reciprocating engine

Table 1: Specifications of Waukesha engine

Engine Model	Waukesha Model F18GL
Engine Characteristics	Turbocharged, intercooled, lean combustion
Engine Configuration	6 Cylinders, inline
Displacement	18 L (1096 cu. in.)
Bore	152 mm
Stroke	165 mm
Speed	1800 rpm
Load Condition (at 1800 RPM)	1360 kPa BMEP
Brake Thermal Efficiency	37%
Piston Skirt Surface Waviness (worn)	10 micron
Piston Skirt Roughness	0.2 micron
Dry Weight	5725 lb.

(This page was intentionally left blank)

4 Parameters Influencing Piston Friction

4.1 Introduction

Piston design parameters fall into two major categories: lubricant selection and piston geometry. Changes to piston geometry have localized effects, since they affect only the power cylinder, but changes to the lubricant have global impacts because the oil flows throughout the engine and affects other components such as the crankshaft and valvetrain. The piston-liner system is highly integrated, and modifying one component often affects the others. In this analysis, lubricant viscosity is considered first because it has a significant influence on the other parameters. The impacts of all design parameters on friction are explained with reference to the Stribeck curve.

4.2 Effect of lubricant viscosity on friction

Oil viscosity has a profound influence on friction, and it interacts with other parameters, such as profile shape and ovality, to modify their effects on friction as well. Increasing viscosity increases hydrodynamic friction by increasing the shear stresses sustained in the oil, and decreasing viscosity tends to reduce hydrodynamic friction by reducing shear stresses. Consequently, highly viscous oils would be expected to produce maximum hydrodynamic friction work.

Reducing viscosity is a potential method to reduce friction, but reducing it beyond a critical point can promote both higher friction and substantially greater wear. Although high-viscosity oil produces greater friction work by increasing shear stresses, the greater shear stresses enable it to support a greater load (at a given sliding speed). The ability of viscous oils to sustain loads hydrodynamically is essential for piston support, since this property helps avoid direct contact between the components. If the viscosity is reduced below the level required for hydrodynamic support, the piston surface will contact the liner surface and incur boundary contact friction. Typically, a design goal is to reduce boundary friction as much as possible, both because boundary friction involves significantly higher friction loss than hydrodynamic friction and because it promotes wear.

4.2.1 Dependence of viscosity on temperature and shear rate (Vogel and Cross equations)

Hydrodynamic friction between the piston and liner is highly dependent on lubricant viscosity, and the viscosity is heavily dependent on temperature. As temperature increases, viscosity decreases dramatically. A robust model will treat viscosity as a function of temperature (instead of assuming a constant value) in order to predict friction accurately.

The temperature dependence of viscosity is specified by the Vogel equation (Eq. 4.1), where T is temperature (in °C), and the other variables are properties of the particular oil used. The θ_1 and θ_2 terms have units of °C, and k has units of cSt. (More details, including property values for various oils, are provided in Appendix B.) Note that the Vogel equation is applicable only to single-grade oils, in which viscosity does not depend on shear rate. Since most large natural-gas engines use straight-weight oil (partially due to cost constraints), the Vogel equation is an accurate correlation between temperature and viscosity for these applications.

$$\nu_0 = k \exp\left(\frac{\theta_1}{\theta_2 + T}\right) \qquad \text{Eq. 4.1}$$

The previous piston model assumed that viscosity was constant throughout the cycle, but this is not a very accurate approximation, since viscosity varies by a factor of 2 between top dead center and bottom dead center (Fig. 4.2). Therefore, the model was modified such that viscosity was calculated from temperature and oil properties according to the Vogel equation; details of changes to the code are provided in Appendix B. The temperature profile was calculated from the Woschni correlation (Eq. B.1) and is shown in Fig. 4.1. At each crank angle increment, the current viscosity of the oil was determined, and Fig. 4.2 illustrates how the viscosity varied throughout the cycle.

Note the approximately sinusoidal nature of the viscosity as the piston moves up and down on the liner: the viscosity decreases toward the top of the stroke. The highest lateral pressure on the piston skirt occurs when the connecting rod force is highest, which happens when cylinder pressure is maximum. The pressure is maximum near TDC just after firing. The TDC position

corresponds to the valleys on the curves in Fig. 4.2, when viscosity is low. Since viscosity is low and lateral pressure is high at TDC, this area is most vulnerable to boundary friction and its concomitant wear. In the field, the top of the liners exhibits the most wear, which is consistent with this prediction.

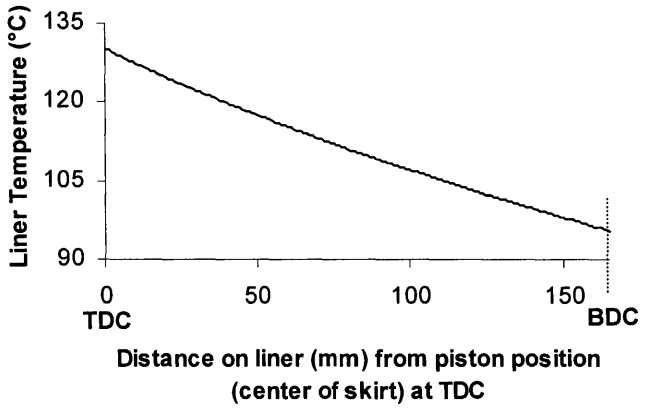

Figure 4.1: Liner temperature vs. position

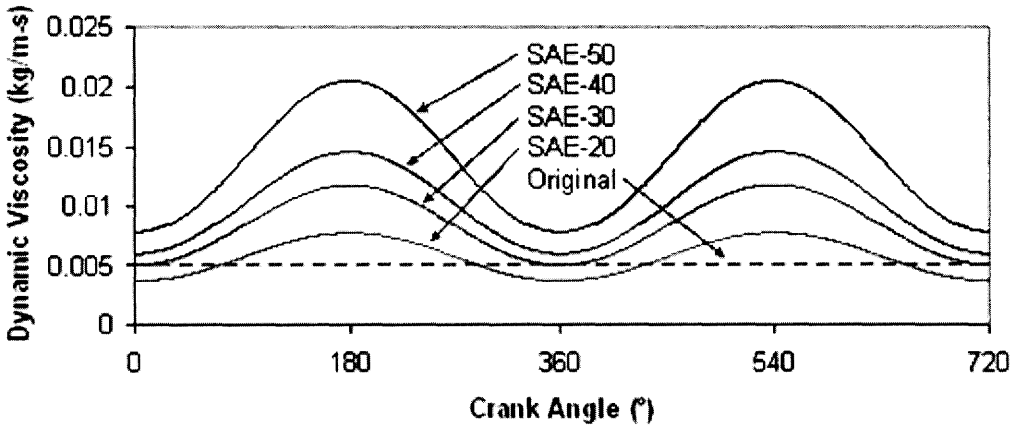

Figure 4.2: Viscosity vs. crank angle for straight-weight oils (original, constant viscosity shown for reference)

All lubricants display a strong dependence of viscosity on temperature. However, the viscosity of multi-grade oils also depends on shear rate—i.e., the ratio of sliding speed to film thickness. Multi-grade oils are formulated so that the viscosity is high when shear rate is low; hence, when piston speed is low near TDC and BDC, the shear rate is also low, and oil is more viscous. This increases hydrodynamic support. However, during mid-stroke when the piston is moving faster, it is already in the hydrodynamic regime, and the high shear rate causes the multi-grade oil to reduce its viscosity, decreasing friction work.

The viscosity characteristics of multi-grade oils are modeled by the Cross Equation (Eq. 4.2), which is explained in detail in Appendix E. In the Cross equation, γ is the absolute value of the shear rate (units of s^{-1}) and β is the critical shear rate (s^{-1}); β depends on temperature according to Eq. E.2. The μ_0 term is the oil viscosity at zero shear rate, μ_∞ is the viscosity when shear rate tends to infinity, m is a correlation constant controlling the width of the transition region, and μ is the viscosity at shear rate γ (i.e., it is the viscosity to be calculated). Note that for single-grade oils, $\mu_\infty = \mu_0$.

$$\mu = \mu_0 \frac{1 + \frac{\mu_\infty}{\mu_0}\left(\frac{\gamma}{\beta}\right)^m}{1 + \left(\frac{\gamma}{\beta}\right)^m} \qquad \text{Eq. 4.2}$$

The oil properties (specified by β, μ_0, & μ_∞) can be optimized to minimize friction. Hypothetically, the oil characteristics could be adjusted such that at high temperatures and low speeds (which are characteristic at TDC), the viscosity increases substantially. However, at high speeds during mid-stroke movement, the viscosity decreases to reduce hydrodynamic friction loss. Finally, at BDC where both speeds and temperatures are low, the viscosity would be increased again. Scenarios similar to this one have been explored for the ring pack[28], and while they cannot be readily implemented in practice, they provide valuable guidance for optimizing multi-grade oils for low-friction operation.

4.2.2 Comparison of modes of lubrication (Stribeck curve)

The viscosity of the oil has a profound effect on friction, both by directly changing the shear stresses in the oil film and by interacting with other design parameters, such as piston profile shape, to modify friction. However, the various modes of lubrication—hydrodynamic, boundary, and mixed—are phenomenologically divergent, and changes in sliding speed, oil viscosity, etc. affect each mode differently. In order to understand the relative contributions of each regime, the Stribeck curve (Fig. 4.3) was developed to illustrate the distribution of hydrodynamic, boundary, and mixed lubrication for various speeds.

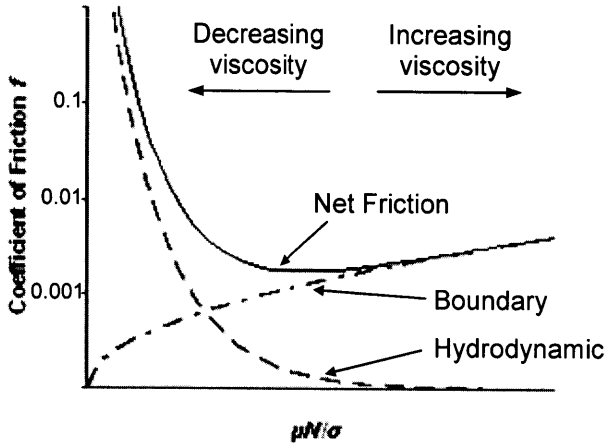

Figure 4.3: Stribeck curve, showing how changing viscosity affects friction

The Stribeck curve indicates how the effective coefficient of friction depends on the dimensionless duty parameter $\mu N/\sigma$, where μ is viscosity, N is sliding speed, and σ is loading force per unit area. If viscosity increases and everything else remains constant, the lubrication regime shifts toward the right (i.e., toward the hydrodynamic part) on the curve. The N parameter refers to relative speed between the piston and liner. At high speeds, the lubrication regime shifts toward the right (hydrodynamic), while at low speeds, such as near the ends of the stroke, boundary lubrication dominates. Finally, as loading pressure σ increases, lubrication shifts toward the left—i.e., toward the boundary regime. These characteristics are borne out by experience in the field: boundary friction is most prevalent when 1) oil viscosity is minimized, 2) sliding speed is minimized, and 3) loading force per unit area is maximized. All three conditions occur at the piston reversal point at the top of the liner, which is also where the most wear (precipitated by boundary contact) is observed.

The Stribeck curve informs design decisions by suggesting the direction in which to change various parameters. The ideal lubrication condition occurs when net friction is minimized; i.e., at the lowest point on the solid curve in Fig. 4.3. As seen from the plot, friction is minimized when the piston is supported by a combination of boundary and hydrodynamic lubrication, with hydrodynamic lubrication bearing the majority of the load. In order to achieve this ideal condition in an engine design, the baseline condition of the engine must first be ascertained. In general, if there is excess hydrodynamic friction, the oil viscosity should be decreased to

minimize friction. However, in the event that boundary friction predominates (i.e., lubrication is on the far left of the Stribeck curve), increasing oil viscosity can actually decrease friction by moving lubrication toward the right on the curve. (Generally, the sliding speed N is fixed by engine speed and geometry, and loading force per unit area σ is fixed by cylinder pressure and connecting-rod geometry, so viscosity is the only significant parameter in the Stribeck curve that can be modified.)

4.2.3 Effect of viscosity on minimum clearance

Minimum clearance, or separation, between the piston and liner is a crucial lubrication parameter because it directly affects wear and boundary friction. If the minimum clearance is large, then the oil film is relatively thick, and the piston is supported hydrodynamically. However, if the minimum clearance is small for significant portions of the cycle, then boundary friction will likely be large as well. Oil viscosity has a direct impact on minimum clearance. As viscosity increases, both the shear stress and the supported load increase as well. Since the supported load is constant for a given engine, the shear stress can be reduced to maintain the same oil film thickness. Since shear stress is inversely proportional to separation distance (as an approximation), one would expect an increase in viscosity to lead to a corresponding increase in minimum separation.

Figures 4.4 and 4.5 depict the model predictions of skirt-liner separation for the entire cycle. To generate the plots, the minimum clearance value for the skirt at each crank angle was determined. A 10 μm waviness value was assumed in this scenario, so when oil film thickness dropped to about 10 μm, boundary contact began. Fig. 4.5 shows a close-up view of the minimum clearance around the 360° crank angle, which is top dead center at the beginning of the expansion stroke, and it clearly shows that an increase in viscosity promotes greater separation between skirt and liner. As stated earlier, this is the point in the cycle when most of the wear is generated, so the greater separation provided by more viscous lubricants can produce substantial reductions in wear. According to Fig. 4.5, low-viscosity oils such as SAE-20 do not provide adequate hydrodynamic pressure to support the piston, and the deficiency must be balanced by increased boundary contact friction, which leads to increased wear.

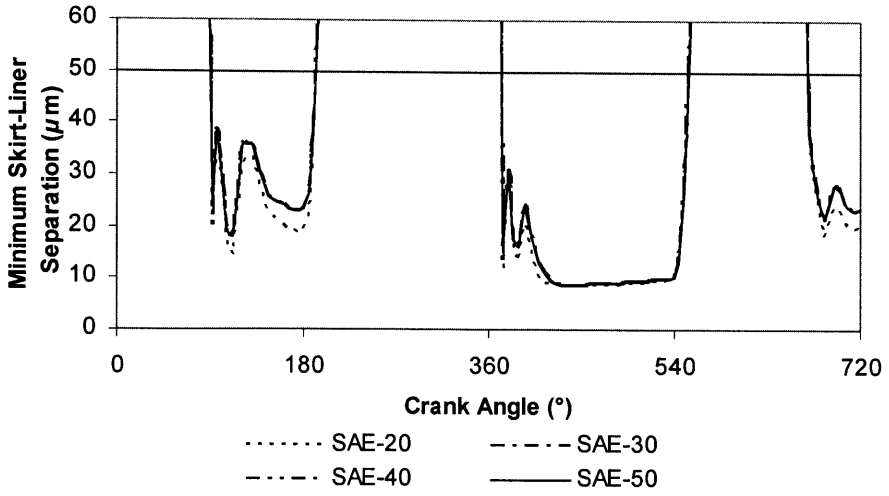

Figure 4.4: Minimum separation vs. oil viscosity (thrust side, 50 μm oil film thickness, 10 μm waviness)

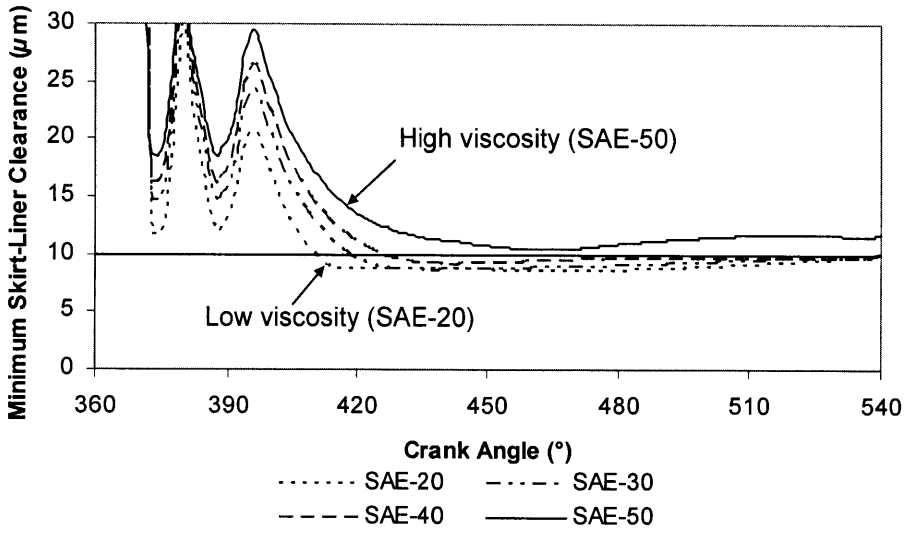

Figure 4.5: Close-up view of minimum separation vs. viscosity (thrust side, 50 μm oil film, 10 μm waviness)

A direct result of the greater separation that results from a more viscous lubricant is that the wetted area decreases. Since the piston "floats" higher in the oil film to produce greater separation, the wetted area decreases proportionally (in this model, a constant oil film thickness is assumed). Figure 4.6 illustrates this trend for the thrust side of the piston skirt; highly-viscous oils like SAE-50 have significantly less wetted area and significantly greater minimum skirt-liner clearance than low-viscosity oils like SAE-20.

Decreasing wetted area (assuming all else held constant) has the additional advantage of decreasing hydrodynamic friction. The off-center areas of the contact patch sustain only moderate pressure (see Fig. 4.15), but they incur significant hydrodynamic drag. Thus, by decreasing the wetted area, viscous oils reduce hydrodynamic friction relative to what it would be with identical wetted areas. However, the reduction in hydrodynamic friction due to decreased wetted area is more than offset by the increase in friction due to increased shear stress, so increasing viscosity always increases hydrodynamic friction.

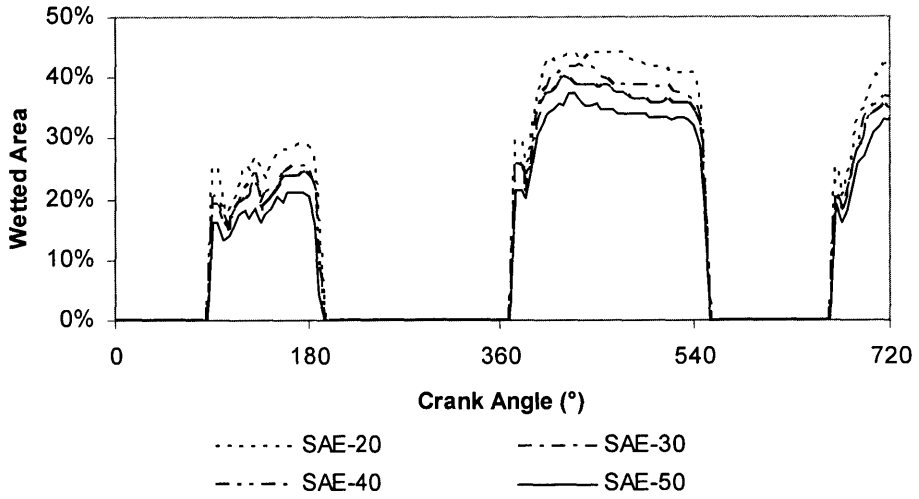

Figure 4.6: Percent wetted area vs. oil viscosity (thrust side, 50 μm oil film thickness, 10 μm waviness)

4.3 Oil film thickness (oil supply)

Oil film thickness, which is controlled by oil supply, has a direct impact on friction. A very thin oil film enables the skirt to easily push the oil aside and scrape the liner, leading to boundary friction. On the other hand, a thick oil film tends to encourage hydrodynamic lubrication by providing more contact between the film and the piston surface, thereby enabling the lateral force to be spread over a larger area. Figure 4.7 provides a schematic comparison. As the film thickness is increased to a certain point, it reduces boundary contact friction to a very small value, which minimizes net friction work loss. If film thickness is increased beyond this critical point, however, no further reductions in boundary friction are available, and hydrodynamic friction increases due to an increase in wetted area. Thus, increasing film thickness beyond the critical point can actually increase net friction.

Large oil film thickness

Large wetted area

Negligible direct surface contact

Primarily hydrodynamic lubrication

Small oil film thickness

Small wetted area

Significant direct surface contact

Primarily boundary lubrication

Figure 4.7: Schematic of large and small oil film thicknesses, showing operational characteristics of each

The relationship between friction work and oil film thickness for the Waukesha F18GL engine is shown in Figure 4.8, which clearly shows a reduction in contact friction as oil film thickness increases, corresponding to predictions. In this example, the boundary contact friction dominates, so the total friction curve follows the same trend. When the film thickness has reached about 80 μm, the boundary contact friction component is negligible, and further increases in film thickness increase hydrodynamic, and therefore net, friction loss.

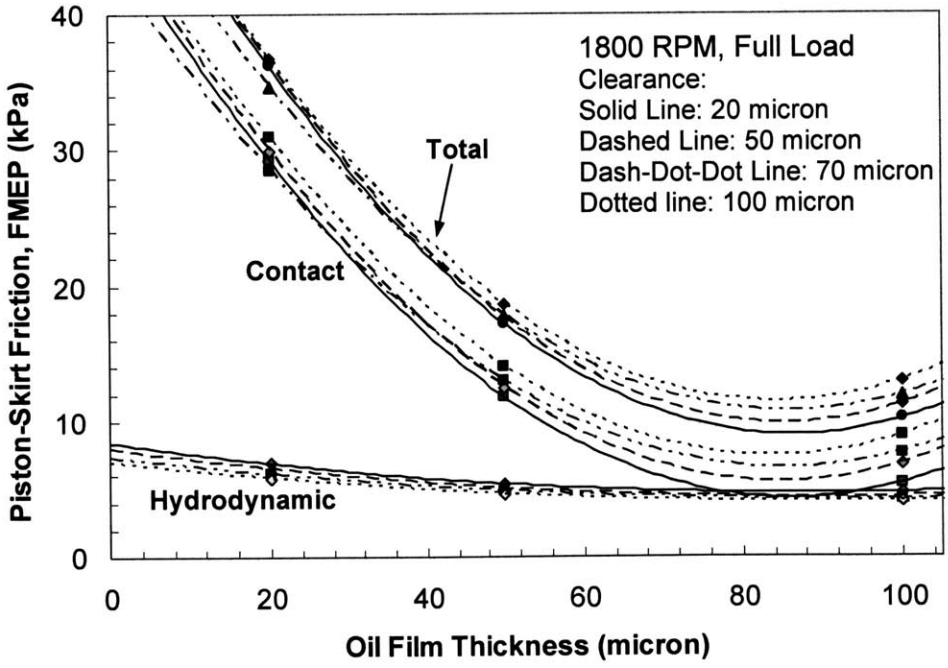

Figure 4.8: Effect of oil film thickness on friction. "Clearance" refers to cold skirt-to-liner clearances

Oil film thickness is dictated by oil supply, and although increasing oil supply can reduce friction, it entails several disadvantages. Increasing oil supply to the skirt will inevitably increase the amount of oil that escapes through the rings and is consumed; the increase in oil consumption is highly undesirable. One obvious disadvantage of heightened oil consumption is that operational costs rise; this is a significant concern for large natural-gas engines, which often hold 30-60 gallons of oil. Another significant disadvantage is that the escaping oil negatively impacts the emissions signature of the engine, and it can also poison certain after-treatment systems (catalytic converters, etc.). Therefore, design changes that reduce friction without resorting to increases in oil supply tend to be preferred, and several such methods are outlined in this report.

4.4 Skirt-liner clearance

The cold clearance between the piston skirt and the liner is a measure of how tightly the piston fits into the bore. A tight fit produces a small skirt-liner clearance, while a loose fit produces a large clearance (Figure 4.9). The clearance changes the *effective* oil film thickness between the skirt and liner. For example, a very tight clearance will push the piston very close to the liner, forcing the oil film away and encountering boundary lubrication, just as if the oil supply and film thickness were small. This is reflected in the friction work loss results shown in Fig. 4.10; as cold clearance is reduced from 0 to 50 μm, friction decreases slightly.

However, as the clearance increases beyond a certain point, the piston starts to "slap" against the liner. At the top of the stroke, the force on the piston reverses and shifts from thrust to anti-thrust orientation. Due to the large forces (both from inertia and from the connecting rod), the accelerations are very high. Therefore, providing a large clearance enables the piston to build up significant lateral momentum as it crosses from thrust side to antithrust side, and this momentum leads to larger forces against the oil film, which increase boundary contact friction. Consequently, if the clearance exceeds a critical value, the increase in slap pressures lead to increased net friction loss, as illustrated in Fig. 4.10. Therefore, the ideal skirt-liner clearance provides sufficient space for the oil but does not provide so much as to encourage piston slap (Fig. 4.11). For the Waukesha F18GL engine under the conditions of this study, the ideal clearance was 50 μm.

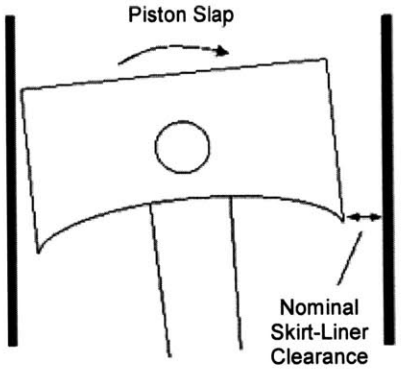

Figure 4.9: Schematic of piston and liner, showing skirt-liner clearance and piston slap

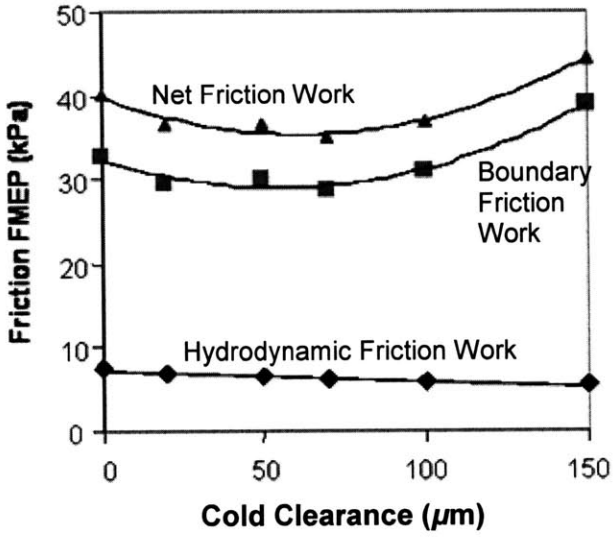

Figure 4.10: Friction work vs. cold clearance (oil film thickness: 20 μm)

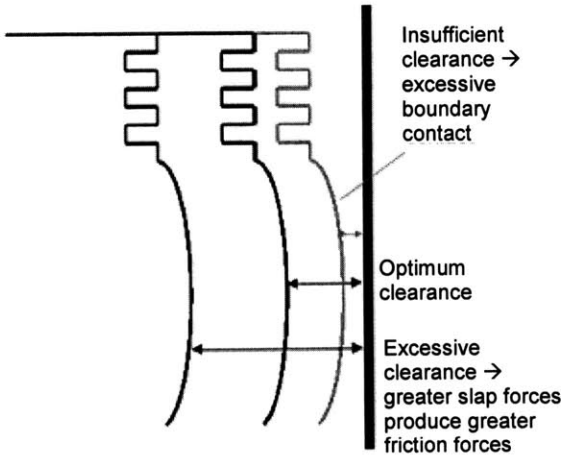

Figure 4.11: Interpretation of results: insufficient clearance produces excessive contact friction, while excessive clearance produces excessive slap

In this study, a constant skirt-liner clearance over the entire stroke was assumed, which is equivalent to treating the liner as having constant diameter. However, in an actual engine, there is a significant temperature gradient between the top and the bottom of the liner, which causes the liner to expand at the top more than at the bottom. Thus, the skirt-liner clearance is hardly constant and may vary substantially over the cycle. In order to reduce piston slap at the top of the liner and provide better guidance for the piston throughout the stroke, many engine designs use an interference fit; that is, the diameter of the cold piston is actually larger than the diameter of the cold liner. Under operational pressure, the piston deforms to provide a snug fit. Such a design minimizes piston slap while retaining sufficient film thickness to provide adequate hydrodynamic support.

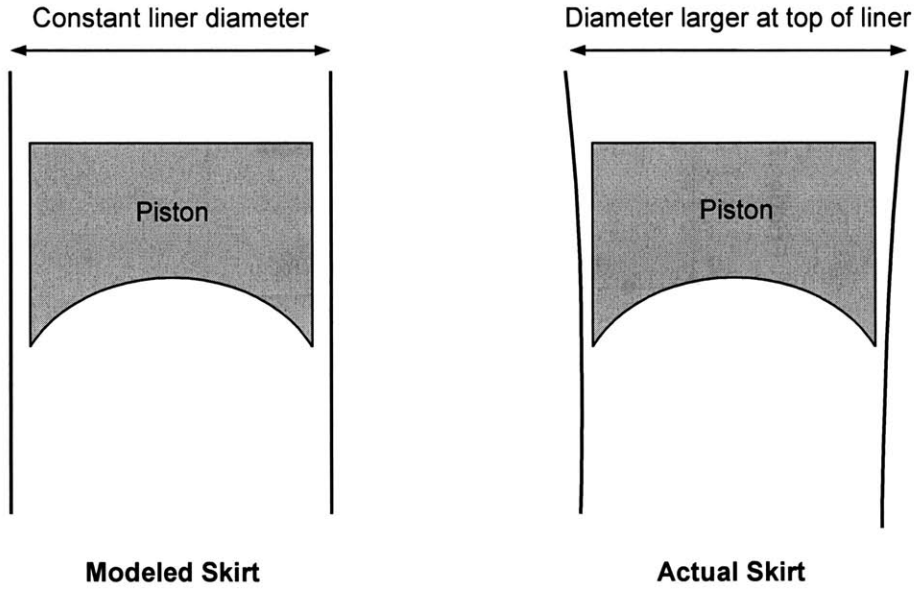

Figure 4.12: Comparison between modeled and actual skirt geometries

4.5 Impact of piston skirt profile on friction

The piston skirt profile has been studied in great depth with the goals of reducing wear, eliminating seizing, etc. This study, however, was concerned with how the piston profile affects friction. The objective for the profile is the same as for the other parameters, which is to maintain piston support in the ideal range on the Stribeck curve—i.e., to balance hydrodynamic and boundary lubrication so as to minimize friction.

In order to minimize friction, support must be concentrated in the hydrodynamic regime. The profile can be designed to promote hydrodynamic lubrication by maximizing the effective oil film thickness (assuming a constant oil supply) over as much of the skirt area as possible. This distributes the pressure as evenly as possible and enables the skirt to maximize the force supported hydrodynamically. Oil film thickness can be made nearly uniform by making the profile as flat as possible and making any changes in clearance as gradual as practical. However, merely designing a nearly-flat profile would be inadequate because the diameter of the hot piston increases more at the top than at the bottom due to temperature differences, thereby distorting the original profile. Moreover, the shape of the piston, particularly at the flexible lower edge, changes significantly as the piston deforms under load. Hence, the profile must be designed such that the hot, deformed skirt profile provides a nearly uniform film thickness.

In order to study a variety of cases, several polynomial shapes were selected to represent a variety of profiles. In Fig. 4.13, these polynomials are shown along with the baseline (Waukesha stock) profile. Each profile is defined by $f(x) = ax^n$, where $f(x)$ is the deviation of the profile from a cylindrical shape, x is vertical distance from the middle of the skirt, n is a nonnegative exponent, and a is a constant. Higher-order polynomials, such as x^8, produce relatively flat profiles over most of the area, and they drop off toward the endpoints. Lower-order polynomials have a sharper peak in the middle of the skirt. Since high-order polynomial shapes provide a flatter surface and more gradual changes in clearance, they would be expected to most effectively promote hydrodynamic lubrication, and this prediction is borne out by the model.

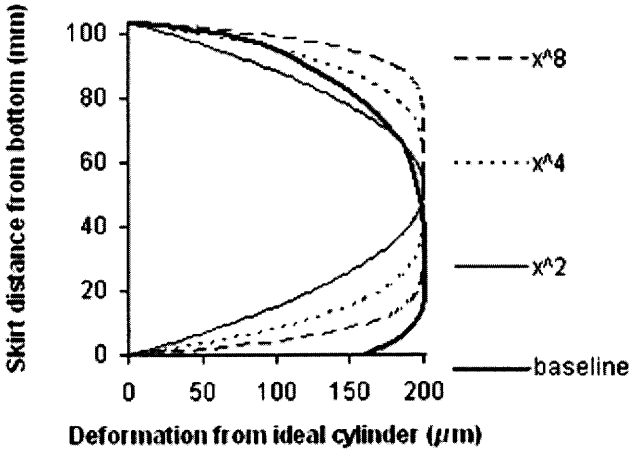

Figure 4.13: Schematic of various profiles

4.5.1 Profile vs. minimum film thickness, wetted area, and pressure distribution

The wetted areas for two profiles, one with sharp curvature and the other with shallow curvature, are illustrated in Fig. 4.14. A constant 50 μm-thick oil film is assumed in this analysis, and the contours show effective clearances between the piston and skirt on the thrust side at a crank angle of 410°. The flatter profile (i.e., higher-order polynomial, x^8) produces not only a larger wetted area but a more gradual progression from high to low clearances. In the profile with sharp curvature, the inadequate hydrodynamic support leads to boundary contact friction, shown as a small triangle in the center of the skirt. As shown in Fig. 4.21, this boundary contact friction dramatically increases friction work loss.

Since both profiles must support the same lateral force, the sharply-curved profile, which has less wetted area, has higher average pressure. More importantly, it has significantly higher peak pressure (Fig. 4.15), which leads to boundary contact. As pressure gradients are reduced by designing a flattened profile, the piston is more likely to remain in the hydrodynamic lubrication regime.

The wetted area decreases as the profile becomes more sharply curved, a trend illustrated for the entire stroke in Fig. 4.16. Since the sharply-curved profile can penetrate more deeply into the oil film, the minimum film thickness is expected to be smaller, and this is confirmed by the model in Fig. 4.17. Note that the sharp profiles drop below the 10 μm waviness value, triggering boundary contact, while the flatter (x^8) profile remains above it (i.e., in the hydrodynamic regime).

Note that the relationship between wetted area and minimum skirt-liner separation is different for piston profile shape as for oil film thickness. When profile shape is changed, wetted area and film thickness change together, but when viscosity is changed, wetted area and film thickness change in opposite directions. For example, when the profile is flattened, both wetted area and separation increase. However, when viscosity is increased, wetted area decreases while minimum separation increases. The difference can be explained phenomenologically. On the one hand, increasing oil viscosity increases the pressure that the oil can sustain, so the increased pressure can be offset by both a decrease in wetted area and an increase in oil film thickness. On the other

hand, making the profile more sharply curved does not change how much pressure the oil can support. Since less area is exposed to the oil, the piston must penetrate more deeply into the film in order to support the same lateral load.

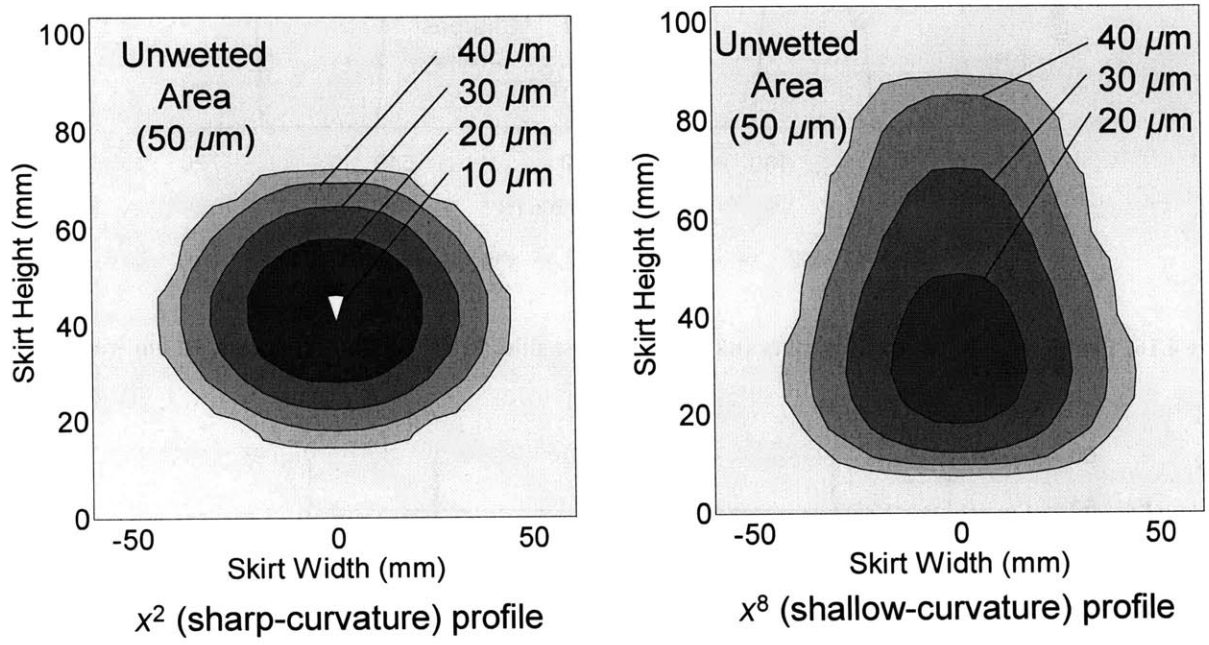

Figure 4.14: Comparison of wetted area for profiles with sharp and shallow curvatures

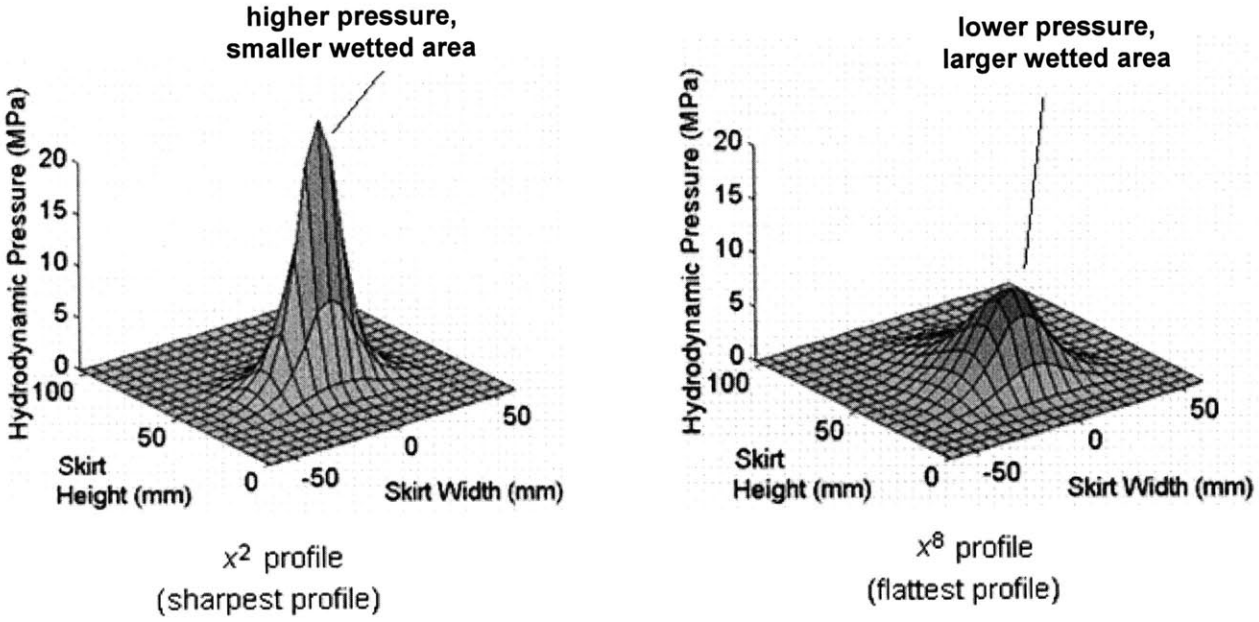

Figure 4.15: Comparison of pressure distributions for profiles with sharp and shallow curvatures

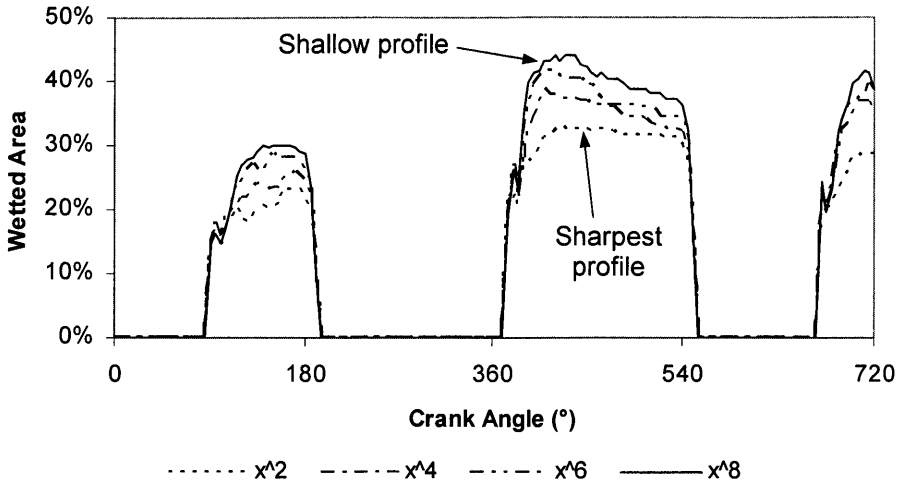

Figure 4.16: Profile vs. wetted area for all crank angles (thrust side, 50 μm oil film thickness, 10 μm waviness)

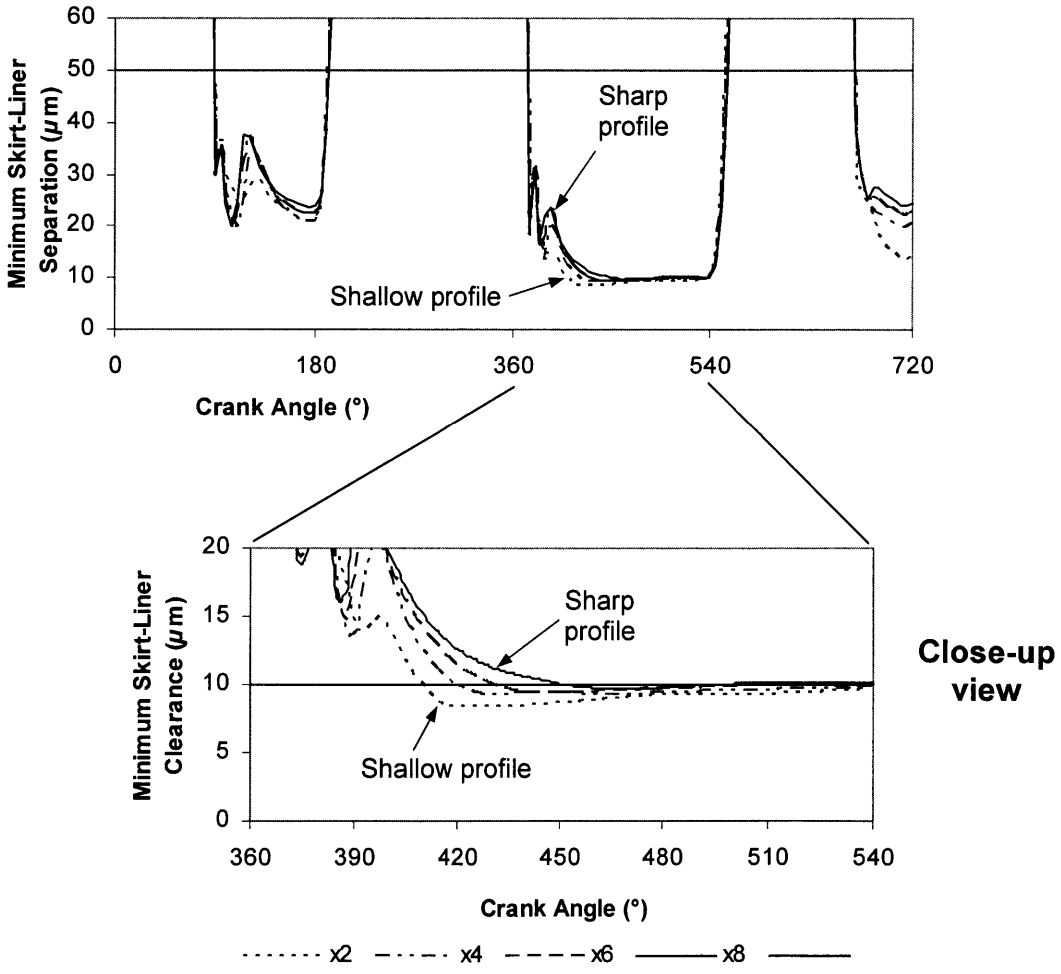

Figure 4.17: Profile vs. minimum separation (thrust side, 50 μm film thickness, 10 μm waviness)

4.5.2 Effect of piston profile design on friction

The results for friction as a function of skirt profile are summarized in Figures 4.18-21. As expected, the sharp piston profiles incur significantly higher boundary work loss because they more effectively penetrate through the oil film. Figure 4.18 illustrates this trend; note that in this case, boundary friction occurs only during the expansion stroke. For most of the stroke, all piston profiles are supported exclusively hydrodynamically, and the only time any boundary friction occurs is during the expansion stroke, when in-cylinder, connecting rod, and skirt pressures are at their peaks. The high lateral pressure corresponds to a high σ (force per unit area) term in the Stribeck curve (Fig. 4.3), which predicted that an increase in σ would shift support toward the left on the curve (i.e., toward boundary lubrication). The boundary friction work is integrated over the cycle to produce Fig. 4.19, which shows a sharp onset of boundary contact during the expansion stroke.

As the profile is flattened, one would expect the hydrodynamic work loss to increase marginally because the wetted area increases, causing hydrodynamic drag to rise. The model output confirms this; Fig. 4.20 shows cycle-integrated hydrodynamic friction increasing as profiles are flattened. Flattening the profile causes hydrodynamic friction to rise marginally, but it drastically reduces boundary friction. Since boundary friction dominates net friction loss, and since boundary contact increases wear, the priority is to shift lubrication toward the hydrodynamic regime. The model suggests that the x^8 (flattest) profile is the best for this purpose. More sophisticated adjustments to the profile shape can be studied on a case-by-case basis; it is hard to generalize because such changes are highly sensitive to the rigidity and geometrical characteristics of each specific piston.

Finally, the results are summarized for baseline SAE-40 oil in Figure 4.21. As the profile becomes more flat, net friction decreases because of drastic reductions in boundary friction. However, if the profile were flattened beyond x^8, the net friction would increase because boundary friction work had already been decreased to a negligible amount, and hydrodynamic friction would increase because of the greater wetted area. Selecting a different oil would modify the lubrication characteristics; see Section 4.5.3 for more details.

One important facet of profile design is that the profile is not constant throughout the cycle. Instead, it deforms in response to pressure and temperature gradients, and piston rotation can change the effective shape. If the piston is designed under the assumption that significant boundary friction will be present (e.g., if it is assumed that the x^2 profile in Fig. 4.21 is representative), it would be advisable to optimize the profile for the first part of the expansion stroke (around 400°, according to Fig. 4.18), since this is the region in which most of the friction loss develops. On the other hand, if the piston is designed to operate primarily in the hydrodynamic regime, work loss is distributed throughout the cycle, and any improvements to the profile must be balanced over the cycle. The latter case is more likely in most practical designs, in which the goal is to avoid boundary lubrication as much as practicable.

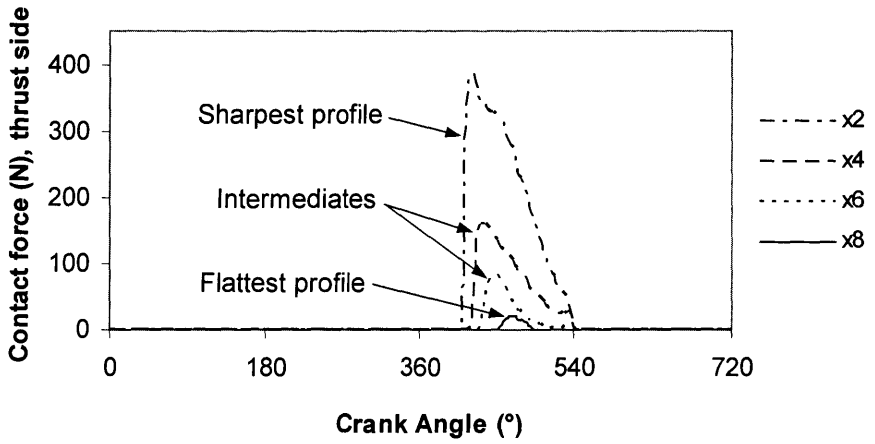

Figure 4.18: Force supported by contact friction (thrust side, 50 μm oil film thickness, 10 μm waviness)

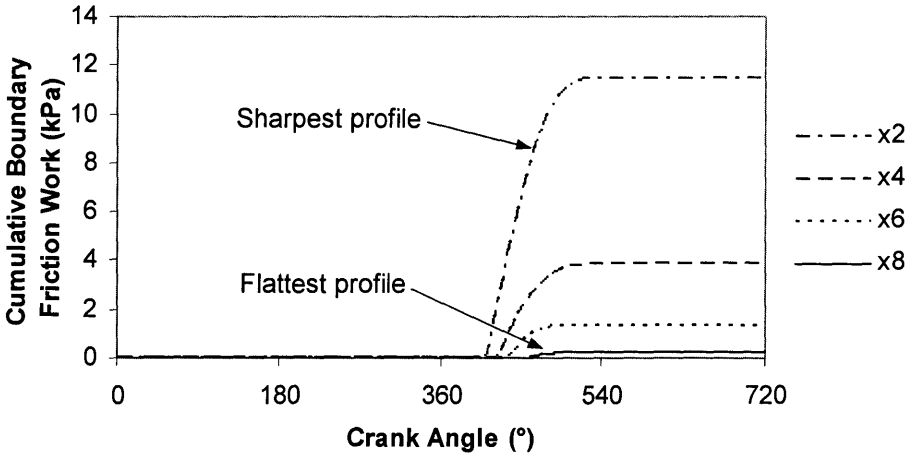

Figure 4.19: Cumulative contact friction work (thrust side, 50 μm oil film thickness, 10 μm waviness)

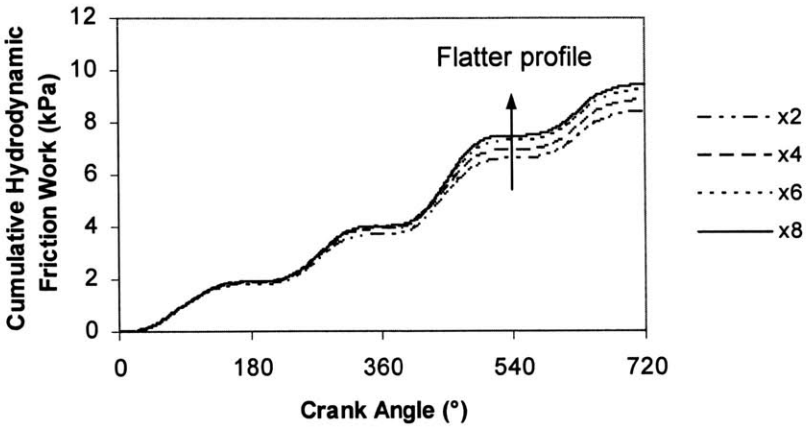

Figure 4.20: Cumulative hydrodynamic friction work (thrust side, 50 μm oil film thickness, 10 μm waviness)

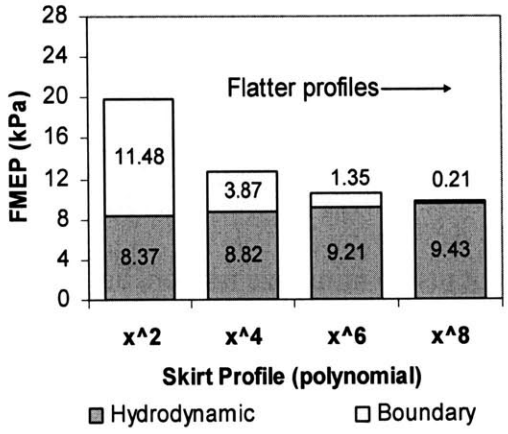

Figure 4.21: Profile vs. net friction work (SAE-40 oil, thrust side, 50 μm oil film thickness, 10 μm waviness)

4.5.3 Relationship between piston profile and viscosity

The profile shape cannot be considered adequately without reference to viscosity. A profile that is optimized for one lubricant may be a poor choice for a different one. In Figure 4.22, the same profiles are tested with two straight-weight lubricants. The low-viscosity oil (SAE-20) produces high friction in all cases because the piston can easily push the oil film aside and enter boundary lubrication. The high-viscosity lubricant (SAE-50), on the other hand, reaches a minimum net friction value at an intermediate profile curvature value (x^6) because the lubricant supports the piston so effectively. In the latter case, the best approach would be to reduce viscosity to reduce net friction, since it is not at risk of boundary lubrication (see Section 4.2 for more details).

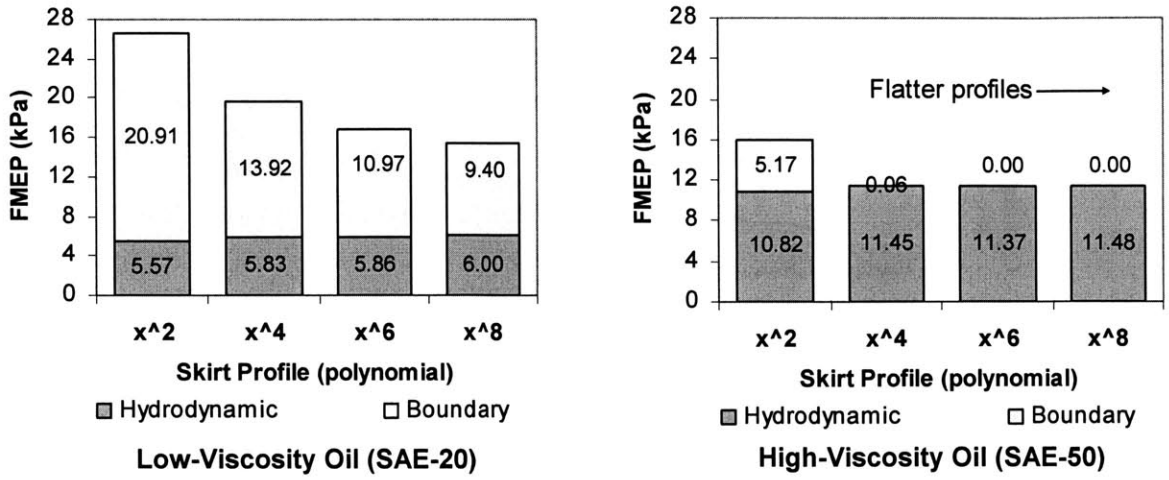

Figure 4.22: Profile vs. net friction work for two different lubricant viscosities (thrust side, 50 μm oil film thickness, 10 μm waviness)

4.6 Piston ovality

The piston profile is designed not just to minimize friction, but also to minimize wear, reduce seizing, enhance guidance, etc. Piston ovality is essentially a piston profile oriented in the horizontal direction, and it fulfills several of the same purposes as the profile. As with the profile, this analysis of ovality focuses on its effect on friction. Figure 4.23 illustrates a cross-section of the piston/skirt system, emphasizing ovality.

When the engine is in operation, the piston skirt deforms in response to pressures stemming from lateral force on the connecting rod and inertial forces. Just as smooth, flattened profiles distribute pressure more evenly and thereby promote hydrodynamic friction, pistons with less ovality have the potential to reduce friction by conforming more closely to the liner. However, the same caveat regarding the profile applies to ovality: the system must be evaluated *after* the piston has been deformed by operational temperature and lateral pressure. The piston model used for this study included both thermal and pressure deformation effects.

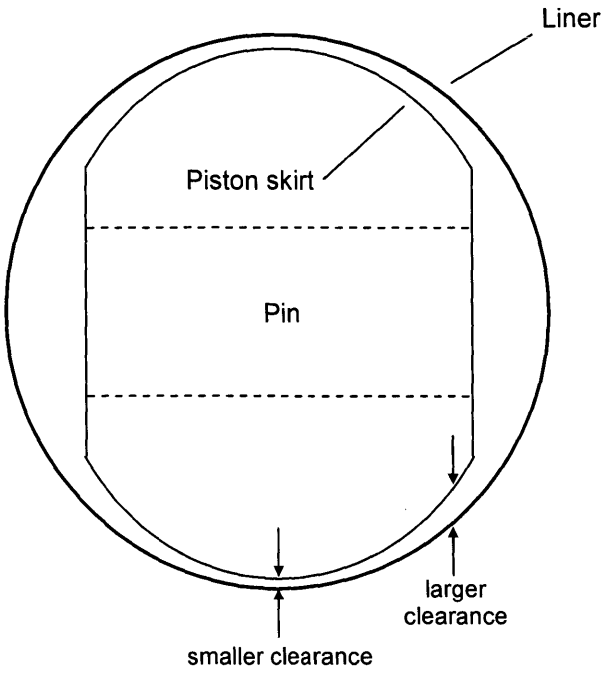

Figure 4.23: Diagram of piston skirt in the liner, showing ovality

4.6.1 Effect of ovality on friction

Ovality is analogous to profile shape because both modify the effective clearance between the piston and liner. The objective of both is to facilitate a relatively flat oil film with gradual gradients in order distribute the lateral force over as large an area as possible. This promotes hydrodynamic lubrication and reduces wear. The ovality is to be adjusted so that it closely matches the shape of the liner, particularly at points in the cycle when the lateral force is high. (A comprehensive model of the engine would include deformation of each component in the power cylinder, including the liner, connecting rod, and pin, but such a model is extremely complex and requires intensive computation for even simple comparisons. The model exercised in this study included only deformation of the piston. However, the principle of piston-liner conformity applies in both types of models.)

Since reducing the ovality (i.e., making the piston more round) enables it to better conform to the liner surface, it is predicted that reducing ovality will also reduce friction. However, it is important to not completely eliminate ovality (i.e., make a perfectly circular piston). The lateral

pressure is highest along the thrust and anti-thrust lines, so these areas will deform the most. A perfectly round piston will thus deform preferentially along the thrust and anti-thrust lines, leading to "negative ovality," or a concave shape that shifts pressure away from the thrust/anti-thrust lines. This could cause instabilities and produce undesirable high-pressure patches.

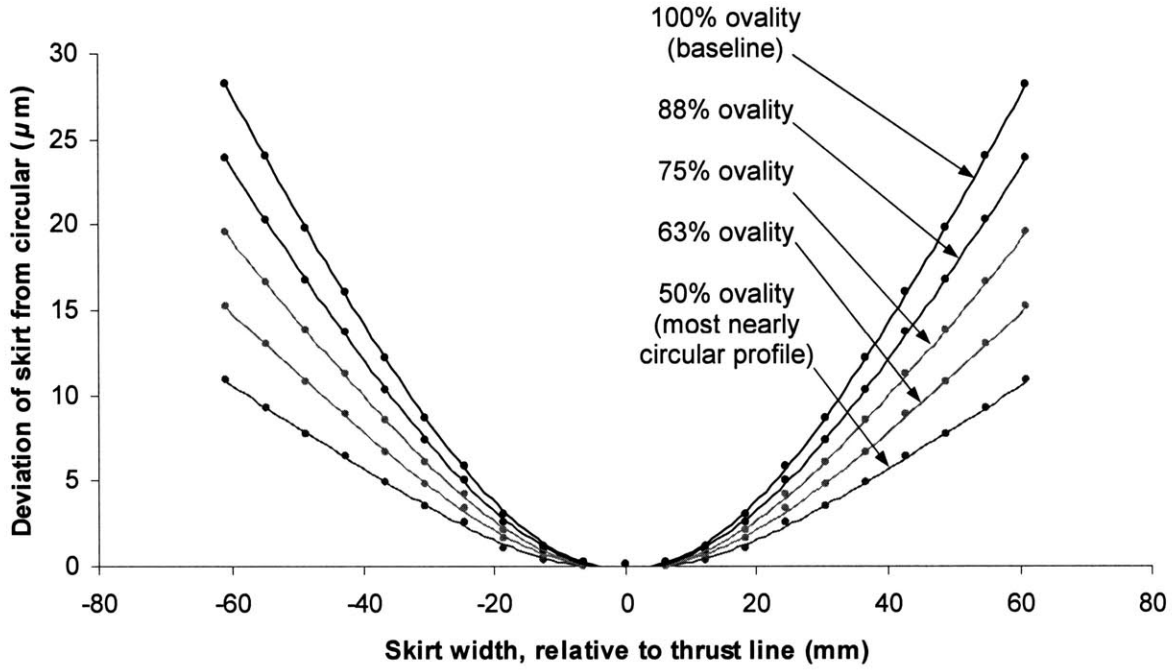

Figure 4.24: Cross-sectional view of piston, showing ovality. The baseline (100%) ovality was reduced to produce a more circular shape that conforms more closely to the liner surface (the *x*-axis in the figure).

In order to study the effect of ovality on friction, the baseline ovality was reduced by various proportions, as shown in Figure 4.24. Reducing ovality is equivalent to making the piston more circular, thereby causing it to conform more closely to the liner. Pistons with several relative ovality values were tested, and their effects on friction are shown in Figures 4.25-27. The model results confirm the prediction that reducing ovality dramatically reduces contact friction (it is eliminated entirely for 63% and 50% ovality pistons), thereby reducing net friction as well.

Since ovality can be adjusted independently of the piston profile, the two parameters can be jointly optimized to achieve ideal results. The profile is difficult to optimize because the piston rotates during the stroke—especially near the top-dead center—effectively changing the profile.

The ovality does not change as much, however, since the piston does not rotate significantly about the thrust/anti-thrust axis. Therefore, in principle, the ovality can be optimized more precisely than the profile. Ideally, the two can be jointly optimized to minimize boundary contact friction while also achieving other objectives, such as smooth guidance throughout the stroke. Joint optimization requires specific, detailed information about the system in question.

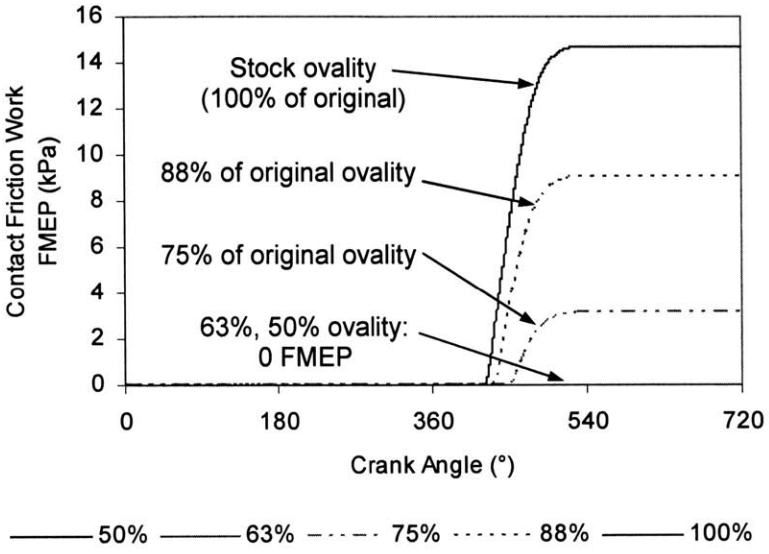

Figure 4.25: Cumulative contact friction work vs. ovality (thrust side, 100 μm oil film thickness, 20 μm waviness). Profiles that are more circular (i.e., have lower ovality) have lower contact friction work loss.

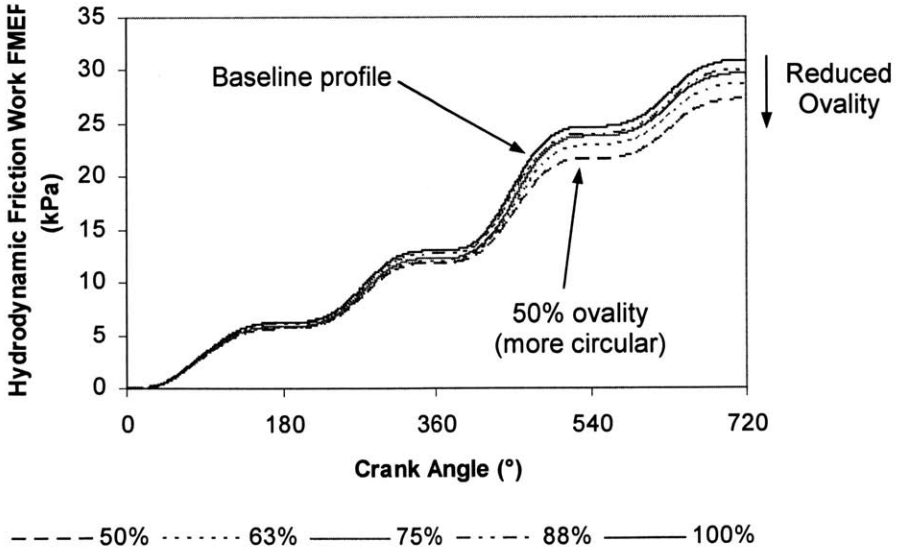

Figure 4.26: Cumulative hydrodynamic friction work vs. ovality (thrust side, 100 μm film thickness, 20 μm waviness). Reducing ovality slightly decreases hydrodynamic friction loss.

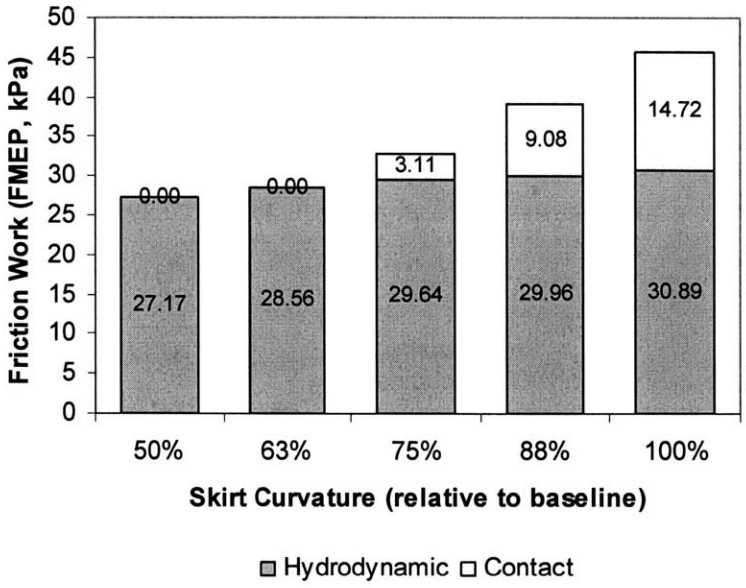

Figure 4.27: Ovality vs. net friction work (SAE-40 oil, thrust side, 100 μm oil film thickness, 20 μm waviness)

4.6.2 Comparison of efficiency of piston ovality changes

If hydrodynamic friction were not limited in the pressure it could support, the most efficient design would support the entire load on the thrust and anti-thrust lines. Figure 4.28 illustrates that if a lateral force—i.e., a force oriented along the thrust/anti-thrust line—is supported at a point offset from that line, a greater normal force must be exerted at the interface. Supporting lateral force at an off-center location requires greater normal force to produce equivalent resistance in the thrust/anti-thrust direction. Moreover, since friction is a function of normal force, supporting the lateral load on off-center locations produces greater friction work loss than centering the pressure along the thrust/anti-thrust line.

A piston with significant ovality will concentrate the force in a high-pressure region on the thrust and anti-thrust lines. However, as Figure 4.25 indicates, this enables the piston to push oil aside and enter the boundary lubrication regime. The modest gain in efficiency by focusing all force on the thrust line is overwhelmed by the drastic increase in contact friction that results from the excessive pressure. In order to minimize net friction, the ovality should be decreased to the point that boundary friction is not significant; even though this spreads pressure to the less-efficient

off-center locations, the reduction in boundary friction more than compensates for this penalty. After the boundary friction is reduced substantially, the ovality should not be reduced further, both to concentrate the pressure near the thrust/anti-thrust lines and to minimize wetted area (and hydrodynamic drag). Minimizing boundary and hydrodynamic friction in this way will enable the piston to operate in the minimum-friction regime on the Stribeck curve.

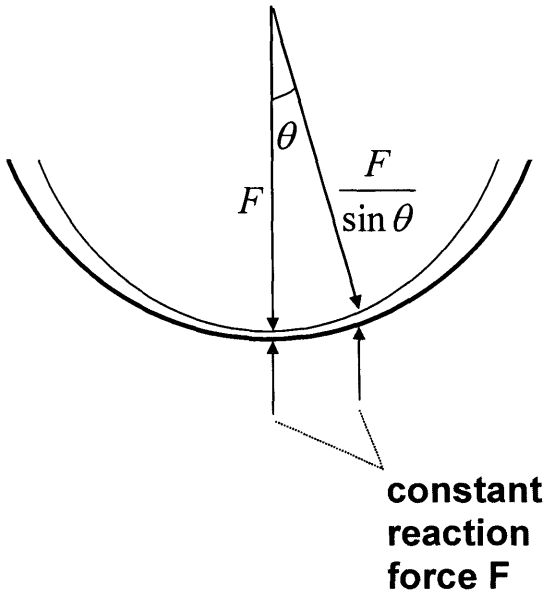

Figure 4.28: Schematic of piston, illustrating how the normal force on an off-center section of the skirt must be greater than the normal force on the thrust/anti-thrust line in order to sustain a constant reaction force

4.7 Piston skirt size

The size of the piston skirt is an important parameter in piston design. For example, a steel piston requires a dramatically different design than an aluminum piston because steel is a much denser material. Steel offers a stiffer structure that can handle much higher in-cylinder pressures, but if it is not designed carefully to reduce weight, it will require much larger connecting rods and other supporting structure, which could nullify any potential advantages. In a typical steel piston design, much of the material is removed, especially in low-stress areas like the periphery of the piston skirt. Figure 4.29 illustrates the difference in skirt size by comparing aluminum and steel pistons from MAHLE that were both designed for heavy-duty engines.

In order to gain a sense of the effect of skirt size on the friction, the baseline Waukesha F18GL piston skirt was scaled by various factors, down to 76% of the original, as shown in Figure 4.30. (Obviously, it is simplistic to change the skirt size without modifying the profile, stiffness, or other characteristics, but this parametric study considered skirt size in isolation.) The effect of skirt size on friction can be understood by observing that smaller skirts must distribute the lateral load over a smaller area (i.e., have higher average and peak pressures), so they tend to have more boundary lubrication and less hydrodynamic lubrication. Indeed, Fig. 4.31 illustrates the dramatic increase in boundary friction as the skirt size is reduced. There is a slight decrease in hydrodynamic lubrication as the skirt gets smaller (Fig. 4.32). Figure 4.33 summarizes the results; for this specific design, it seems to be best to make this skirt as large as possible.

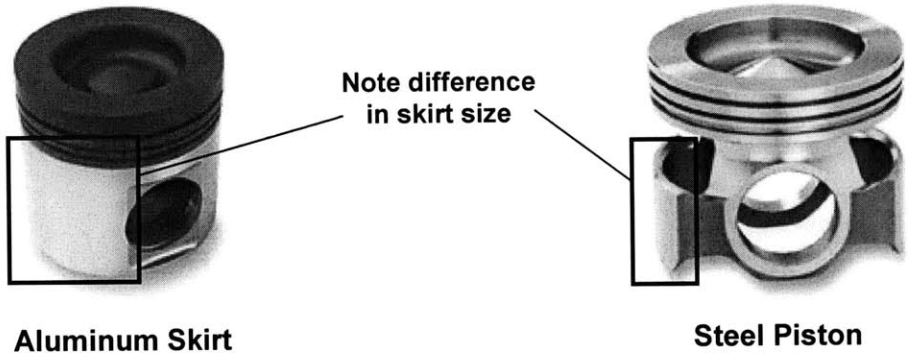

Figure 4.29: Comparison of aluminum and steel piston designs. MAHLE FERROTHERM® piston (aluminum skirt, steel crown) on left; MAHLE MONOTHERM® (all-steel) at right; both designed for heavy-duty engines

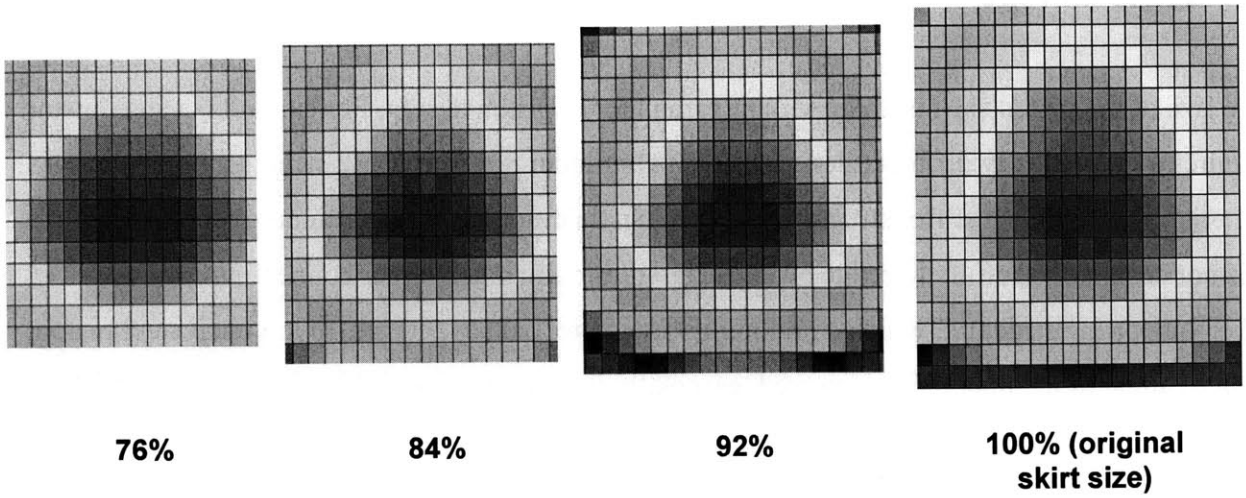

Figure 4.30: Schematic of skirts used in skirt size comparison

In actual piston designs, the tendency of smaller skirts to operate in the boundary lubrication regime can be offset by other design changes. For instance, the ovality can be adjusted to spread the load horizontally. Also, the profile can be adjusted to spread as much pressure in the center region as possible. As seen in Figure 4.15, most of the pressure is borne in the center of the skirt. Since the steel MONOTHERM® piston (shown in Figure 4.29) spreads the load horizontally across its width, it does not incur significant friction disadvantages by reducing skirt height.

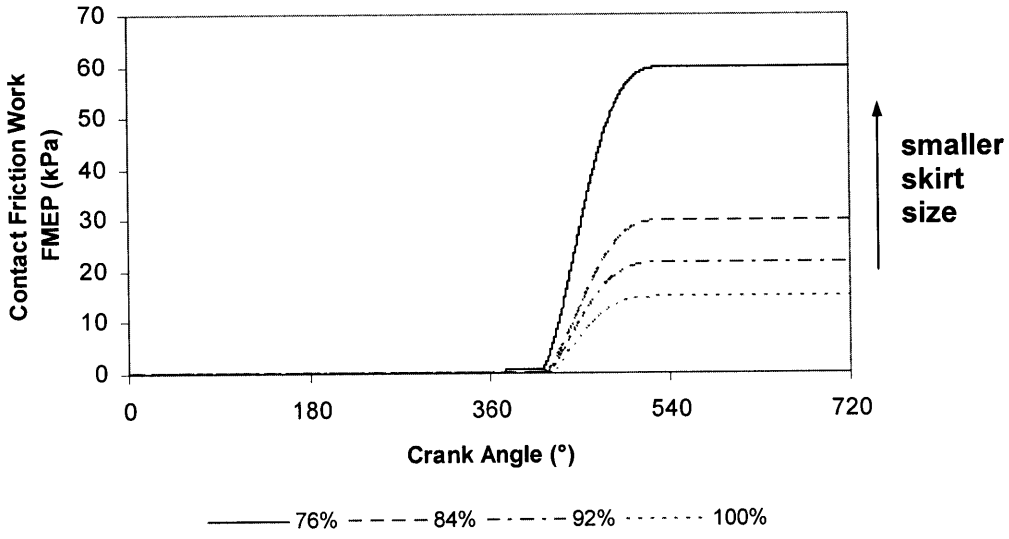

Figure 4.31: Cumulative contact friction work (thrust side, 100 μm oil film thickness, 20 μm waviness)

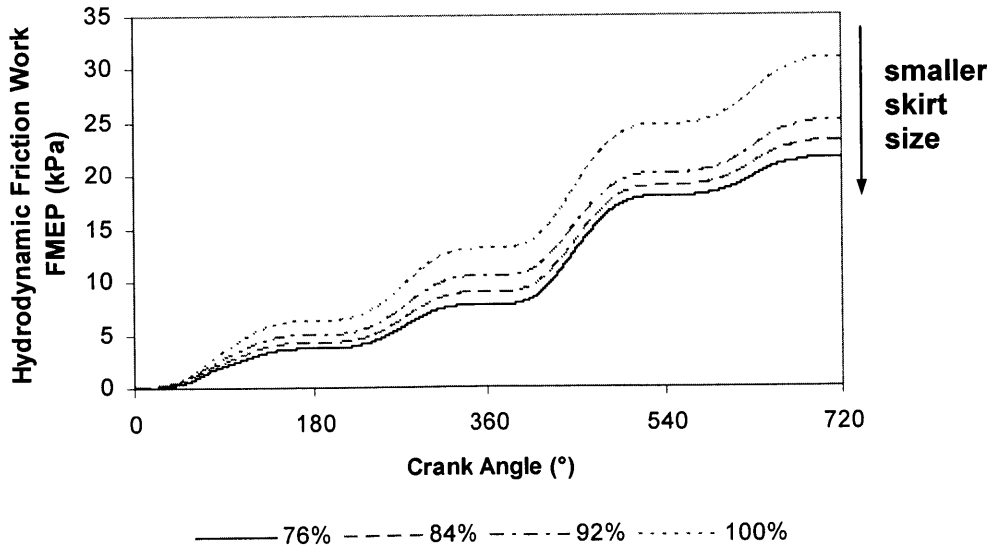

Figure 4.32: Cumulative hydrodynamic friction work (thrust side, 100 μm film thickness, 20 μm waviness)

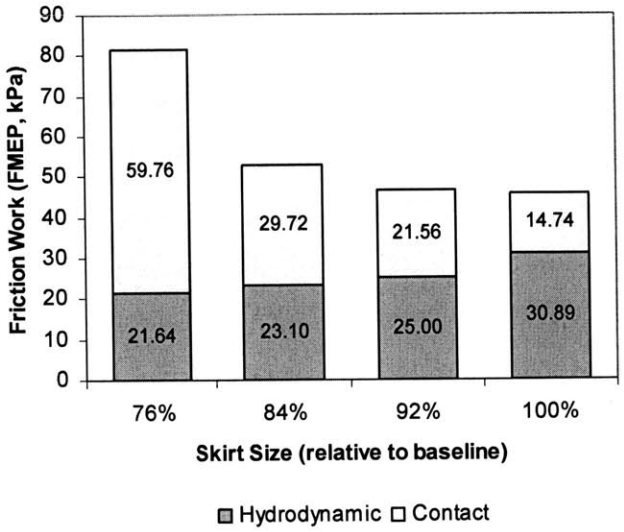

Figure 4.33: Skirt size vs. friction work (SAE-40 oil, thrust side, 100 μm oil film thickness, 20 μm waviness)

4.8 Skirt surface waviness

Pistons typically have a waviness pattern machined into them. The waviness marks enhance hydrodynamic lubrication by serving as oil reservoirs; the surface tension keeps oil in the valleys between the wave peaks even when the bulk oil supply is negligible, and when the piston is under pressure, the oil in the valleys serves as an alternate oil supply. Moreover, the grooves between the peaks help prevent seizing by providing a flow path for oil and preventing a vacuum from developing between the skirt and liner surfaces. However, if the waviness pattern is too pronounced, the peaks will serve the same function as a sharp profile (described in Section 4.5). In effect, the peaks will push the oil film aside and contact the liner surface directly, leading to boundary lubrication. Therefore, it is expected that excessive waviness will be highly detrimental to friction, but that a moderate amount of waviness will provide oil retention and guidance without significant friction losses.

The analytical piston model was exercised to determine the effect of waviness height on friction. In this model, a simple sawtooth pattern was used, as shown in Figure 4.34. However, actual pistons are machined in various ways, leading to sinusoidal or other shapes (e.g., Fig. 4.37). Moreover, the peaks of the waviness pattern, regardless of their original shape, tend to get

sheared off during operation, leading to a "negatively skewed" condition; i.e., the average depth of the valleys is greater in magnitude than the average height of the peaks.

The liner also affects oil flow and retention. In typical large natural-gas engines, liners have a honing pattern that serves much the same purpose as the waviness pattern on the piston: the grooves retain oil by surface tension and serve as an alternate supply, and they also provide flow paths for oil. Unlike the piston, in which grooves are machined circumferentially, the grooves in the liner are often oriented at an angle relative to the horizontal. The honing angle, as it is called, has a modest impact on friction, as studied by Jocsak[22]; it is found that shallow honing angles (relative to the horizontal) encourage oil to flow laterally rather than move up or down the liner, which would be undesirable. Due to limitations on complexity of this model, the liner surface was assumed to be smooth. (In addition, the flow factor approximation of surface effects on hydrodynamic lubrication, summarized in Section 3.4, requires that one of the two interacting surfaces be smooth.) Since the lubrication principles for the ring (studied by Jocsak) apply also to the piston, it is reasonable to assume that shallow honing angles would minimize friction for both.

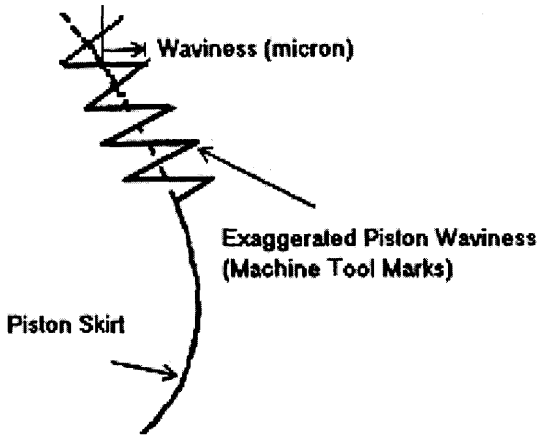

Figure 4.34: Schematic of waviness marks in piston skirt

4.8.1 Waviness vs. friction

If the peaks on the skirt surface can penetrate easily through the oil film to the skirt surface, they will build up contact pressure, thwarting hydrodynamic lubrication. The effects of waviness

height on friction, as calculated by the model, confirm this prediction; as waviness increases past a certain critical value, friction increases dramatically. Figure 4.35 shows that as the waviness increases beyond 5 microns, friction increases rapidly. This data suggests that it would be inadvisable to use a waviness amplitude of more than 10 microns in the Waukesha piston with the given oil film thickness and skirt-liner clearance.

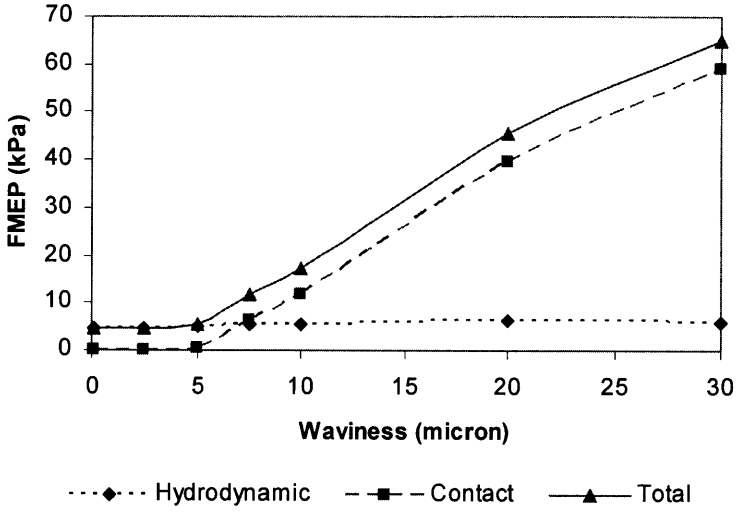

Figure 4.35: Friction vs. waviness for standard Waukesha piston (skirt-liner clearance: 20 micron, oil film thickness: 50 micron; baseline profile and ovality)

4.8.2 Waviness vs. roughness

Surface roughness refers to the natural deviations of an actual surface from a geometrically smooth shape. Any metal shape has natural surface roughness that is related to the method of manufacture, degree of polishing, and other factors. In a ring surface, surface roughness plays an important role because it serves much the same purpose as waviness on a piston surface: the valleys serves as oil reservoirs, and the gaps between the peaks provide flow paths for oil. In a piston, however, the waviness amplitude is greater than the roughness amplitude, often by an order of magnitude. The difference between roughness and waviness in the model is illustrated in Figure. 4.36. Thus, although roughness would be expected to play an important role in a piston with a nominally smooth (un-honed) surface, roughness only slightly modifies the effective amplitude of the waviness peaks in typical pistons. Therefore, roughness amplitude is expected to have a negligible effect on friction.

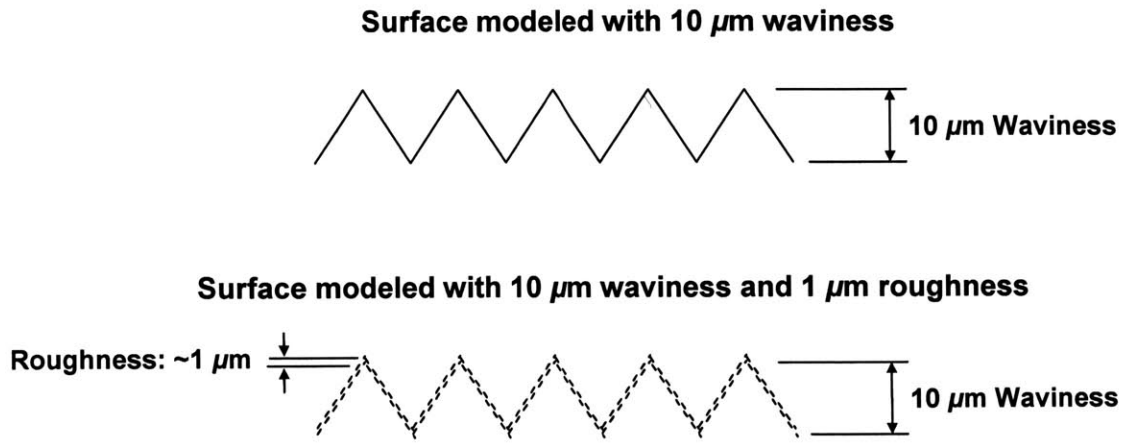

Figure 4.36: Schematic of surface waviness with and without roughness

Tests were conducted to evaluate the effect of roughness on friction, but they showed a negligible effect, as expected. In the model, surface waviness was on the order of 10 microns, while surface roughness was on the order of only one micron, which are typical values for large natural-gas engines. The model, which assumed a sawtooth pattern for waviness, confirmed that changes in roughness had little impact on net friction.

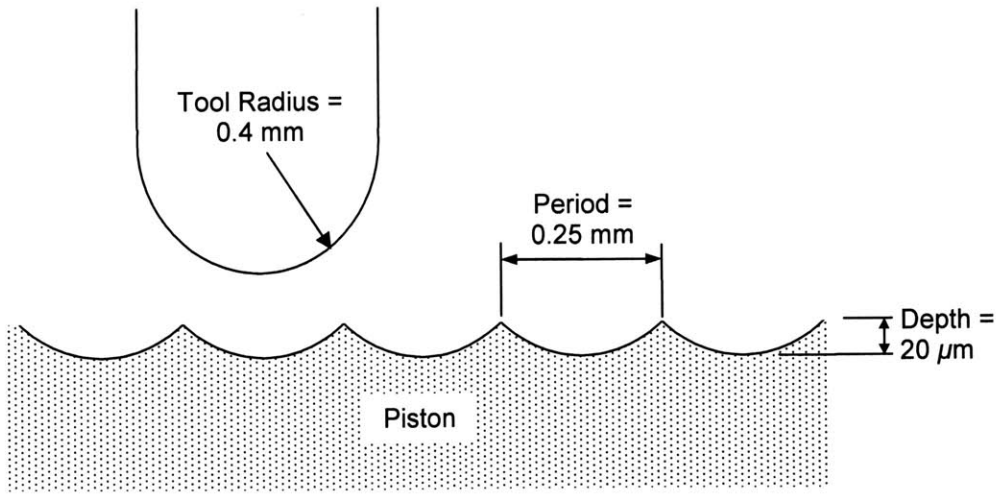

Figure 4.37: Waviness patterns, showing unworn (new) pattern at top and worn profile below

In an actual Waukesha engine, a tool with a circular profile was used to etch the waviness patterns in the piston profile (specification illustrated in Fig. 4.37). The initial waviness was 20 μm, and the pattern closely approximated the sawtooth pattern assumed in the model. However, it is known that normal wear on the skirt shears off the peaks of the waviness marks, roughly halving wave height and producing a worn profile in which much of the exposed surface is smooth (Figure 4.38). Therefore, it is possible that the characteristic roughness of the metal could significantly affect friction. It is very difficult to model a surface with both undulations and flat areas (Figure 4.38b) because such a surface resists accurate stochastic characterization, which is needed for the present model.

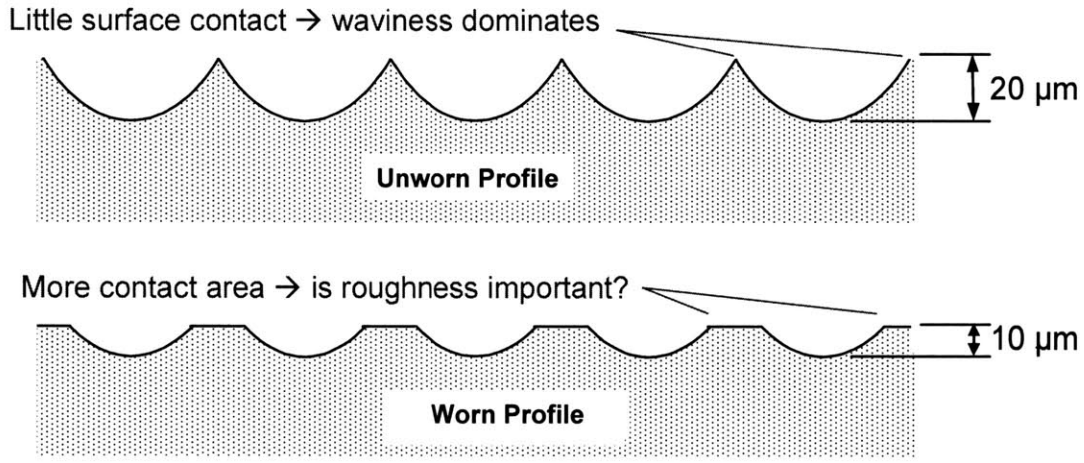

Figure 4.38: Waviness patterns, showing unworn (new) pattern at top and worn profile below

4.8.3 Other effects of waviness

The present model cannot fully characterize the effects of waviness because it does not include such factors as vacuum pressure between the skirt and liner. If the skirt and liner are very smooth, it is possible for them to form a tight seal, which would inhibit motion (slapping motion or normal vertical movement). This could result in seizing. Hence, even though smaller waviness amplitude may reduce friction, any further reductions in height must be approached with caution.

Another important phenomenon related to waviness is surface tension in the oil. A surface with significant waviness can store oil on its greater surface area, and it can retain more oil in its

crevices. When the piston moves to areas with poor oil supply (e.g., when a nearly-dry piston scrapes over a nearly-dry liner surface near top-dead center on the upstroke), the oil in the gaps provides a cushion for the piston. Hence, although reducing waviness height may shift lubrication toward the hydrodynamic regime, it may have the unintended consequence of reducing oil supply, which could have a greater adverse effect.

4.9 Summary of changes

Each of the parameters studied above has the potential to affect friction, but they offer varying benefits. Figure 4.39 provides a rough comparison of each effect, assuming everything else remains constant. Obviously, the improvements are not additive; for example, if the waviness is excessive, profile curvature will no longer have much of an effect on friction. In order to reduce friction, the piston should be designed to provide a relatively even skirt-liner clearance in order to enhance hydrodynamic lubrication and avoid boundary lubrication. This can be achieved by using a relatively flat profile, adjusting piston ovality to match the liner shape, and reducing waviness peaks so they do not contact each other. Moreover, selecting the lubricant such that the viscosity is high enough to provide adequate hydrodynamic support, but not so high that is induces excessive drag, is also crucial to controlling friction. A key takeaway from this study is that the piston-liner system is highly-integrated, and changing one variable affects many other parameters.

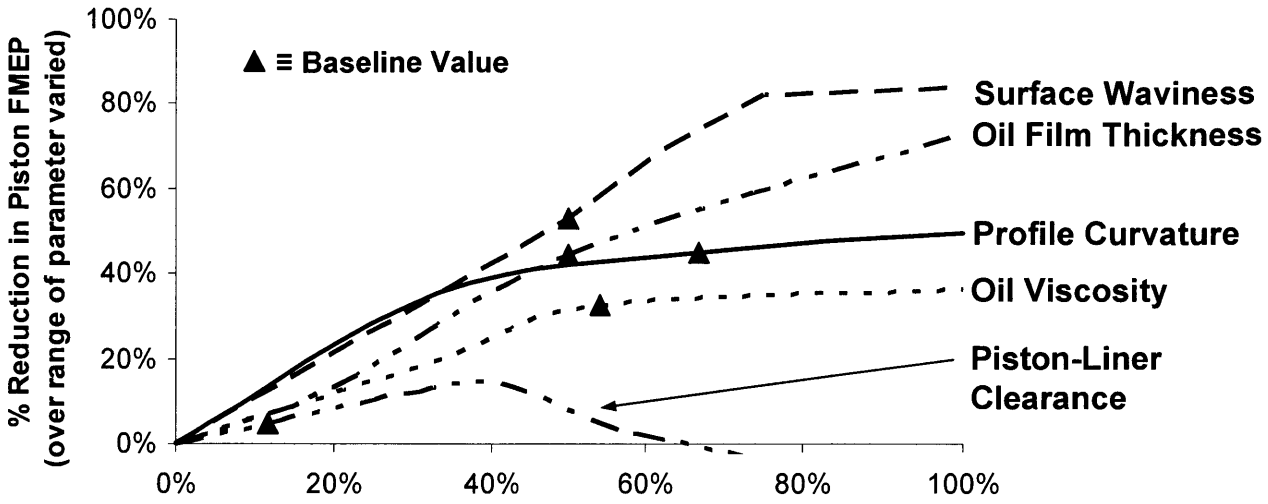

End of Range (0%)	% Change in Parameter	End of Range (100%)
20 μm	Surface Waviness	0.1 μm
0 μm	Oil Film Thickness	100 μm
x^2	Profile Curvature	Flattest (x^6)
0 μm	Piston-Liner Clearance	150 μm
8.1 cSt	Oil Viscosity (100° C)	20.4 cSt

Figure 4.39: Comparison of effects of various piston design parameters on friction; baseline values reflect parameters selected for the default engine

5 Deterministic Algorithm

A significant drawback of the numerical model of the piston is that it takes a substantial amount of time to compute the Reynold's equation and stiffness matrix, both of which involve solutions of linear algebraic systems. As summarized in Section 3.5, the algorithm must solve the Reynold's equation via matrix reduction assuming a rigid skirt, determine the deformation characteristics via the stiffness matrix, adjust the oil film thickness values in the Reynold's equation, and then solve again. This iterative process must continue until the pressure and film thickness values converge on a common solution.

Would it be possible to combine the stiffness matrix and Reynold's equation into a combined algebraic system, which could then be solved directly? Although this linear system would be larger than either of its constituents, it would avoid the iteration process and potentially yield substantial gains in numerical efficiency. This section explores a proposed algorithm that would provide a deterministic (i.e., non-iterative) solution.

5.1 Background

5.1.1 Reynold's equation

Hydrodynamic lubrication in a thin-film situation is described by the Reynold's equation, which was described in Section 2.1 and derived in detail in Appendix A. The Reynold's equation is a nonlinear second-order differential equation, and it is shown in Eq. 5.1 in simplified form. This is called the "1-D Reynold's equation" because it varies spatially only in the x direction.

$$\frac{\partial}{\partial x}\left(h^3 \frac{\partial p}{\partial x}\right) = -6\mu U \frac{\partial h}{\partial x} + 12\mu \frac{\partial h}{\partial t} \qquad \text{Eq. 5.1}$$

where:

- $x \equiv$ independent distance variable (an additional variable y is used in 2-D Reynold's equation)
- $h \equiv$ clearance height (a function of x)

- $p \equiv$ pressure (a function of x)
- $\mu \equiv$ oil viscosity (treated as a constant)
- $U \equiv$ relative speed between contacting surfaces (constant for each crank angle at given RPM)
- $t \equiv$ independent time variable

5.1.2 Rigid-Skirt Solution

Since μ and U are treated as constants, only two dependent variables, p and h, remain (ignoring the time-dependent term for the present). Unfortunately, since p and h comprise factors of a product in the Reynold's equation, they cannot be treated independently because they are nonlinearly dependent terms. To circumvent this issue, the skirt and liner can be assumed to be rigid, which makes the h (oil film thickness) terms constant (Fig. 1). Since h is constant, the Reynold's equation can be solved easily for the pressure map p by expressing it as a second-difference discreetization and solving it via linear algebra. The process is outlined below.

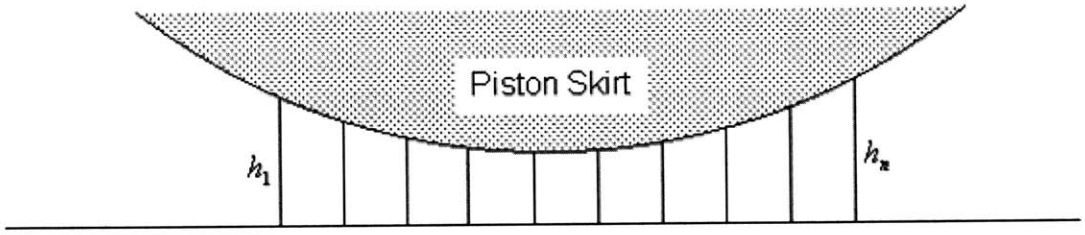

Figure 5.1: Schematic of the 1-D piston skirt and cylinder liner; the clearance heights are shown as h_1-h_n

The Reynold's equation (1-D form shown in Eq. 5.2) can be expressed as a second-difference equation according to the process described in Section 3.2.2 and illustrated in Figure 5.2. The second-difference approximation to the second-derivative is shown in Eq. 5.3.

$$\frac{\partial}{\partial x}\left(h^3 \frac{\partial p}{\partial x}\right) = -6\mu U \frac{\partial h}{\partial x} + 12\mu \frac{\partial h}{\partial t} \qquad \text{Eq. 5.2}$$

$$\frac{\partial}{\partial x}\left(h^3 \frac{\partial p}{\partial x}\right) \approx \frac{\left(h^3_{i+1/2} \frac{p_{i+1} - p_i}{\Delta x}\right) - \left(h^3_{i-1/2} \frac{p_i - p_{i-1}}{\Delta x}\right)}{\Delta x} = \frac{h^3_{i+1/2} p_{i+1} - \left(h^3_{i+1/2} + h^3_{i-1/2}\right) p_i + h^3_{i-1/2} p_{i-1}}{(\Delta x)^2} \qquad \text{Eq. 5.3}$$

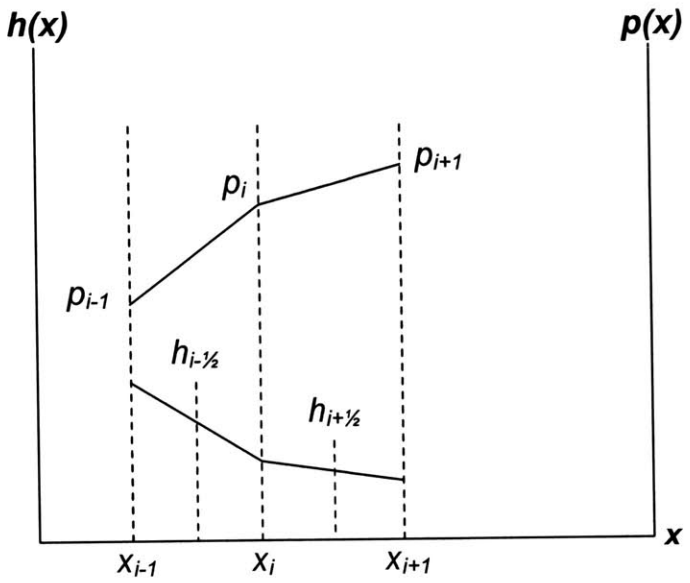

Figure 5.2: Illustration of second-difference approximation for a second derivative

As described previously, the centered $h_{i+½}$ and $h_{i-½}$ terms can be expressed in terms of their neighbors, h_{i-1}, h_i, and h_{i+1}, which are located at actual node points. The process, shown below, produces the overall equation Eq. 5.4.

$$\frac{h_{i+1/2}^3 p_{i+1} - \left(h_{i+1/2}^3 + h_{i-1/2}^3\right) p_i + h_{i-1/2}^3 p_{i-1}}{(\Delta x)^2} = -6\mu U \frac{h_{i+1} - h_{i-1}}{2\Delta x} + 12\mu \frac{h_i - h_i(t = t_{j-1})}{\Delta t} \longrightarrow$$

Second Difference — Centered Difference — Backward Difference (in time dimension)

$$\frac{\left(\frac{h_i + h_{i+1}}{2}\right)^3 p_{i+1} - \left(\left(\frac{h_i + h_{i+1}}{2}\right)^3 + \left(\frac{h_i + h_{i-1}}{2}\right)^3\right) p_i + \left(\frac{h_i + h_{i-1}}{2}\right)^3 p_{i-1}}{(\Delta x)^2} = -6\mu U \frac{h_{i+1} - h_{i-1}}{2\Delta x} + 12\mu \frac{h_i - h_i(t = t_{j-1})}{\Delta t}$$

$$\left(h_i + h_{i+1}\right)^3 p_{i+1} - \left(\left(h_i + h_{i+1}\right)^3 + \left(h_i + h_{i-1}\right)^3\right) p_i + \left(h_i + h_{i-1}\right)^3 p_{i-1} =$$
$$-24\mu U (\Delta x)^2 \frac{h_{i+1} - h_{i-1}}{\Delta x} + 96\mu (\Delta x)^2 \frac{h_i - h_i(t = t_{j-1})}{\Delta t} \qquad \text{Eq. 5.4}$$

Note that, in the time derivative in Eq. 5.4, h_i represents the local node at the current time step, and $h_i(t = t_{j-1})$ represents the time value at the previous step. In this way, the time dependence is treated as a constant offset in each new time step, which helps constrain the problem. Finally, the discreetized Reynold's matrix is input into a matrix, shown in Eq. 5.5. All terms except for the p_i terms must be known and treated as constants. The matrix shown in Eq. 5.5 represents the process by which the legacy algorithm computes the rigid-skirt Reynold's solution for hydrodynamic pressure. The model must solve this system for each iteration step at each time step—a computationally intensive process.

$$\begin{bmatrix} 1 & & & & & & \\ h_{2-} & -(h_{2-}+h_{2+}) & h_{2+} & & & & \\ & h_{2-} & -(h_{2-}+h_{2+}) & h_{2+} & & & \\ & & \ddots & \ddots & \ddots & & \\ & & & h_{2-} & -(h_{2-}+h_{2+}) & h_{2+} & \\ & & & & & 1 & \end{bmatrix} \begin{bmatrix} p_1 \\ p_2 \\ p_3 \\ \vdots \\ p_n \\ p_{n+1} \end{bmatrix} = -24\mu\Delta x \begin{bmatrix} 1 \\ U(h_3 - h_1) - 4\Delta x(h_2 - h_2(t = t_1))/\Delta t \\ U(h_4 - h_2) - 4\Delta x(h_3 - h_3(t = t_2))/\Delta t \\ \vdots \\ U(h_{n+1} - h_{n-1}) - 4\Delta x(h_n - h_n(t = t_{n-1}))/\Delta t \\ 1 \end{bmatrix} \quad \text{Eq. 5.5}$$

$$h_{n+} \equiv h_n + h_{n+1}$$

$$h_{n-} \equiv h_n + h_{n-1}$$

5.1.3 Compliant-Skirt Solution

Unfortunately, the rigid-skirt assumption is unrealistic. When subjected to operational forces, the skirt deforms significantly, changing the effective oil film thickness. Moreover, since the pressure depends on the cube of oil film thickness, small deformations have a dramatic effect on the pressure terms. The skirt and liner are shown schematically in Fig. 5.3; note that the h values for oil film thickness in the Reynold's equation are distinct from Δh values for deformation predicted by the stiffness matrix. However, they are related by the fact that a Δh deformation is

added algebraically to the old h to get a new h value. Traditionally, and in the simulation runs described above, the clearance h and pressure p terms were solved iteratively, as illustrated in Fig. 5.4. The Reynold's equation is first solved assuming a rigid skirt; then the pressure terms are input to the stiffness matrix to produce deformation terms, which are used to adjust the oil film thickness terms in the Reynold's equation. The process is repeated until convergence is reached.

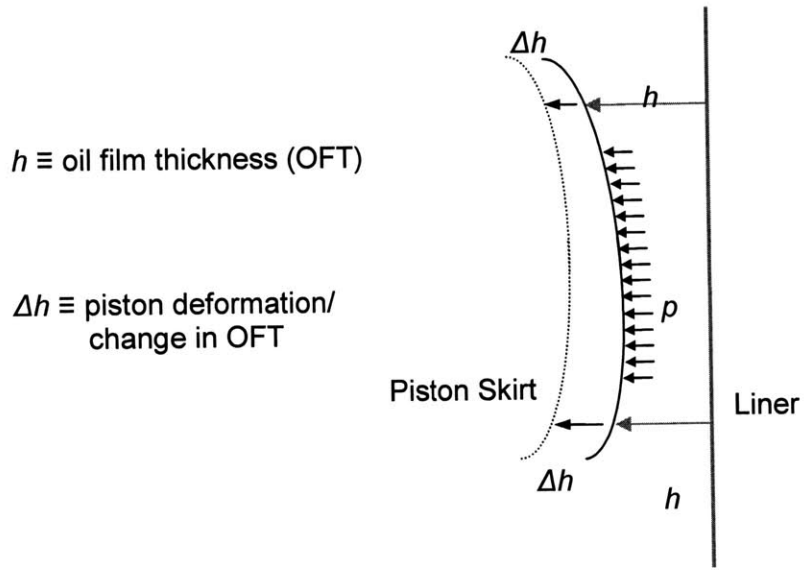

Figure 5.3: Schematic of skirt and liner, distinguishing between oil film thickness (h) and deformation (Δh)

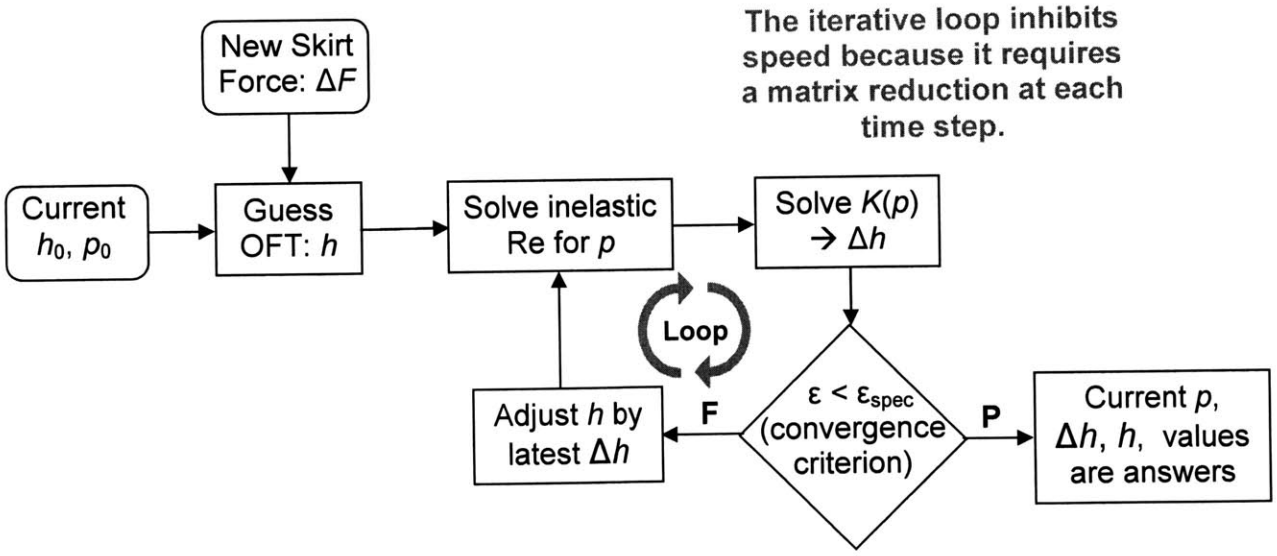

Figure 5.4: System diagram of iterative algorithm

5.2 Semi-Deterministic Solution

5.2.1 Background

Both the Reynold's equation and the stiffness matrix show relationships between pressure and oil film thicknesses. The objective of a deterministic algorithm is to combine both of these relationships into one common (i.e., simultaneous) solution. In general, simultaneous solutions are restricted to linear systems. However, in the Reynold's equation, the second derivative of pressure includes an h^3 term, which is obviously not linear. After the Reynold's equation is discreetized, the p and h terms appear as ph^3 terms (Eq. 5.4), which are clearly nonlinear.

The piston model operates by stepping slowly through an engine cycle in small increments. At each increment, all the variables (including pressure and film thickness) are calculated before progressing to the next time step. Moreover, the output from one crank angle is used as input to the next crank angle. This characteristic—gradual progression from one value to another—can be harnessed to linearize the Reynold's equation.

Any continuous function can be approximated as a Taylor polynomial, whose accuracy is dependent upon the order of the polynomial, the projection distance (i.e., the distance from the known point to the calculated point), and the degree of linearity of the function. Since the time steps in the simulation are small, the changes in the pressure and film thickness between successive steps are also small. Therefore, a first-order Taylor approximation of the Reynold's equation can linearize it without introducing excessive error.

5.2.2 First-order Taylor approximation of Reynold's equation

The first term in the 1-D Reynold's equation was discreetized in Eq. 5.3 as a second-difference. In order to combine all variables on one side, the Reynold's equation is rearranged to form a function $f(h, p)$ which always equals zero. (It is easier to take derivatives of a zero-valued function; the advantage of this approach will be detailed in the next section.) For the sake of

simplicity, the time dependence is ignored; the backward difference can be replaced easily, as described previously.

$$f(h,p)=\frac{(h_i+h_{i+1})^3\cdot\frac{p_{i+1}-p_i}{\Delta x}-(h_i+h_{i-1})^3\cdot\frac{p_i-p_{i-1}}{\Delta x}}{2^3\Delta x}+6\mu U\frac{h_{i+1}-h_{i-1}}{2\Delta x}=0 \qquad \text{Eq. 5.6}$$

This can be rearranged to the following:

$$f(h,p)=(h_i+h_{i+1})^3(p_{i+1}-p_i)-(h_i+h_{i-1})^3(p_i-p_{i-1})+24\mu U(h_{i+1}-h_{i-1})\Delta x=0 \qquad \text{Eq. 5.7}$$

5.2.3 Partial Derivatives of Reynold's Equation

Although both the Reynold's equation and stiffness matrix correlate pressure and film thickness values, the variables are not directly comparable. As explained in Section 5.1.3, the Reynold's equation uses the total height (h) variables, while the stiffness matrix uses deformation (Δh) variables, which represent how the oil film changes from the nominal position. As a result, p and h variables cannot simply be placed together in a combined Reynold's equation/stiffness matrix system and solved directly. The equations can be made compatible, however, by determining the effect of each upon a common variable. It is natural to pick the original input variable, ΔF (change in net force) as this common variable.

When the model steps to a new crank angle increment, it usually changes the amount of force that must be supported by the piston skirt (this force is calculated primarily by determining the connecting rod force from the inter-cylinder pressure and crank angle). As this force F increases, it tends to increase the pressure terms in the Reynold's equation. However, the increased pressure terms cause the piston to deform, increasing effective oil film thickness, h. The increased separation tends to reduce the pressure. Hence, the Reynold's equation and stiffness matrix have opposite effects on the net force. The goal of a deterministic algorithm is to find the amount of deformation that balances these effects.

The Reynold's equation determines how a change in film thickness changes hydrodynamic pressure. The stiffness matrix determines how a change in pressure changes the skirt profile, and hence, the oil film thickness. *The partial derivative of the Reynold's equation, ∂p/∂h, shows how the stiffness (∂h) affects the pressure terms in the original Reynold's equation (∂p).*

The Taylor approximation for $f(h,p)$ is summarized in Eq. 5.8. By rearranging the function so that the right-hand side is always zero, the constant term in the Taylor approximation is eliminated. Note that in this first-order Taylor approximation, the higher-order terms (H.O.T.) are neglected (this assumption is reconsidered in section 5.3).

$$f(h,p) = \cancel{f(h_0,p_0)}^{0} + \frac{\partial f(h_0,p_0)}{\partial h}\Delta h + \frac{\partial f(h_0,p_0)}{\partial p}\Delta p + \text{H.O.T.} = 0 \qquad \text{Eq. 5.8}$$

where $h = h_0 + \Delta h$ and $p = p_0 + \Delta p$

Eq. 5.9 shows the first derivative of $f(h,p)$, with partial derivatives shown in Eq. 5.10-11. Once again, these first derivates treat the Reynold's equation as though it behaves linearly in the region under consideration; this simplification will be considered in depth in Section 5.3.

$$\begin{aligned}\partial f(h,p) = \; & 3(h_i + h_{i+1})^2 (p_{i+1} - p_i)(\partial h_i + \partial h_{i+1}) - 3(h_i + h_{i-1})^2 (p_i - p_{i-1})(\partial h_i + \partial h_{i-1}) \\ & + 24\mu U(\partial h_{i+1} - \partial h_{i-1})\Delta x \\ & + (h_i + h_{i+1})^3 (\partial p_{i+1} - \partial p_i) - (h_i + h_{i-1})^3 (\partial p_i - \partial p_{i-1}) = 0\end{aligned} \qquad \text{Eq. 5.9}$$

$$\frac{\partial Re(h_0,p_0)}{\partial p}\Delta p = (h_{i-1} + h_i)\cdot\Delta p_{i-1} - ((h_{i-1} + h_i) + (h_i + h_{i+1}))\cdot\Delta p_i + (h_i + h_{i+1})\cdot\Delta p_{i+1} \qquad \text{Eq. 5.10}$$

$$\begin{aligned}\frac{\partial Re(h_0,p_0)}{\partial h}\Delta h = & \left[3(h_{i-1} + h_i)^2 (p_{i-1} - p_i) - 24\mu U\Delta x\right]\cdot\Delta h_{i-1} + \\ & \left[3(h_{i-1} + h_i)^2 (p_{i-1} - p_i) + 3(h_{i+1} + h_i)^2 (p_{i+1} - p_i) - \frac{96\mu(\Delta x)^2}{\Delta t}\right]\cdot\Delta h_i + \\ & \left[3(h_{i+1} + h_i)^2 (p_{i+1} - p_i) + 24\mu U\Delta x\right]\cdot\Delta h_{i+1}\end{aligned} \qquad \text{Eq. 5.11}$$

Rearrangement of Eq. 5.8 produces Eq. 5.12. Forcing the $f(h,p)$ equation to be zero always forces the derivative to be zero at all times also, so the partial derivative can be equated; this is a handy result.

$$\begin{aligned}
&\left[-3(h_i + h_{i-1})^2 (p_i - p_{i-1}) - 24\mu U\Delta x\right]\cdot \Delta h_{i-1} + \\
&\left[3(h_i + h_{i+1})^2 (p_{i+1} - p_i) - 3(h_i + h_{i-1})^2 (p_i - p_{i-1})\right]\cdot \Delta h_i + \\
&\left[3(h_i + h_{i+1})^2 (p_{i+1} - p_i) + 24\mu U\Delta x\right]\cdot \Delta h_{i+1} \\
&= \\
&\left[(h_i + h_{i-1})^3\right]\cdot \Delta p_{i-1} + \\
&\left[-(h_i + h_{i+1})^3 - (h_i + h_{i-1})^3\right]\cdot \Delta p_i + \\
&\left[(h_i + h_{i+1})^3\right]\cdot \Delta p_{i+1}
\end{aligned} \qquad \text{Eq. 5.12}$$

The partial derivatives of the Reynold's equation (expressed in $f(h,p)$ form) can be summarized as in Eq. 5.13. The general idea is that by inputting a map of either changes in pressure or changes in film thickness, the effect of the Reynold's equation on the other variable can be calculated easily through a linear system. Of course, this works only because the Reynold's equation has been made linear, and this approximation is valid only for "small" deviations. The definition of "small deviations" will be considered later.

$$\begin{bmatrix} \dfrac{\partial f(h,p)}{\partial h} \end{bmatrix}\begin{bmatrix} \Delta h \end{bmatrix} = \begin{bmatrix} \dfrac{\partial f(h,p)}{\partial p} \end{bmatrix}\begin{bmatrix} \Delta p \end{bmatrix} \qquad \text{Eq. 5.13}$$

5.2.4 Linear System Formulation

The formulae shown in Eq. 3.18 and Eq. 5.13 describe linear relationships between Δp and Δh that are produced by skirt deformation and hydrodynamic pressure, respectively. Since both of these physical processes operate on the piston simultaneously, it is necessary to include both in a common solution.

If both correlations are simply added together, as in Eq. 5.14 and 5.15, they describe a relationship between Δp and Δh that combines both stiffness and hydrodynamic pressure. Note that they are inverse functions of each other: Eq. 5.14 translates Δp into Δh, while Eq. 5.15 translates Δh into Δp. However, this approach assumes knowledge of either the Δp or Δh map, which is obviously unavailable prior to solution.

$$\left[\left[\frac{\partial f(h,p)}{\partial p}\right]^{-1}\left[\frac{\partial f(h,p)}{\partial h}\right]+\left[K\right]\right]\left[\Delta h\right]=\left[\Delta p\right] \qquad \text{Eq. 5.14}$$

$$\left[\left[\frac{\partial f(h,p)}{\partial h}\right]^{-1}\left[\frac{\partial f(h,p)}{\partial p}\right]+\left[K\right]^{-1}\right]\left[\Delta p\right]=\left[\Delta h\right] \qquad \text{Eq. 5.15}$$

In order to achieve an actual combined solution, it is necessary to first define a *change* to the initial state. This change affects both the Δp or Δh maps, and the combined equation will predict these changes. Theoretically, any change to the pressure or oil film maps can be chosen—either uniform or non-uniform changes can work. However, the most physically realistic change is a uniform change in oil film thickness, since additional lateral force on the piston tends to push it deeper into the oil film.

To initialize the algorithm, the rigid Reynold's equation is solved for pressure in response to a constant change in oil film thickness. The constant change in film thickness is called ΔH, and the rigid-skirt pressure change is ΔP. Then the task of the simultaneous solution is to determine both Δh (the change in film thickness relative to ΔH) and Δp (the change in film pressure relative to ΔP).

The simultaneous solution is developed by first considering the Reynold's equation and stiffness matrix separately. In Eq. 5.16, the derivative of the Reynold's equation is evaluated at $h = h_0 +$

ΔH, which is known. In Eq. 5.17, the stiffness matrix solves for deformation Δh in response to the net pressure ($\Delta P + \Delta p$).

$$\left[\quad \frac{\partial f(h_0 + \Delta H, p_{\Delta H})}{\partial p} \quad\right]\left[\Delta p\right] = \left[\quad \frac{\partial f(h_0 + \Delta H, p_{\Delta H})}{\partial h} \quad\right]\left[\Delta h\right] \qquad \text{Eq. 5.16}$$

$$\left[\quad K \quad\right]\left[\Delta h\right] = \left[\Delta P\right] + \left[\Delta p\right] \qquad \text{Eq. 5.17}$$

These equations can be combined in the system shown in Eq. 5.18:

$$\begin{bmatrix} \left[\dfrac{\partial f(h_0 + \Delta H, p_{\Delta H})}{\partial p}\right] & -\left[\dfrac{\partial f(h_0 + \Delta H, p_{\Delta H})}{\partial h}\right] \\ -\left[\quad I \quad\right] & \left[\quad K \quad\right] \end{bmatrix} \begin{bmatrix} [\Delta p] \\ [\Delta h] \end{bmatrix} = \begin{bmatrix} [0] \\ [\Delta P] \end{bmatrix} \qquad \text{Eq. 5.18}$$

5.2.5 Force balance

Eq. 5.19 unites the effects of the Reynold's equation and stiffness equation so that the predicted changes from each source agree. Perhaps the most important aspect of this linearized system, however, is that it allows a straightforward calculation of net force in order to meet the overall constraint of force balance. When all the pressure terms are integrated with respect to area, they produce the net lateral force supported hydrodynamically by the piston. This force must be equal to the external and inertial forces in order to preserve force balance.

Because the system is linear throughout, the entire matrix can be scaled to match the external force. The scaling factor κ is determined by calculating the ratio between the external force and the integral of pressure terms, as shown in Eq. 5.19. This scaling factor is then applied to the Reynold's equation derivative (Eq. 5.20) and the combined system (Eq. 5.21). The value of this approach is that it enables the program to initially select any random value of ΔH (and hence, ΔP). The linear system determines the shape of the pressure and film thickness maps, and then the force balance criterion scales them down to the correct magnitudes at the end.

$$\kappa = \frac{\Delta F}{\sum (\Delta P_i + \Delta p_i) \cdot \Delta A_i} \qquad \text{Eq. 5.19}$$

$$\kappa \left[\frac{\partial Re(p_0, h_0)}{\partial p} \right] [\Delta P] = \kappa \left[\frac{\partial Re(p_0, h_0)}{\partial h} \right] [\Delta H] \qquad \text{Eq. 5.20}$$

$$\kappa \begin{bmatrix} \left[\frac{\partial Re(p_0, h_0)}{\partial p} \right] & -\left[\frac{\partial Re(p_0, h_0)}{\partial h} \right] \\ -[I] & [K] \end{bmatrix} \begin{bmatrix} [\Delta p] \\ [\Delta h] \end{bmatrix} = \kappa \begin{bmatrix} [0] \\ [\Delta P] \end{bmatrix} \qquad \text{Eq. 5.21}$$

5.3 Error analysis

The useful characteristics of the system, such as the scalability of the net force and the simultaneous solution itself, are a direct result of the linearization of the Reynold's equation. How accurate is this approximation? In this section, the system is analyzed step by step to isolate and evaluate the magnitude of the error. The basic objective is to determine whether the higher-order terms that were neglected in the Taylor polynomial expansion of the Reynold's equation can be properly neglected.

5.3.1 Linearized equation vs. original equation

The first step in the analysis is to express the Reynold's equation as a zero-valued function, as explained previously:

$$f(h,p) = (h_i + h_{i-1})^3 p_{i-1} - \left((h_i + h_{i+1})^3 + (h_i + h_{i-1})^3\right)p_i + (h_i + h_{i+1})^3 p_{i+1} + 24\mu\Delta x\left(U(h_{i+1} - h_{i-1}) - 4\Delta x \frac{h_i - h_i(t = t_{j-1})}{\Delta t}\right) = 0 \qquad \text{Eq. 5.22}$$

This function is linearized by considering only the first partial derivatives of the discreetized system. Note that the function is renamed from $f(h,p)$ to $Re(h,p)$ for clarity:

$$f(h,p) = Re(h,p) = \cancel{Re(h_0,p_0)}^{0} + \frac{\partial Re(h_0,p_0)}{\partial h}\Delta h + \frac{\partial Re(h_0,p_0)}{\partial p}\Delta p + \text{H.O.T.} = 0 \qquad \text{Eq. 5.23}$$

where $h = h_0 + \Delta h$

and $p = p_0 + \Delta p$

Then the higher-order terms are analyzed. In Eq. 5.24, the second-order, third-order, and fourth-order terms in the (H.O.T.) expression are explicitly stated:

$$\begin{aligned}\text{H.O.T.} = \text{O}(h^2, p^2) = &\frac{1}{2!}\cdot\frac{\partial^2 Re(h_0,p_0)}{\partial h^2}(\Delta h)^2 + \frac{1}{2!}\cdot\frac{\partial^2 Re(h_0,p_0)}{\partial p^2}(\Delta p)^2 + \\ &\frac{1}{3!}\cdot\frac{\partial^3 Re(h_0,p_0)}{\partial h^3}(\Delta h)^3 + \frac{1}{3!}\cdot\frac{\partial^3 Re(h_0,p_0)}{\partial p^3}(\Delta p)^3 + \\ &\frac{1}{4!}\cdot\frac{\partial^4 Re(h_0,p_0)}{\partial h^4}(\Delta h)^4 + \frac{1}{4!}\cdot\frac{\partial^4 Re(h_0,p_0)}{\partial p^4}(\Delta p)^4 + \\ &\text{O}(h^5) + \text{O}(p^5)\end{aligned} \qquad \text{Eq. 5.24}$$

The pressure terms are considered first. Note that in the original discreetized equation (Eq. 5.7), the function already depends linearly on pressure p. Thus, all higher-order terms in p are already zero. (This does not mean that the actual Reynold's equation depends linearly on pressure; it is only saying that after the Reynold's equation is discreetized into algebraic form according to Eq.

5.7, the dependence on pressure is only first-order.) The following equation shows the reduced equation.

$$\begin{aligned}\text{H.O.T.} = O(h^2, p^2) = &\frac{1}{2!}\cdot\frac{\partial^2 Re(h_0, p_0)}{\partial h^2}(\Delta h)^2 + \cancel{\frac{1}{2!}\cdot\frac{\partial^2 Re(h_0, p_0)}{\partial p^2}(\Delta p)^2} + \\ &\frac{1}{3!}\cdot\frac{\partial^3 Re(h_0, p_0)}{\partial h^3}(\Delta h)^3 + \cancel{\frac{1}{3!}\cdot\frac{\partial^3 Re(h_0, p_0)}{\partial p^3}(\Delta p)^3} + \\ &\frac{1}{4!}\cdot\frac{\partial^4 Re(h_0, p_0)}{\partial h^4}(\Delta h)^4 + \cancel{\frac{1}{4!}\cdot\frac{\partial^4 Re(h_0, p_0)}{\partial p^4}(\Delta p)^4} + \\ &O(h^5) + \cancel{O(p^5)}\end{aligned} \qquad \text{Eq. 5.25}$$

The oil film thickness dependence, on the other hand, is cubic. Therefore, the quadratic and cubic terms in the Reynold's equation discreetization are nonzero, but quartic and higher terms drop out:

$$\begin{aligned}\text{H.O.T.} = O(h^2, p^2) = &\frac{1}{2!}\cdot\frac{\partial^2 Re(h_0, p_0)}{\partial h^2}(\Delta h)^2 + \cancel{\frac{1}{2!}\cdot\frac{\partial^2 Re(h_0, p_0)}{\partial p^2}(\Delta p)^2} + \\ &\frac{1}{3!}\cdot\frac{\partial^3 Re(h_0, p_0)}{\partial h^3}(\Delta h)^3 + \cancel{\frac{1}{3!}\cdot\frac{\partial^3 Re(h_0, p_0)}{\partial p^3}(\Delta p)^3} + \\ &\cancel{\frac{1}{4!}\cdot\frac{\partial^4 Re(h_0, p_0)}{\partial h^4}(\Delta h)^4} + \cancel{\frac{1}{4!}\cdot\frac{\partial^4 Re(h_0, p_0)}{\partial p^4}(\Delta p)^4} + \\ &\cancel{O(h^5)} + \cancel{O(p^5)}\end{aligned} \qquad \text{Eq. 5.26}$$

The equation of higher-order terms is shown in reduced form below:

$$\text{H.O.T.} = O(h^2, p^2) = \frac{1}{2!}\cdot\frac{\partial^2 Re(h_0, p_0)}{\partial h^2}(\Delta h)^2 + \frac{1}{3!}\cdot\frac{\partial^3 Re(h_0, p_0)}{\partial h^3}(\Delta h)^3 \qquad \text{Eq. 5.27}$$

The critical question in regard to the error analysis is whether the neglected higher-order terms are significant. In order to evaluate this question, take the ratio of the higher-order terms to the original terms. In Eq. 5.28, this ratio is shown as the sum of the ratios for each constituent (oil

film thickness and pressure), and in Eq. 5.29, the equation is described explicitly. For a given crank angle, the partial derivatives with respect to h and the Δh increment can be substituted into Eq. 5.29; if the ratio is small, then the linearization approximation is relatively accurate.

$$\frac{H.O.T.}{Re(h,p)} = \frac{H.O.T.(h)}{\dfrac{\partial Re(h_0,p_0)}{\partial h}\Delta h} + \frac{H.O.T.(p)}{\dfrac{\partial Re(h_0,p_0)}{\partial p}\Delta p} \qquad \text{Eq. 5.28}$$

$$\frac{H.O.T.}{Re(h,p)} = \frac{\dfrac{1}{2!}\cdot\dfrac{\partial^2 Re(h_0,p_0)}{\partial h^2}(\Delta h)^2 + \dfrac{1}{3!}\cdot\dfrac{\partial^3 Re(h_0,p_0)}{\partial h^3}(\Delta h)^3}{\dfrac{\partial Re(h_0,p_0)}{\partial h}\Delta h} + \frac{0}{\dfrac{\partial Re(h_0,p_0)}{\partial p}\Delta p} \qquad \text{Eq. 5.29}$$

In general, however, the partial derivatives of the Reynold's equation function are not known, so they must be approximated. The first observation is that the equation is dominated by its cubic terms, so for order-of-magnitude approximations, it can be represented as h^3. Then the second and third derivatives are known and simple, and the $H.O.T./Re(h,p)$ ratio reduces to the following:

$$Re(h_0,p_0) \approx h^3 \;\rightarrow$$

$$\frac{H.O.T.}{Re(h,p)} \approx \frac{\dfrac{\partial^2(h^3)}{\partial h^2}(\Delta h)^2 + \dfrac{\partial^3 Re(h^3)}{\partial h^3}(\Delta h)^3}{\dfrac{\partial Re(h^3)}{\partial h}\Delta h} \approx \frac{6h(\Delta h)^2 + 6(\Delta h)^3}{3h^2\Delta h} \qquad \text{Eq. 5.30}$$

This correlation is simpler than the previous one, but is still someone difficult because neither h (the original oil film thickness) nor Δh (the change in film thickness since the last step) are known. The additional approximation that Δh is much less than h is stipulated, which causes the (Δh) in the numerator to drop out, leading to the simple statement that Δh must be less than h (Eq. 5.31). Another way to express this idea is that if Δh is much less than h, then the higher-order terms are negligible. This is a reasonable result, since the higher-order terms in the Taylor polynomial expansion operate on Δh, and a small Δh will get even smaller as it is raised to a higher power.

$$\frac{H.O.T.}{Re(h,p)} \approx \frac{6h(\Delta h)+6(\Delta h)^2}{3h^2} \approx \frac{6h(\Delta h)}{3h^2} \approx \frac{\Delta h}{h} << 1 \qquad \text{Eq. 5.31}$$

This condition is easy to implement in an actual algorithm, which can simply find the maximum ratio between the change in h and the previous h value. If the ratio is above a certain threshold, say 10%, then the time step (i.e., crank angle) is bisected (or otherwise decreased). The threshold is determined by the user to represent the preferred balance between accuracy and computational speed.

5.3.2 Evaluation of actual data in a legacy simulation run

Is the simplification that Δh be much less than h realistic? In order to get a rough idea of typical values, the legacy (baseline) simulation program was exercised for a typical case, and the output was analyzed to determine the worst-case $\Delta h/h$ ratio. It can be seen that for most crank angles, the $\Delta h/h$ ratio is negligible, implying that linearization of the Reynold's equation is very accurate. The only times the ratio exceeds 5% are for very short periods in the cycle which correspond to piston slap or other significant lateral motion. For sections that have excessive error (e.g., for the tiny increment just after TDC = 360° in the Fig. 5.5, corresponding to piston slap), the crank angle should be reduced (e.g., use an increment of 0.25° instead of 0.5°).

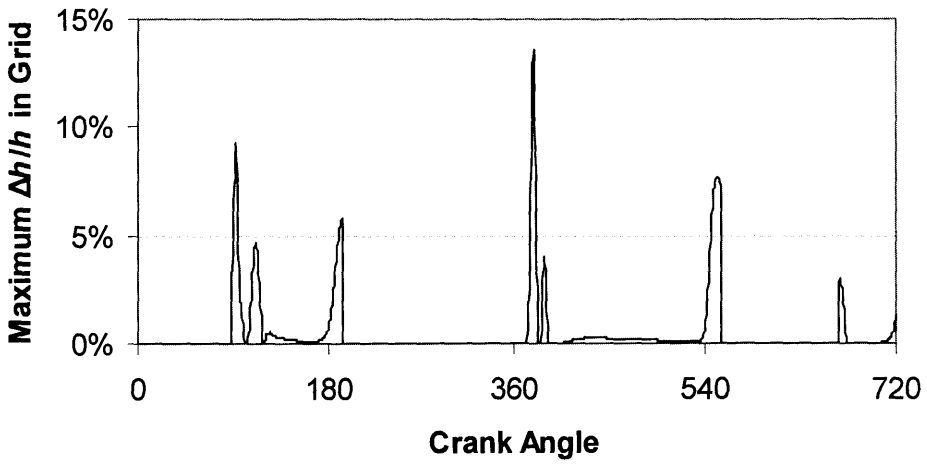

Figure 5.5: Plot of worst-case (i.e., maximum) $\Delta h/h$ ratios for a complete cycle, using old simulation with 5° increments (thrust side, with SAE-40 oil, shallow x^8 profile, 70 μm oil film thickness, 10 μm waviness)

5.4 Future work

5.4.1 Implementation

A significant challenge is to implement the algorithm into the code of the current model. Since the proposed algorithm is fundamentally different from the legacy iterative algorithm, extensive changes to the core operation of the model are needed. Fig. 5.6 is a flowchart of subroutine calls used in the piston model.

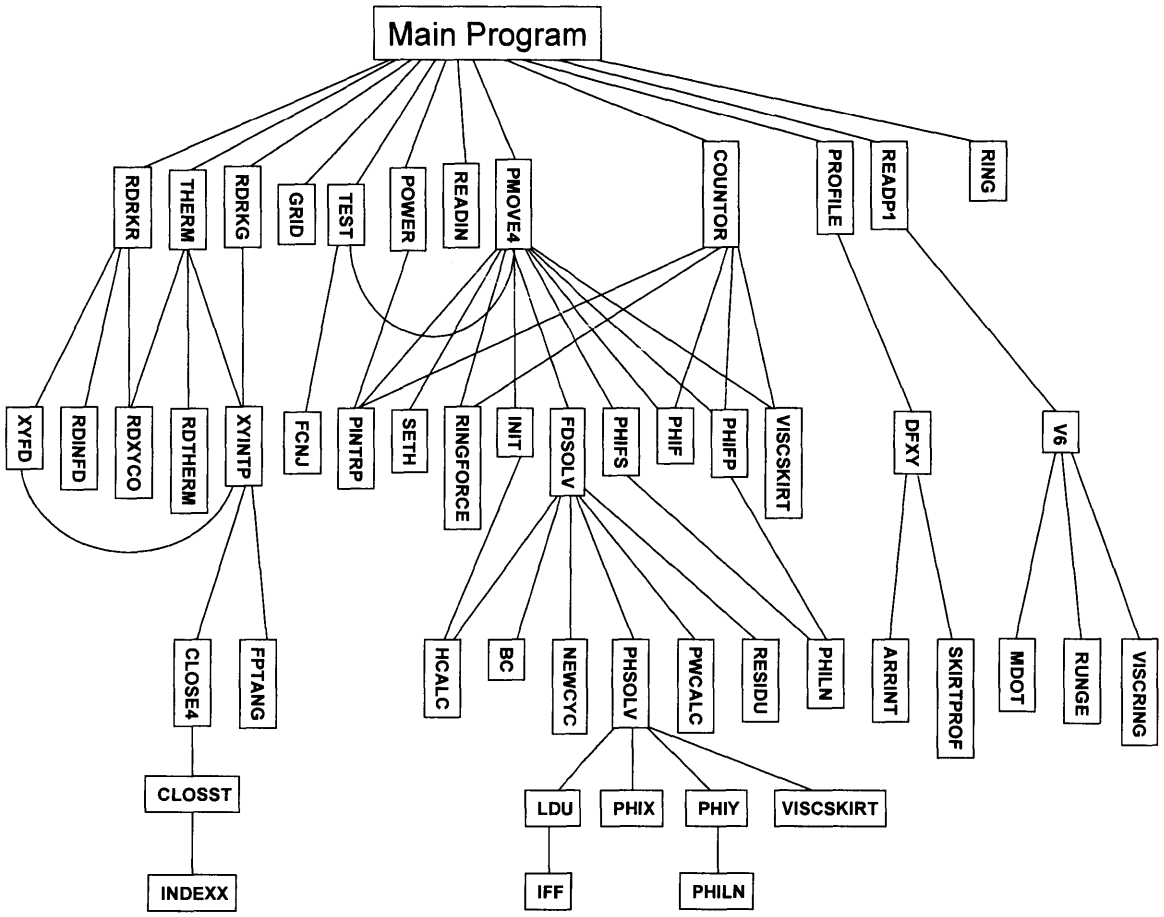

Figure 5.6: Flow chart of subroutine and function calls in piston model, illustrating the flow of operations. The crucial subroutine DIVPAG, which is a Fortran ISML subroutine, is not shown here.

In the interest of brevity, the purpose of each subroutine in the model will not be described. However, the iteration process is controlled by an implicit backward differentiation implemented

by the DIVPAG subroutine. The IVPAG class of subroutines is one of the ISML (International Mathematical and Statistical Libraries) libraries written for FORTRAN. It is a sophisticated algorithm for solving an initial-value problem for ordinary differential equations using either Adams-Moulton's or Gear's backward differentiation method, and it calls other subroutines multiple times until it reaches convergence. The *IMSL Fortran Subroutines for Mathematical Applications* documentation summarizes the algorithm as follows:

> The routine IVPAG solves a system of first-order ordinary differential equations of the form $y' = f(t, y)$ or $Ay' = f(t, y)$ with initial conditions where A is a square nonsingular matrix of order N. Two classes of implicit linear multistep methods are available. The first is the implicit Adams-Moulton method (up to order twelve); the second uses the backward differentiation formulas BDF (up to order five). The BDF method is often called Gear's stiff method. In both cases, because basic formulas are implicit, a system of nonlinear equations must be solved at each step. The deriviative matrix in this system has the form $L = A + \eta J$ where η is a small number computed by IVPAG and J is the Jacobian. When it is used, this matrix is computed in the user-supplied routine FCNJ or else it is approximated by divided differences as a default. Using defaults, A is the identity matrix. The data structure for the matrix L may be identified to be real general, real banded, symmetric positive definite, or banded symmetric positive definite. The default structure for L is real general.[27]

In the piston model, the subroutine pmove4 was specially designed to work with DIVPAG. As can be seen from Fig. 5.6, pmove4 is connected to many other subroutines, so by extension, many interconnected subroutines were designed specifically to function with DIVPAG. In order to implement the deterministic linearization algorithm, those subroutines need to be modified or rewritten to accommodate the updated methodology.

5.4.2 Mathematical analysis

In the field of differential equation analysis, a crucial question is whether a particular algorithm is stable. Some discreetization schemes have the potential to provide accurate results, but for

some input parameters, they diverge and fail. In order for the deterministic method to be robust, the stability must be assured at each time step. Further work is needed in this area, but it would be ideal if the algorithm could test for and guarantee stability at each time step rather than just guessing at appropriate values for convergence. This objective is complicated, however, by discontinuous effects, which are considered next.

5.4.3 Discontinuous effects

As explained in Section 3.6, the current model considers several discontinuous effects. The first is the oil film thickness, which requires a more complicated formulation than a fully-flooded assumption; the program needs to set pressure to 1 bar whenever the separation exceeds the input oil film thickness. Figure 5.7 illustrates the oil film, showing the discontinuity between the smooth piston imprint and the defined oil film thickness. Another important effect is cavitation, in which the model must set pressure to zero whenever the predicted pressure falls below atmospheric. Finally, the transition to asperity pressure is governed by a minimum separation threshold, which introduces a third discontinuity.

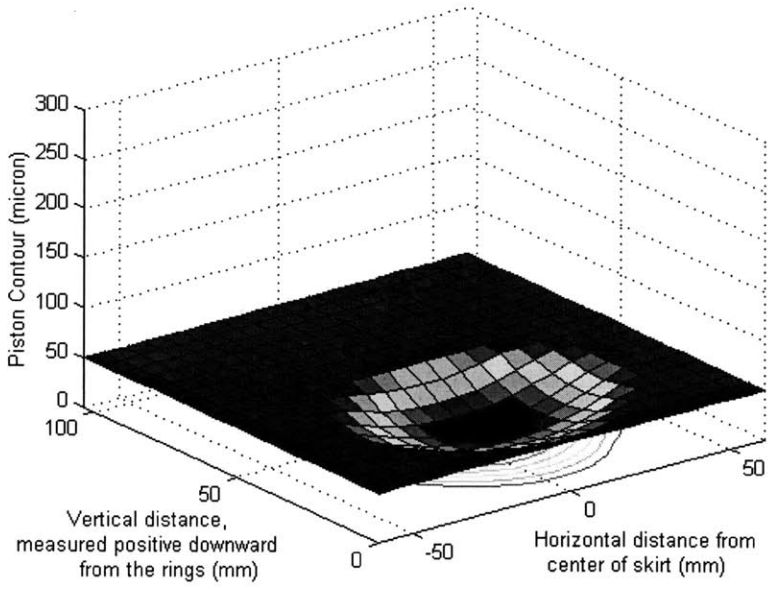

Figure 5.7: Illustration of the oil film, showing piston imprint. The interface between the piston imprint and oil film is discontinuous, which complicates the solution of the hydrodynamic differential equation.

In the legacy iterative algorithm, implicit methods, which guess a solution and then test it against constraints, were used. It is straightforward to include discontinuities into the test solution (or guess) because they can simply be defined; however, including discontinuities in an explicit algorithm is far more difficult. A significant challenge relates to where to define the boundary conditions, since they shift during operation. Each of the three sources of discontinuities is considered in turn.

If a constant oil film thickness is assumed, the boundary between wetted surface and unwetted area is dynamic (changing with time). As the piston penetrates deeper into the oil film in order to sustain a greater load, it becomes exposed to more nodes (see schematic in Fig. 5.8). Each node corresponds to both a $h_{i,j}$ variable and a $p_{i,j}$ variable, which must be solved by the combined matrix (Eq. 5.18). Therefore, as the piston skirt moves in and out of the oil film, the matrix size changes. (Alternatively, the matrix could solve for all nodes at each time step, but the unwetted nodes would have to be artificially set to 1 bar to reflect the fact that unwetted areas are under atmospheric pressure.) The shifting boundary conditions significantly complicate the mathematics and make the algorithm more complex.

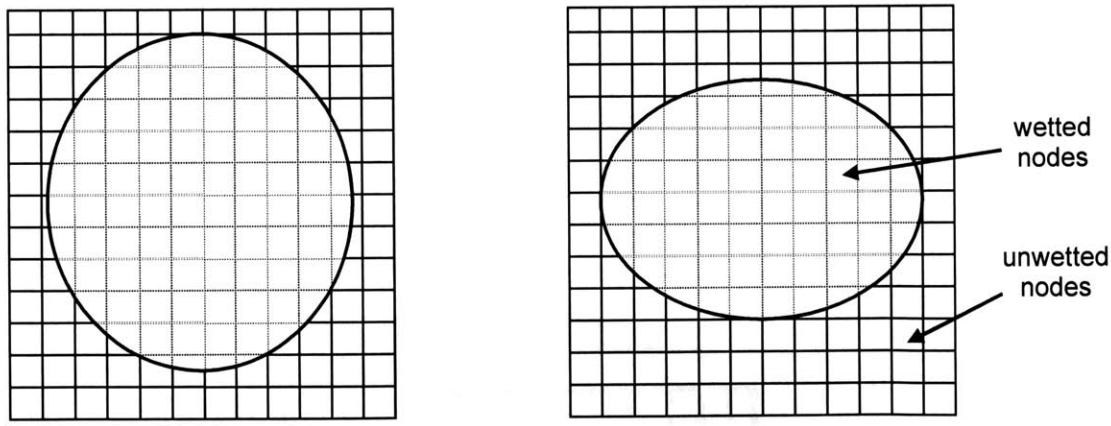

Figure 5.8: Schematic of skirt and piston footprint, illustrating the effect of oil film thickness on wetted nodes at different points in the cycle (a fully-flooded skirt would treat all nodes as wetted).

If cavitation is included in the solution method, any nodes that are exposed to a calculated negative pressure must be set to atmospheric. (More sophisticated cavitation models are

available, but simply setting negative pressures to 1 bar is a useful approximation.) As illustrated in Figure 5.9, including cavitation in the model changes the boundary further and switches some previously wetted nodes to unwetted. The algorithm must not only account for the new status of these nodes, but must also reassign the boundary conditions to the nodes that are still under hydrodynamic support.

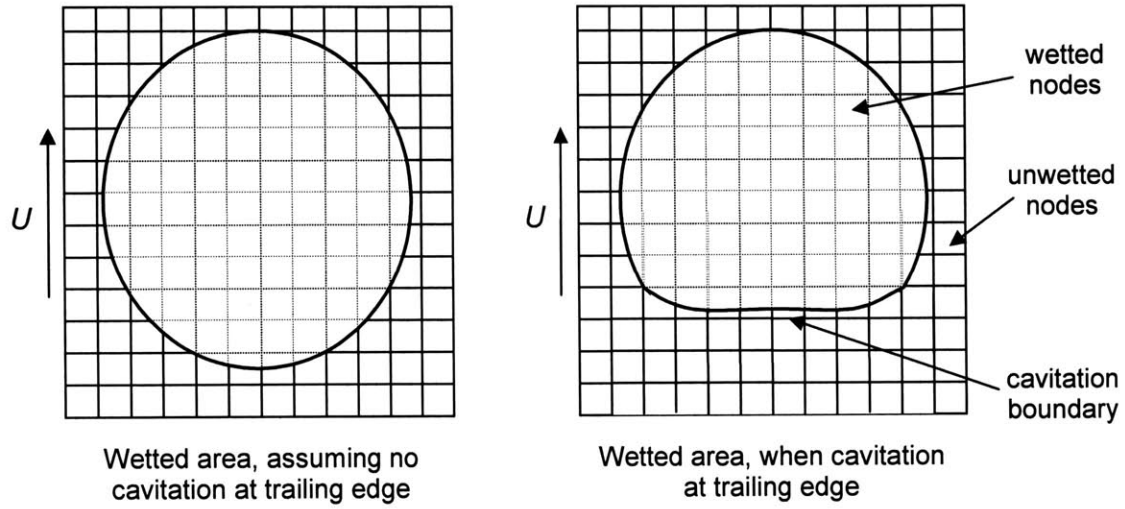

Figure 5.9: Schematic of skirt and piston footprint, showing the effect of cavitation on wetted nodes

The third discontinuous phenomenon is asperity contact, which can play a very significant role in friction calculations. Usually asperity contact occurs at only a few nodes, but the pressures at these nodes are typically far greater than the average hydrodynamic pressure. If the model determines that the oil film thickness will fall below a certain threshold (typically the amplitude of the machined grooves), it assumes boundary lubrication (see Section 3.6.3 for more details). However, the nodes undergoing asperity contact must be removed from the solution matrix because they are no longer under hydrodynamic support.

In contrast to the other two sources of discontinuity, which simply set the nodal pressure to a low value (usually 1 bar), the nodes under asperity contact are under very high pressures, usually much higher than those under hydrodynamic support. The combined solution matrix (Eq. 5.18) includes the deformation due to hydrodynamic pressure, but it does not consider the additional deformation due to asperity pressure. In order to provide an accurate estimate of deformation, the

asperity contact pressure must be included in the stiffness matrix calculation, even though it falls outside the domain of the hydrodynamic pressure solution matrix.

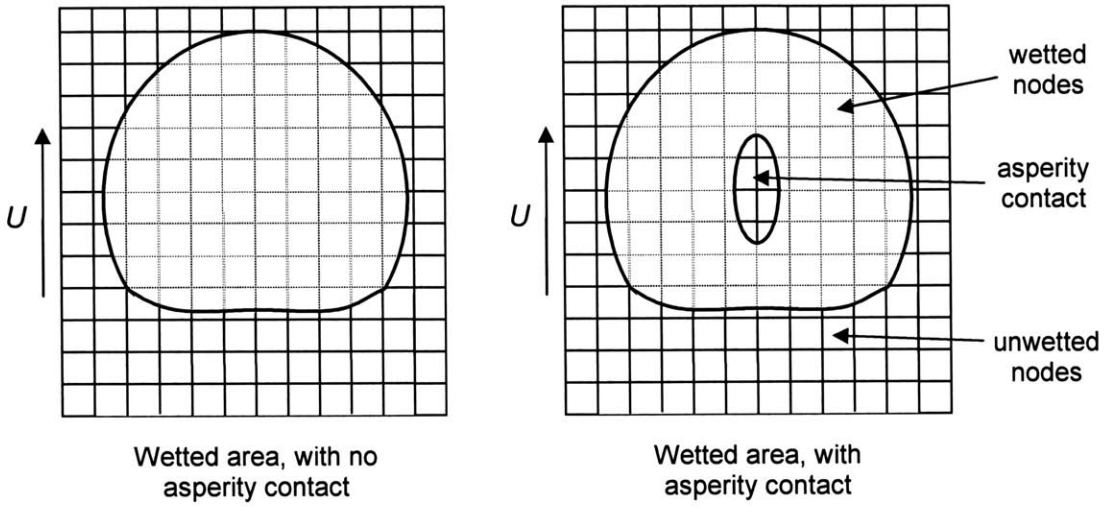

Figure 5.10: Schematic of skirt and piston footprint, showing the effect of asperities on nodes exposed to hydrodynamic lubrication

5.4.4 Testing and comparison against legacy model and experiments

The combined matrix presented in Eq. 5.18 has the potential to increase speed by eliminating or drastically reducing iteration. However, the larger matrix exacts a modest efficiency penalty because it is twice as large each of the two matrices it replaces (i.e., the discreetized Reynold's equation matrix and the stiffness matrix). A system of equations can be solved by the LU factorization method with speed on the order of $2n^2$, where n is the length of the matrix. In the legacy system, several linear systems of size n are solved multiple times until they converge. Ideally, the new, linearized matrix (of size $2n$) will only need to be solved once, but it will take 4 times as long as solving one of the smaller matrices. Hence, the solution time for this approach will be equivalent to about at least 2 iterations (i.e., two size-n matrix solutions at each step) in the legacy system. (Some advanced matrix solution methods, such as multi-grid algorithms, may be able to reduce this time further).

After the algorithm is implemented, it needs to be tested in two major areas. It must first be tested to demonstrate that it offers superior speed and numerical efficiency, since that was the

justification for it in the first place. It must also be tested for accuracy: does it predict solutions similar to those calculated with the legacy iterative approach? Finally, the results ought to be compared with appropriately designed experiments to ensure that the modeling approach is accurate.

(This page was intentionally left blank)

6 Conclusions

6.1 Summary

The parameters of the piston-liner system of a reciprocating engine are complex and highly interdependent, but numerical models have enabled significant progress to be made toward understanding them. In this project, which focused on reducing friction, the effects predicted by the model comport with physical intuition. Reducing viscosity reduces hydrodynamic friction while also reducing hydrodynamic pressure, but excessive reduction in viscosity makes the system vulnerable to boundary contact, which increases net friction. Thus, the strategy is to design the power cylinder system to operate primarily in the hydrodynamic lubrication regime while utilizing the lowest-viscosity oil practical.

The model confirmed that increasing oil film thickness (by increasing oil supply) tends to increase hydrodynamic support, which can supplant high-friction boundary contact. Thus, increasing oil film thickness can reduce friction losses. However, excessive oil supply can increase hydrodynamic drag needlessly and lead to heightened oil consumption, which can have serious negative consequences for aftertreatment and exhaust. Therefore, methods other than simply increasing oil film thickness are preferred.

Changes to the design of the piston can promote hydrodynamic lubrication without increasing the supply or viscosity of the oil. The piston and liner geometry can be modified to maintain a smooth, even distribution of film thickness and hydrodynamic pressure. By avoiding pressure concentrations and the sharp film thickness gradients that cause them, the piston skirt is less likely to push the oil film aside and enter the boundary lubrication mode. The model confirmed that a relatively flat piston profile provides the best hydrodynamic support over the majority of the cycle because it conforms most closely to the liner. Likewise, a profile that contains minimal ovality (i.e., is nearly as circular as the liner) maintains an even distribution of film thickness and pressure, thereby maximizing hydrodynamic support and minimizing friction loss.

Some pistons are constructed of steel, which is significantly denser than the aluminum that is typically used. In order to reduce weight, much of the material is removed, including some around the piston skirt. Changing skirt size is expected to have a major impact on the distribution between hydrodynamic and boundary lubrication. The model predicted that smaller skirt sizes are at greater risk for boundary lubrication, with its concomitant increase in friction, since they concentrate the same lateral force over a smaller area. Therefore, if a smaller skirt surface is necessary, the other variables, such as piston profile and ovality, must be approached with great care to ensure adequate hydrodynamic support.

Finally, surface modifications can be selected to minimize friction. Although circumferential grooves (waviness) retain oil by surface tension and provide useful flow paths for oil, they can dramatically increase friction if their amplitude is excessive. The model predicts that if the amplitude is significantly greater than the average clearance between piston and liner, then the peaks of the grooves will penetrate through the oil film and scrape against each other, leading to boundary contact and its concomitant friction and wear. Therefore, waviness amplitude should be no larger than what is needed to provide adequate oil pathways and retain sufficient oil by surface tension. Moreover, the model indicated that the naturally-occurring asperities on the piston surface do not significantly affect friction, provided that they are substantially smaller than the machined grooves.

The contributions of each parameter to friction reduction are not additive, since each parameter affects the others. The most effective strategy is to combine a variety of techniques to achieve an overall decrease in friction while avoiding significant disadvantages. For example, the piston profile and piston ovality must be considered together because they both affect the separation between the skirt and liner. The waviness amplitude, skirt size, and cold skirt-liner clearance must be evaluated together with viscosity, since a low-viscosity lubricant tends to promote boundary lubrication and consequent high friction. By applying the computer model to a specific power cylinder arrangement, an optimized combination of design changes can be selected to minimize net friction loss and improve reliability.

6.2 Future work

The current piston model requires a substantial amount of time to run, particularly as precision—and consequently, matrix size—increases. The iterative process used to solve both the Reynold's equation and stiffness matrix for common pressure and film thickness variables simultaneously requires a large matrix to be solved many times for each crank angle increment. A deterministic method, which would combine the Reynold's equation and stiffness matrix in a single linear system, was described in this project, but it requires further development and implementation. The algorithm linearizes the Reynold's equation, which introduces a measure of error but allows the equation to be combined with the linear stiffness matrix in a linear algebraic system, which enables it to be solved directly. If appropriate error bounds on this linearization are established, this method could significantly improve the performance of the model.

The effects of piston stiffness ought to be investigated further. This project sought to develop parametric relationships that could be applied to a wide variety of pistons, but it is difficult to follow a similar approach when studying piston stiffness because stiffness is highly sensitive to the specific construction of each particular piston. The internal structure of the piston (webbing, material type, etc.) determines how the skirt surface deforms through a complex relationship determined by finite-element analysis. It is difficult to formulate general correlations that predict how structural changes in any piston will influence friction. Instead, it is more appropriate to use the model as a practical design tool to compare specific engine systems for which detailed information (i.e., detailed geometry and stiffness matrices) are known.

Finally, any modification to the piston design must be approached with a holistic perspective, since few improvements in engine design come without concomitant disadvantages. Some changes that reduce friction loss, such as reducing skirt ovality, may have deleterious effects on reliability or the integrity of the surface finish. Other changes may be desirable, but they could be prohibitively difficult or costly to manufacture. The usefulness of the model is that it can evaluate a wide variety of modifications through a system-wide approach in order to predict their cumulative effect on friction and reliability.

(This page was intentionally left blank)

References

[1] Richardson, D.E., "Review of Power Cylinder Friction for Diesel Engines," Internal Report, Cummins Engine Company.

[2] Richardson, D.E., ASME Paper 99-ICE-196, 1999 ASME-ICED Spring Conference.

[3] Primus, R.J., Flynn, P.F., "The Assessment of Losses in Diesel Engines Using Second-Law Analysis," ASME, *Computer-Aided Engineering and Energy Systems*, Vol. 3: Second Law Analysis and Modeling, pp. 61-68, 1986.

[4] Rao, V.D.N., *et al.*, "Engine Studies of Solid Film Lubricant Coated Pistons," SAE Paper 970009, 1997.

[5] Ting, L.L., "A Review of Present Information on Piston Ring Tribology," SAE Paper 852355, 1985.

[6] Patton, K.J., Nitschke, R.G., Heywood, J.B., "Development and Evaluation of a Friction Model for Spark-Ignition Engines," SAE Paper 890836, 1989.

[7] Kovach, J.T., Tsakiris, E.A., and Wong, L.T., "Engine Friction Reduction for Improved Fuel Economy," SAE Paper 820085, 1982.

[8] Hamai, K., *et al.*, "Development of a Friction Prediction Model for High Performance Engines," STLE, Lubrication Engineering, Volume 47, pp. 567-573, 1990.

[9] Koch, F., *et al.*, "PIFFO – Piston Friction Force Measurements During Engine Operation," SAE Paper 960306, 1996.

[10] Betz, G., Gabele, H., Assmus, H-O, "Friction Power and Noise Behaviour of the Piston Assembly," IMechE, C375/019, 1989.

[11] Goenka, P.K., Meernik, P.R., "Lubrication Analysis of Piston Skirts," SAE Paper 920490, 1992.

[12] Pinkus, Oscar and Sternlicht, Beno, "Theory of Hydrodynamic Lubrication", McGraw-Hill, 1961.

[13] Frene, J., Nicolas, D., Degueurce, B., Berthe, D., Godet, M., Hydrodynamic Lubrication: Tribology Series (Vol. 33), Elsevier, 1997.

[14] Tian, T., "Modeling the Performance of the Piston Ring Pack in Internal Combustion Engines", Ph.D. Thesis, Department of Mechanical Engineering, Massachusetts Institute of Technology, June 1997.

[15] Greenwood, J.A. and Tripp, J., "The Contact of Two Nominally Flat Surfaces," Proceedings of the Institute of Mechanical Engineers, 1971.

[16] Wong, V.W., Tian, T., Lang, H., Ryan, J., "A Numerical Model of Piston Secondary Motion and Piston Slap in Partially Flooded Elastohydrodynamic Skirt Lubriction," SAE Paper 940696, 1994.

[17] Mansouri, S.H., Wong, V.W., "Effects of Piston Design Parameters on Piston Secondary Motion and Skirt-Liner Friction," SAE Paper 2004-01-2911, 2004.

[18] Ryan, J.P., Wong, V. W., Lyon, R.H., Hoult, D.P., Sekiya, Y., Kobayashi, Y. and Aoyama, S., "Engine Experiments on the Effects of Design and Operational Parameters on Piston Secondary Motion and Piston Slap," SAE Paper 940695 (1994).

[19] Wong, V.W., Smedley, G., Tian, T., "Piston Ring Design for Reduced Friction in an Advanced Natural-Gas Power Generation Engine," CIMAC Paper No. 263 (2004).

[20] Smedley, G., Mansouri, S.H., Tian, T., Wong, V.W., "Friction Reduction Via Piston and Ring Design for an Advanced Natural Gas Reciprocating Engine," ASME ICEF2004-879 (2004).

[21] Patir, N. and Cheng, H.S., "Application of Average Flow Model to Lubrication Between Rough Sliding Surfaces," ASME Journal of Lubrication Technology, 1979.

[22] Jocsak, J. "The Effects of Surface Finish on Piston Ring-pack Performance in Advanced Reciprocating Engine Systems", M.S. Thesis, Department of Mechanical Engineering, Massachusetts Institute of Technology, June 2005.

[23] Zhu, D., Cheng, H.S., Arai, T. and Hamai, K., "A Numerical Analysis for Piston Skirts in Mixed Lubrication—Part I: Basic Modeling," ASME Paper 91-Trib-66, STLE/ASME Tribology Conference, St. Louis (1991).

[24] Zhu, D., Hu, Y., Cheng, H.S., Arai, T. and Hamai, K., "A Numerical Analysis for Piston Skirts in Mixed Lubrication—Part II: Deformation Considerations," ASME Paper 92-Trib-22, ASME-STLE Joint Tribology Conference, San Diego (1992).

[25] Woschni, G., and Zeilinger, K., "Vorausberechnung de s Kolbenringverhaltens," FVV Workshop, *Tribosystem Kolben-Kolbenring-Zylindgerlaufflache*, 10, Okt., 1989, VDMA-Haus Frankfurt.

[26] Cameron, A., "Basic Lubrication Theory," New York: Halsted Press, 1981.

[27] Visual Numerics, *IMSL Fortran Subroutines for Mathematical Applications*, Math/Library Volumes 1 and 2, Online Manual, 2000.

[28] Takata, R. "Effects of Lubricant Viscosity and Surface Texturing on Ring-pack Performance in Internal Combustion Engines", M.S. Thesis, Department of Mechanical Engineering, Massachusetts Institute of Technology, June 2006.

(This page was intentionally left blank)

Appendix A: Derivation of Fundamental Equations

Source: Grant Smedley, S.M. Thesis: *Piston Ring Design for Reduced Friction in Motion Internal Combustion Engines,* MIT, May 2004.

A.1 Shear Stress Between the Ring and the Liner and Volumetric Flow Rate of Oil

The shear stress generated between the ring and the liner and the volumetric flow rate of oil can be determined by applying conservation of mass and momentum to a fluid element under the ring surface as follows.

Conservation of Mass[12-13]:

$$\frac{d\rho}{dt}+\frac{\partial}{\partial x}(\rho u)+\frac{\partial}{\partial y}(\rho v)+\frac{\partial}{\partial z}(\rho w)=0 \qquad \text{Eq. A.1}$$

Conservation of Momentum (Navier-Stokes Equations)[12-13]:

x-direction:

$$\rho\left(\frac{\partial u}{\partial t}+u\frac{\partial u}{\partial x}+v\frac{\partial u}{\partial y}+w\frac{\partial u}{\partial z}\right)=-\frac{\partial p}{\partial x}+\mu\left(\frac{\partial^2 u}{\partial x^2}+\frac{\partial^2 u}{\partial y^2}+\frac{\partial^2 u}{\partial z^2}\right)+\rho X$$

y-direction:

$$\rho\left(\frac{\partial v}{\partial t}+u\frac{\partial v}{\partial x}+v\frac{\partial v}{\partial y}+w\frac{\partial v}{\partial z}\right)=-\frac{\partial p}{\partial y}+\mu\left(\frac{\partial^2 v}{\partial x^2}+\frac{\partial^2 v}{\partial y^2}+\frac{\partial^2 v}{\partial z^2}\right)+\rho Y \qquad \text{Eq. A.2}$$

z-direction:

$$\rho\left(\frac{\partial w}{\partial t}+u\frac{\partial w}{\partial x}+v\frac{\partial w}{\partial y}+w\frac{\partial w}{\partial z}\right)=-\frac{\partial p}{\partial z}+\mu\left(\frac{\partial^2 w}{\partial x^2}+\frac{\partial^2 w}{\partial y^2}+\frac{\partial^2 w}{\partial z^2}\right)+\rho Z$$

For this particular case and in most bearing lubrication applications, the following assumptions are valid[12-13]:

1. Height of fluid film y << x, z (film curvature can be ignored)
2. Negligible pressure variation across fluid film $\Rightarrow \frac{\partial p}{\partial y} = 0$
3. Laminar flow
4. No external forces act on fluid film $\Rightarrow X = Y = Z = 0$
5. Fluid inertia is small compared to viscous shear $\Rightarrow$ LHS terms in Eq. (A.2) neglected
6. All velocity gradients are negligible compared to $\frac{\partial u}{\partial y}, \frac{\partial w}{\partial y}$.

With the above assumptions, Eq. (A.2) reduces to:

$$\frac{1}{\mu}\frac{\partial p}{\partial x} = \frac{\partial^2 u}{\partial y^2}$$
$$\frac{1}{\mu}\frac{\partial p}{\partial z} = \frac{\partial^2 w}{\partial y^2} \qquad \text{Eq. A.3}$$

An expression for shear stress can be obtained as follows. The following boundary conditions are needed:

$$u(y = 0) = 0$$
$$u(y = h) = U$$

Integrating the x-direction component of Eq. (A.3) with respect to y and applying the above boundary conditions, an expression for $u(y)$ can be obtained:

$$u(y) = \frac{1}{2\mu}\frac{dp}{dx}(y^2 - hy) + \frac{Uy}{h} \qquad \text{Eq. A.4}$$

It should be noted that performing the integration in this way assumes that the viscosity is not a function of the distance from the liner in the cross-flow direction. However, for a shear-thinning fluid, the viscosity is a function of the local shear rate, which is given by the rate of change of the

velocity in the cross-flow direction. Although many oils are shear-thinning fluids, it has been shown in [14] that accurate results can be obtained for these oils by approximating the viscosity as the piston speed divided by the average distance between the nominal lines defining the ring and liner surfaces. Therefore, the above integration is still valid even in these cases.

Shear stress is given by:

$$\tau(x) = \mu \left. \frac{\partial u}{\partial y} \right|_{y=0}$$

Using Eq. (A.4):

$$\tau(x) = \frac{\mu U}{h} - \frac{h}{2}\frac{dp}{dx} \quad . \qquad \text{Eq. A.5}$$

The volumetric flow rate can also be derived using the above results:

$$Q(x) = \int_0^h u(y)dy$$

Using Eq. (A.4):

$$Q(x) = -\frac{h^3}{12\mu}\frac{dp}{dx} + \frac{Uh}{2} \qquad \text{Eq. A.6}$$

A.2 Derivation of the Reynolds Equation

A relationship between the film height and width and the pressure distribution under the ring surface can be derived by applying conservation of mass and conservation of momentum to a fluid element under the ring surface.

Starting again with Eq. (A.3), the following boundary conditions can be applied, which assume that the motion of the ring surface occurs only in the x-direction:

$$u(y=0)=0$$
$$u(y=h)=U$$
$$w(y=0)=0$$
$$w(y=h)=0$$

Integration of Eq. (A.3) and application of the above boundary conditions yields the following result:

$$u=\frac{1}{2\mu}\frac{\partial p}{\partial x}y(y-h)+\frac{h-y}{h}U$$
$$w=\frac{1}{2\mu}\frac{\partial p}{\partial z}y(y-h) \qquad \text{Eq. A.7}$$

Substitution of Eq. (A.7) into the expression for conservation of mass given by Eq. (A.1) yields:

$$\frac{\partial}{\partial y}(\rho v)=-\frac{\partial}{\partial x}(\rho u)-\frac{\partial}{\partial z}(\rho w) \qquad \text{Eq. A.8}$$

The following boundary conditions will be applied[12-13]:

$$v(y=0)=\frac{\partial h}{\partial t}$$
$$v(y=h)=0$$

Now, integrating Eq. (A.8) with respect to y and applying the boundary conditions, assuming an incompressible lubricant, yields[12-13]:

$$\frac{\partial}{\partial x}\left(\frac{h^3}{\mu}\frac{\partial p}{\partial x}\right)+\frac{\partial}{\partial z}\left(\frac{h^3}{\mu}\frac{\partial p}{\partial z}\right)=6U\frac{\partial h}{\partial x}+12\frac{\partial h}{\partial t} \qquad \text{Eq. A.9}$$

This is the two-dimensional Reynolds Equation for incompressible lubricants. This equation relates the pressure distribution in the oil film with the film height and width between the ring and the liner.

Appendix B: Temperature Dependence of Lubricant Viscosity

B.1 Introduction

Oil formulation has a significant impact on engine operation by affecting friction, operating characteristics, and reliability. Changing oil viscosity affects engine friction by modifying the way engine surfaces, such as the piston, rings, and connecting rods, slide against each other. The original piston model assumed a constant oil viscosity for the entire cycle, but as shown Section B.3, viscosity changes by a factor of 2 throughout the cycle, so this assumption is suspect.

The piston program reads input data from a text file named `INPUT.INP`. In order to modify the program to include the temperature dependence of viscosity, several additional inputs, such as the temperatures and lubricant properties, must be added. A new namelist, `$OILVISC`, is added to represent these values. This appendix details how the source code was changed to accommodate temperature dependence.

B.2 Static viscosity (original program)

The original program used the variable `VISLUB` to refer to the dynamic viscosity of the oil around the skirt. It used two additional variables, `MUOIL` and `NUO`, to refer to the dynamic and kinematic viscosities around the rings. Each of these viscosities was assumed to be constant, and the original values are given below:

Table 2: Viscosity properties used in legacy program

Variable	Value	Units
VISLUB	0.005035	kg/m-s
MUOIL	0.01	kg/m-s
NUO	0.000015	m^2/s

Although viscosity was assumed to be constant, the oil around both the piston skirt and rings changes effective viscosity during the cycle because the liner temperature varies substantially.

B.3 Temperature profile along liner

In order to calculate the change in viscosity as a function of temperature, the temperature profile must first be determined. The Woschni correlation was used[25]:

$$T(l) = T_{TDC} - (T_{TDC} - T_{BDC})\sqrt{l/S} \qquad \text{Eq. B.1}$$

where $T(l)$ is the liner temperature, l is the liner location (measured downward from TDC), and T_{TDC} and T_{BDC} are temperatures at TDC and BDC. The top and bottom temperatures are given as inputs, replacing `VISLUB`, `NUO`, and `MUOIL`.

The temperature of the oil varies slightly between the top of the skirt and the bottom of the skirt, and it varies quite substantially between the TDC and BDC positions. It would be very difficult to index all nodes for local viscosity, in part because many of the nodes are unwetted. In order to improve speed and simplicity, an average (mid-point) viscosity was calculated for the piston skirt, and a different viscosity was calculated for the piston rings, but both were functions of crank angle. The error introduced by averaging over the skirt length is small compared with the baseline program, which averages over the entire stroke. Furthermore, the viscosity calculated by the mid-point viscosity is probably close to the actual viscosity calculated by a full nodal analysis.

B.4 Interface between geometry and temperature

The square-root temperature profile is shown schematically in Figure B.1, and the piston schematic is shown alongside it. The reference temperatures were `TTOP`, the temperature at the top of the liner, and `TBOTTOM`, the temperature at the bottom.

From Figure B.2, it is clear that at TDC, the mid-point of the piston skirt lies a distance of (`RTL` + 0.5 · `SKIRTL`) below the top temperature (`TTOP`) position. As the piston moves downward,

this distance increases by s, the distance between the TDC position and the current position. The s equation is as follows, where a is the crank radius and l is the connecting rod length:

$$s = (a+l) - \left(a\cos\theta + \sqrt{l^2 - a^2\sin^2\theta}\right) \qquad \text{Eq. B.2}$$

The square root dependence is given by the following equation:

$$T(x) = TTOP - \left(\frac{TTOP - TBOTTOM}{\sqrt{DISPLIN}}\right)\cdot\sqrt{x} \qquad \text{Eq. B.3}$$

where x is simply:

$$x = s + RTL + \frac{SKIRTL}{2} \qquad \text{Eq. B.4}$$

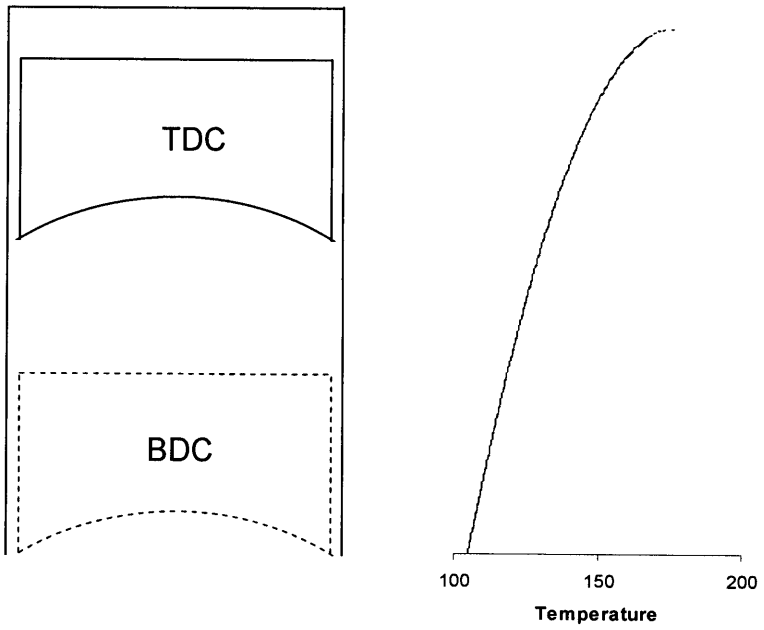

Figure B.1: Temperature variation along cylinder liner using Woschni (square root) correlation

The calculation of viscosity for the rings (to produce functional muoil) was the same in every respect except the calculation of x. Rather than reaching from TTOP to the middle of the skirt, x only reached to the middle of the ring pack, as shown in Figure B.3. This was accomplished by

replacing (RTL + 0.5 · SKIRTL) with TRSR, the distance between TTOP and the mid-point between the top ring and second ring:

$$x = s + TRSR$$

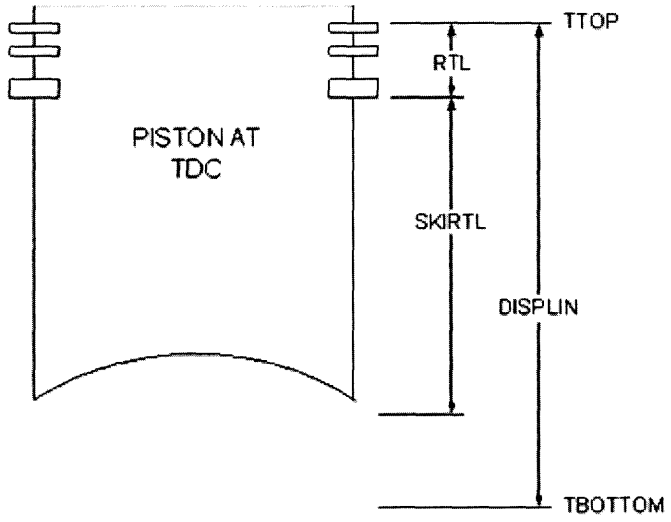

Figure B.2: Schematic of piston, showing variables used (in $OILVISC namelist in INPUT.INP file)

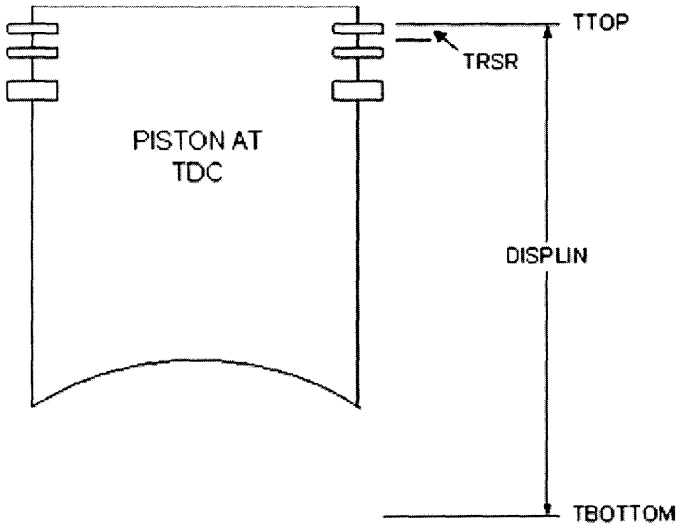

Figure B.3: Schematic of piston, showing variables used (in $OILVISC namelist in INPUT.INP file)

The program calculated a reference temperate at each crank angle. For the skirt, the reference temperature was assumed to be the temperature at the middle of the skirt, and the reference temperature for the rings was located at the midpoint of the ring pack. Figure B.4 shows how

these reference points vary with crank angle; they follow a simple sinusoidal relationship. Figure B.5 matches these reference points to the square-root temperature correlation discussed earlier to illustrate how the temperature at the reference points varies with crank angle.

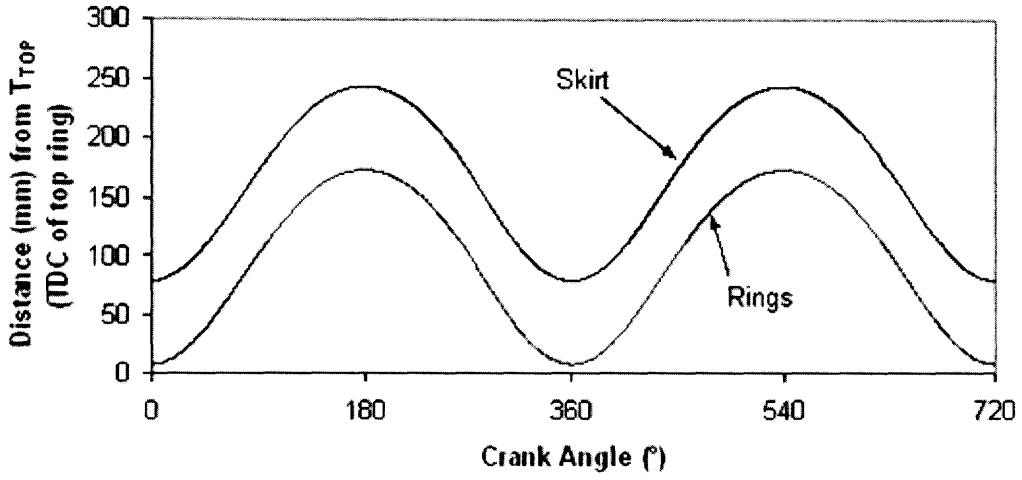

Figure B.4: Distance of reference points (skirt: midpoint; ring: midpoint between top ring and second ring) from reference temperature (i.e., liner temperature at top ring at TDC)

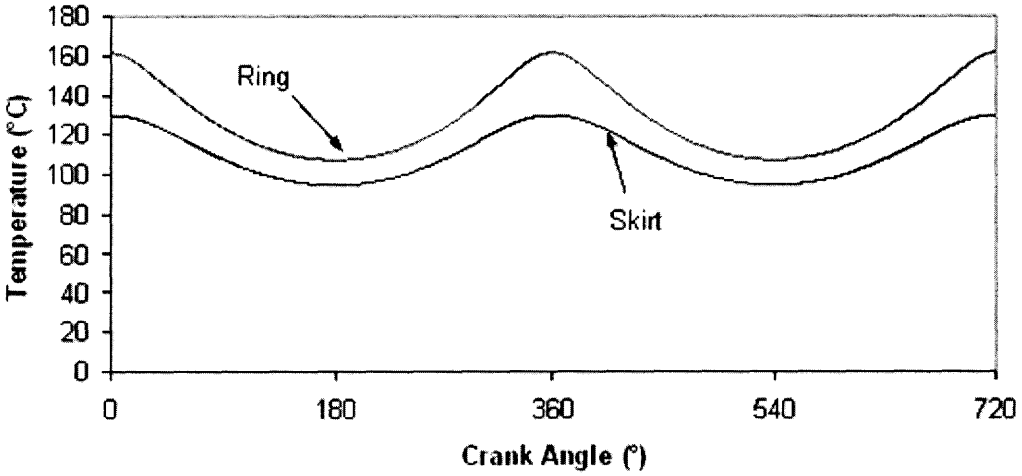

Figure B.5: Temperature distribution at skirt and ring mid-points as a function of crank angle

B.5 Vogel relationship

The Vogel equation (Eq. B.5) correlates viscosity with temperature. The piston model was modified to use Vogel equation parameters instead of assuming a constant viscosity value.

$$\nu_0 = k \exp\left(\frac{\theta_1}{\theta_2 + T}\right) \quad \rightarrow \quad \mu = \rho \cdot k \exp\left(\frac{\theta_1}{\theta_2 + T}\right) \qquad \text{Eq. B.5}$$

The θ_1 and θ_2 terms have units of °C, and k has units of cSt. In the field, the engine uses only straight-weight oils because it operates continuously under relatively uniform loading; therefore, no shear thinning information was included in the Vogel equation. The parameters used in the Vogel equation were obtained from *Basic Lubrication Theory*[26]. The densities were assumed to be constant as given at 100° C, since they do not vary much over the approximately 35-55° C range under consideration. The k values were determined by linear interpolation from the given points. Figures B.8-10 illustrate how crank angle and oil weight affect actual viscosity at the skirt mid-point.

Oil Type	ρ (kg/m^3)	k (cSt)	θ_1 (°C)	θ_2 (°C)
SAE-20	832	0.0580	1028	108.0
SAE-30	839	0.0274	1361	123.3
SAE-40	848	0.0272	1396	121.7
SAE-50	852	0.0223	1518	122.6

* Note: the actual value in the book was 884; this was assumed to be a typo for 848.

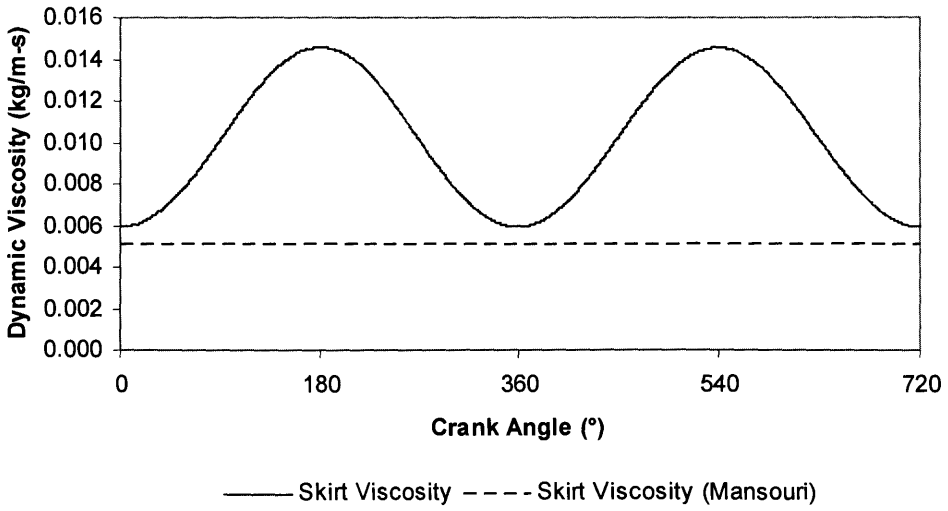

Figure B.6: Skirt viscosity vs. crank angle for SAE-40 oil (original skirt viscosity shown for reference)

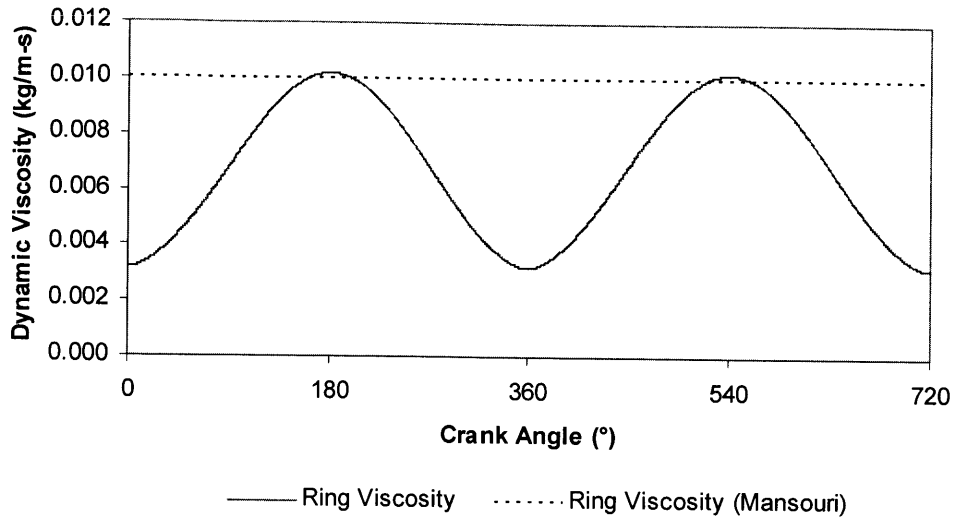

Figure B.7: Ring pack viscosity vs. crank angle for SAE-40 oil (original viscosity shown for reference)

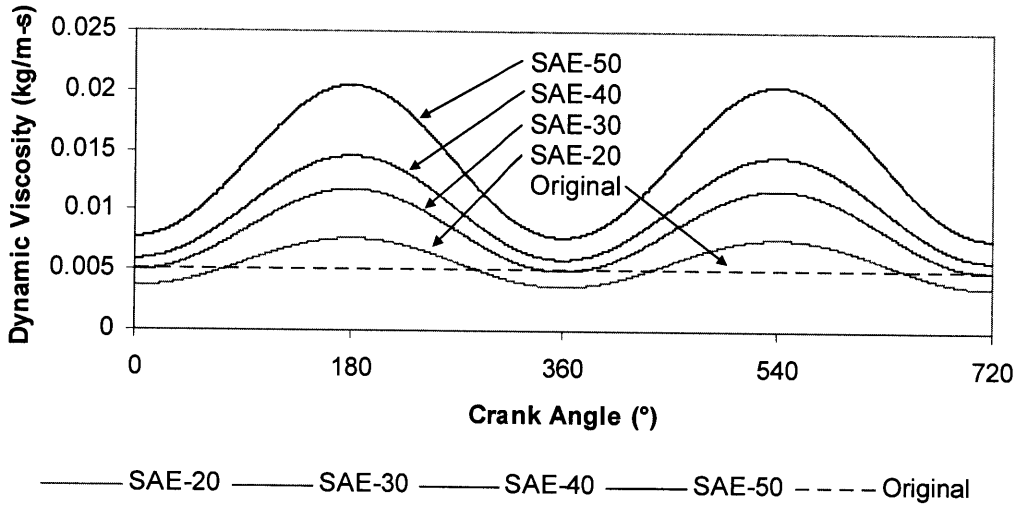

Figure B.8: Skirt viscosities at skirt mid-point as functions of crank angle for various straight-weight oils (original skirt viscosity shown for reference)

In section B.6, a detailed list of changes to the original source code is provided.

B.6 Log of Changes

Input file (INPUT.INP)

1. Rearranged order of inputs in `INPUT.INP` to match `engine` namelist
2. Add new namelist `OILVISC` that contains the parameters for the oil

```
$OILVISC
  TTOP = 175.6666667,
  TBOTTOM = 104.537263,
  DISPLIN = 0.188,
  RTL = 0.0187,
  TRSR = ,
  ZK = 0.09,
  THETA1 = 965.75,
  THETA2 = 92.74,
  RHO = 850,
 $END
```

Viscosity at piston skirt (VISLUB) in main program (MAIN.F)

1. Add new namelist `OILVISC`:

```
namelist /OILVISC/ TTOP,TBOTTOM,DISPLIN,RTL,TRSR,ZK,THETA1,
     THETA2,RHO
```

2. Add new common block `oilvisc`:

```
common /oilvisc/ TTOP,TBOTTOM,DISPLIN,RTL,TRSR,ZK,THETA1,
     THETA2,RHO
```

3. Add readin feature for `oilvisc`:

```
read (8,oilvisc)
```

4. Place common block at the top to allocate memory:

```
common /oilvisc/ TTOP,TBOTTOM,DISPLIN,RTL,TRSR,ZK,THETA1,
     THETA2,RHO
```

5. Added subroutine `viscskirt`, which calculates the oil viscosity at the mid-point of the piston skirt at the current crank angle:

```
subroutine viscskirt(ca,rmu)
implicit real*8 (a-h,o-z)
COMMON /ENG/ PSTDIA,STROKE,CONROD,SKIRTL,skirtw,cylinl,rofs,
  &   PLCLR,CP,CG,A,BCG,RLRING(3),RMPST,RMWRST,RMCONR,CRMEFR,E1YNG,
```

```
 &   E2YNG,POISR1,POISR2,WAVHGT,WAVLEN,ROUGHS,RPM,RIPP,IP
common /oilvisc/ TTOP,TBOTTOM,DISPLIN,RTL,TRSR,ZK,THETA1,
 &   THETA2,RHO
  include 'fdsolv.par'
crankrad=stroke/2
carad=ca*pi/180
verttravel = skirtl/2 + rtl + (crankrad + conrod) -
 &   (crankrad * cos(carad) +
 &   sqrt(conrod**2 - crankrad**2 * sin(carad)**2))
skirttemp=ttop-(ttop-tbottom) / sqrt(displin) * sqrt(verttravel)
rmu = rho * zk * exp(theta1/(theta2 + skirttemp))/1000000
return
end
```

6. Delete static assignment of oil viscosity:

   ~~`rmu = vislub`~~

7. Remove `vislub` variable from `ENG` common statement:

```
COMMON /ENG/ PSTDIA,STROKE,CONROD,SKIRTL,skirtw,cylinl,rofs,
 &   PLCLR,CP,CG,A,BCG,RLRING(3),RMPST,RMWRST,RMCONR,CRMEFR,E1YNG,
 &   E2YNG,POISR1,POISR2,WAVHGT,WAVLEN,ROUGHS,RPM,RIPP,IP
```

8. Remove `VISLUB=0.005035` declaration from `INPUT.INP` namelist
9. At every point at which CA is changed, call `viscskirt` to calculate the current viscosity:
   a. Initialize crank angle in main program:

```
      CA = CAINIT
    call viscskirt(ca,rmu)
```

   b. Increment crank angle in main program:

```
      ca = ca + dca
    call viscskirt(ca,rmu)
```

   c. Increment crank angle in subroutine `countor`:

```
      ca = cainit + t*rpm*6.
    call viscskirt(ca,rmu)
```

   d. Increment crank angle in subroutine `pmove4`:

```
      ca = cainit + t*rpm*6.
       call viscskirt(ca,rmu)
```

   e. Increment crank angle in subroutine `power`:

```
      ca = cainit + tt*rpm*6.
    call viscskirt(ca,rmu)
```

The original static skirt viscosity was VISLUB, and it was assigned to the constant rmu in the original program. The rmu variable was used in the subroutines countor, phsolv, and power, and it was used a total of 6 times. Under normal operation, subroutines countor and power are called at each crank angle by the main program, but if convergence cannot be obtained, subroutine pmove4 is called. All three of them call the viscskirt subroutine to calculate rmu.

Viscosity in ring-pack (MUOIL, NUO) in main program (MAIN.F)

The viscosity calculation for the ring area was performed virtually identically to that of the skirt. The only parameter that was changed was the distance between TTOP and the viscosity measuring point, which is now the midpoint between the top and second rings (TRSR).

1. Modify common block ringdata so that it does not have muoil or nuoil:

```
common /ringdata/tw,wtmol,vol1,vol2,vol3,vol4,a13,a35,g,cd,
&      rcr,conlen,bore,rt1,rw1,rt2,rw2,rmass1,rmass2,
&      ct10,ct20,cb10,cb20,vrp1,vrp2,ct1,ct2,cb1,cb2,
&      crvh,delta
```

2. Modify namelist ringdata so that it does not have muoil or nuoil:

```
namelist /ring/tw,wtmol,vol2,vol3,vol4,a13,a35,g,cd,
&       bore,rt1,rw1,rt2,rw2,rmass1,rmass2,
&       ct10,ct20,cb10,cb20,
&       crvh,delta
```

3. Add common block oilvisc after every instance of ringdata common block:

```
namelist /OILVISC/ TTOP,TBOTTOM,DISPLIN,RTL,TRSR,ZK,THETA1,
     THETA2,RHO
```

4. Delete MUOIL = 0.01 and NUO=.000015 from INPUT.INP.
5. Eliminate all instances of memory allocation for muoil and nuoil:

```
~~real nuo,muoil~~
```

6. Add memory allocation in V6 subroutine; note that it is real*8, not real:

```
real*8 muoil,nuo
```

7. Eliminate `muoil` and `nuoil` from this memory call:

```
real nuo,muoil,mstep
```

becomes

```
real mstep
```

8. Eliminate `muoil` and `nuoil` from this memory call:

```
REAL MO1,MO2,MO3,MO4,NUO,MUOIL,W
```

becomes

```
REAL MO1,MO2,MO3,MO4,W
```

9. Add new subroutine `viscring` to calculate viscosity of oil around rings:

```
subroutine viscring(ca,muoil,nuo)
implicit real*8 (a-h,o-z)
real*8 nuo,muoil
COMMON /ENG/ PSTDIA,STROKE,CONROD,SKIRTL,skirtw,cylinl,rofs,
 &   PLCLR,CP,CG,A,BCG,RLRING(3),RMPST,RMWRST,RMCONR,CRMEFR,E1YNG,
 &   E2YNG,POISR1,POISR2,WAVHGT,WAVLEN,ROUGHS,RPM,RIPP,IP
common /oilvisc/ TTOP,TBOTTOM,DISPLIN,RTL,TRSR,ZK,THETA1,
 &   THETA2,RHO
  include 'fdsolv.par'
crankrad=stroke/2
carad=ca*pi/180
verttravel = trsr + (crankrad + conrod) - (crankrad * cos(carad)+
 &   sqrt(conrod**2 - crankrad**2 * sin(carad)**2))
skirttemp=ttop-(ttop-tbottom) / sqrt(displin) * sqrt(verttravel)
muoil = rho * zk * exp(theta1/(theta2 + skirttemp))/1000000
nuo = zk * exp(theta1/(theta2 + skirttemp))/1000000
return
end
```

10. In subroutine `V6`, add a call to subroutine `viscring` after `FLOW` function; note that crank angle is now `th`:

```
call viscring(th,muoil,nuo)
```

Other changes

Placed integer values at the end of the common block declaration so that compiler would not produce a warning:

Original:

```
      COMMON /ENG/ PSTDIA,STROKE,CONROD,SKIRTL,skirtw,cylinl,rofs,
     &   PLCLR,CP,CG,A,BCG,RLRING(3),RMPST,RMWRST,RMCONR,CRMEFR,E1YNG,
     &   E2YNG,POISR1,POISR2,WAVHGT,WAVLEN,ROUGHS,RPM,RIPP,IP
```

Modified:

```
      COMMON /ENG/ PSTDIA,STROKE,CONROD,SKIRTL,skirtw,cylinl,rofs,
     &   PLCLR,CP,CG,A,BCG,RLRING(3),RMPST,RMWRST,RMCONR,CRMEFR,E1YNG,
     &   E2YNG,POISR1,POISR2,WAVHGT,WAVLEN,ROUGHS,RPM,RIPP,IP
```

Original:

```
       COMMON /COM8/ P1OLD,CT1OLD,CT2OLD,CB1OLD,CB2OLD,
      &   TOPMIN,TOPMOT,DWNMIN,DWNMOT,CMIN,CMOT,ONE3M,DOTM12
```

Modified:

```
       COMMON /COM8/ P1OLD,CT1OLD,CT2OLD,CB1OLD,CB2OLD,
      &   TOPMIN,TOPMOT,DWNMIN,DWNMOT,CMIN,CMOT,ONE3M,DOTM12,INTRVL
```

Appendix C: Inlet Boundary Condition in Reynold's Equation

At the inlet, the lubricant has height h_∞ as it moves at speed U. At some point, the piston comes into contact with it; at this point, the lubricant has height h_{inlet}, as shown in the figure below:

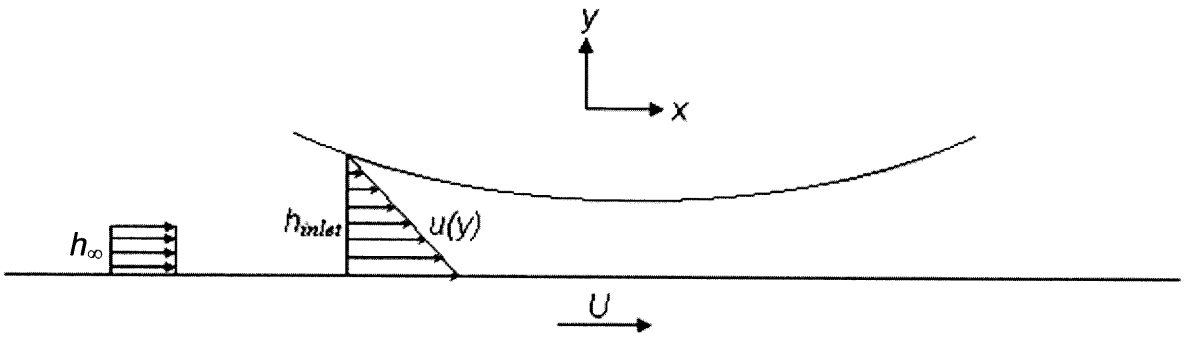

The flow between the piston and liner can be approximated by a fully-developed flow between two parallel plates, provided the following two conditions are valid:

1. The curvature of the plate is negligible.
2. The transition region is small compared with the wetted length.

Typically, the variations in h are very small compared with the wetted length $(x_2 - x_1)$, so the first approximation is valid. If viscous diffusion is the only mechanism driving the transition from stationary to Couette flow, the length of the transition region is given by:

$$l_E \approx \frac{h_0^2}{\nu} U \qquad \text{Eq. C.1}$$

where h_0 is the minimum film thickness, ν is the kinematic viscosity of the oil, and U is the relative velocity of the plates (modeled here as the velocity of the liner against a stationary piston). By the approximation below, the transition region l_E is much smaller than the wetted length L, so condition 2 is also valid.

$$\frac{l_E}{L} = \frac{h_0^2}{\nu}\frac{U}{L} \ll 1 \qquad \text{Eq. C.2}$$

For a parallel plane condition, the flow is invariant in the x direction (*i.e.*, the profile looks similar at various points across the wetted region). Hence, continuity requires that vertical speed not change:

$$\frac{\partial v}{\partial y} = 0 \qquad \text{Eq. C.3}$$

Since $v = 0$ at $y = 0$, v must be 0 everywhere, which is intuitively correct—oil is not moving normal to the liner surface.

A simplified form of the Navier-Stokes equation is shown below along with the aforementioned boundary condition:

$$\begin{aligned} 0 &= -\frac{1}{\rho}\frac{\partial p}{\partial x} + \nu\frac{\partial^2 u}{\partial^2 y} \\ 0 &= \frac{\partial v}{\partial y} \end{aligned} \qquad \text{Eq. C.4}$$

The first equation shows that p is not a function of y; hence, the first term in that equation can only be a function of x, while the second term can only be a function of y. This can only be true if both terms are constant. Therefore, the pressure gradient is a constant. By integrating the x-momentum equation twice, the output is:

$$0 = -\frac{y^2}{2}\frac{dp}{dx} + \mu u + Ay + B \qquad \text{Eq. C.5}$$

One boundary condition is $u = U$ at $y = 0$ requires that $B = -\mu U$. The other boundary condition, $u = 0$ at $y = h_{inlet}$, requires that:

$$A = \frac{\mu U}{h_{inlet}} + \frac{h_{inlet}}{2}\frac{dp}{dx} \qquad \text{Eq. C.6}$$

Combining terms, the velocity profile $u(x)$ is:

$$u(y) = \left(\frac{1}{2\mu}\frac{dp}{dx}\right)y^2 - \left(\frac{U}{h_{inlet}} + \frac{h_{inlet}}{2\mu}\frac{dp}{dx}\right)y + U \qquad \text{Eq. C.7}$$

At the inlet, pressure is atmospheric, the same as free-stream pressure. Thus, the pressure variation is considered to be zero at the entrance only, reducing the equation to:

$$u(y) = U\left(-\frac{1}{h_{inlet}}y + 1\right) \qquad \text{Eq. C.8}$$

Note that velocity now varies linearly in y. Applying conservation of volume, the mass coming in from the free stream is equal to the mass passing through the inlet (h_{inlet}):

$$\begin{aligned} Uh_\infty &= \int_{y=0}^{y=h_{inlet}} u(y)dy \\ &= \int_{y=0}^{y=h_{inlet}} U\left(-\frac{1}{h}y + 1\right)dy = U\int_{y=0}^{y=h_{inlet}}\left(-\frac{1}{h}y + 1\right)dy = U\left[-\frac{1}{2h}y^2 + y\right]_{y=0}^{y=h_{inlet}} = \frac{1}{2}Uh_{inlet} \qquad \text{Eq. C.9} \\ \rightarrow\ h_\infty &= \frac{1}{2}h_{inlet} \end{aligned}$$

Hence, at the entrance, the inlet height is approximately twice the free-stream height.

(This page was intentionally left blank)

Appendix D: Reynold's Exit Boundary Condition

The Reynold's exit boundary condition is:

$$\left.\frac{\partial p}{\partial x}\right|_{x=\text{exit}} = 0 \qquad \text{Eq. D.1}$$

This condition can be discreetized by applying the backward-difference approximation:

$$\frac{\partial p}{\partial x} \approx \frac{p_{n+1} - p_n}{\Delta x} = 0 \qquad \text{Eq. D.2}$$

Since the discreetization is merely a truncated Taylor polynomial, a more accurate version can be achieved by taking more terms, as shown below:

$$p(x - \Delta x) \approx p(x) - \Delta x \frac{\partial p}{\partial x} + \frac{\Delta x^2}{2} \frac{\partial^2 p}{\partial x^2} + O(x^3) \qquad \text{Eq. D.3}$$

This is then discreetized as follows; note that second derivative is approximated by a (centered) second difference around the p_n term rather than the exit (p_{n+1}) term:

$$p(x - \Delta x) \approx p_{n+1}(x) - \Delta x \frac{\partial p}{\partial x} + \frac{\Delta x^2}{2} \frac{p_{n-1} - 2p_n + p_{n+1}}{(\Delta x)^2} + O(x^3) \qquad \text{Eq. D.4}$$

Truncating the $O(x^3)$ error term and equating $p(x - \Delta x) = p_n$, the equation can be rearranged as follows:

$$\frac{\partial p}{\partial x} = \frac{p_{n+1} - p_n}{\Delta x} + \frac{\Delta x}{2}\frac{p_{n-1} - 2p_n + p_{n+1}}{(\Delta x)^2} \rightarrow$$

Eq. D.5

$$\frac{\partial p}{\partial x} = \frac{p_{n-1} - 4p_n + 3p_{n+1}}{2\Delta x} = 0$$

If a matrix is used, this equation can be easily inputted on an additional row.

Appendix E: Lubricant Analysis

Many friction characteristics are heavily dependent on lubricant viscosity, as evidenced by both the piston model and general experience in the field. However, viscosity is not constant for a particular lubricant; rather, it varies with temperature, shear rate, and a host of other minor factors. The viscosity of all lubricants, whether single-grade or multi-grade, typically depends strongly on temperature. Moreover, the viscosity of multi-grade lubricants depends on shear rate, while the viscosity of single-grade ("straight weight") oils does not. This Appendix outlines the basic formulae used to quantify the two phenomena.

The Vogel equation gives the relationship between low-shear kinematic viscosity and temperature (Taylor, et al., 1994):

$$\nu_0 = k \exp\left(\frac{\theta_1}{\theta_2 + T}\right) \qquad \text{Eq. 4.1}$$

where ν_0 is the kinematic viscosity of the low shear rate oil in cSt, k (units of cSt), θ_1 (°C), and θ_2 (°C) are correlation constants for a particular oil, and T is the oil temperature in °C. The Vogel equation is typically used in the piston model because it accurately correlates temperature and viscosity for single-grade oils, which are usually used in the large stationary engines under consideration.

Other engines, such as those used in automotive applications, commonly use multi-grade oils, whose viscosity depends not only on temperature but also on shear rate. Typically, the viscosity is relatively high at low shear rates and relatively low at high shear rates. The advantage of this characteristic is that the viscosity is relatively high at the ends of the stroke, when the piston is moving comparatively slowly, and is therefore near the boundary lubrication regime. However, the viscosity decreases in the middle of the stroke, when the shear rate is high; this reduces hydrodynamic friction which predominates at that point. The shear rate dependence is described by the Cross equation, shown below:

$$\mu = \mu_0 \frac{1 + \frac{\mu_\infty}{\mu_0}(\frac{\gamma}{\beta})^m}{1 + (\frac{\gamma}{\beta})^m} \qquad \text{Eq. E.2}$$

where γ is the absolute value of the shear rate (units of s^{-1}), β is the critical shear rate (s^{-1}), μ_0 is the oil viscosity at zero shear rate, μ_∞ is the viscosity when shear rate tends to ∞, m is a correlation constant controlling the width of the transition region, and μ is the viscosity at shear rate γ. Note that for single-grade oils, $\mu_\infty = \mu_0$.

The critical shear rate β is temperature dependent according to the following correlation (Taylor, et al., 1994):

$$\beta = 10^{(c_1 + c_2 T)} \qquad \text{Eq. E.2}$$

where c_1 and c_2 are parameters specific to a particular lubricant, and T is oil temperature in °C.

The constants for both the Vogel equation and the Cross equation for a variety of lubricants are shown in Table 3. These constants are culled from several published papers on oil properties by Ian Taylor at Shell. (Note that the last three oils are single-grade, and thus shear-thinning effect does not occur for these oils. Hence, $\mu_\infty/\mu_0 = 1$ is used, and the values of c_1 and c_2 are irrelevant to the calculations and can be arbitrarily assigned.)

The oil property data in Table 3 has the following two limitations:

- The properties shown are for representative oils, but these properties vary by manufacturer and additive constituent. Although it is typically good to obtain precise data for the specific brand and type of oil being used, this table serves as an approximate guide when such data is unavailable.

- Oil density was assigned to be 850 kg/m^3 for all oils. Although dynamic viscosity is used in the friction calculations, kinematic viscosity was used as input for historical reasons. Some

values of k were derived under the assumption that density was 850 kg/m^3, so this density value should be used in the Cross equation regardless of the actual density value.

Table 3: Constants used in Vogel equation used to calculate viscosity

Oil Grade	k (cSt)	θ_1 (°C)	θ_2 (°C)	μ_∞ / μ_0	c_1	c_2 (°C^{-1})
0W40	0.01341	1986.4	189.7	0.67	2.5	0.026
5W20	0.04576	1224	134.1	0.94	2.5	0.029
5W40	0.15	1018.74	125.91	0.8	2.3	0.0225
10W30	0.1403	869.72	104.4	0.76	2.3	0.0225
10W50A	0.0352	1658.88	163.54	0.49	2.43	0.0218
10W50B	0.0507	1362.4	129.8	0.52	2.28	0.0269
15W40A	0.1223	933.46	103.89	0.9	2.3	0.0225
15W40B	0.03435	1424.3	137.2	0.79	2.5	0.026
20W50	0.0639	1255.46	117.7	0.84	2.3	0.0225
SAE10	**0.0258**	**1345.42**	**144.58**	**1**	**2.3**	**0.0225**
SAE30	**0.0246**	**1432.29**	**132.94**	**1**	**2.3**	**0.0225**
SAE50	**0.0384**	**1349.94**	**115.16**	**1**	**2.3**	**0.0225**

The effect of the Cross equation constants is illustrated in Fig. E.1. Several hypothetical multi-grade oils, whose low-shear viscosities and high-shear viscosities were identical, were compared by using different Cross equation parameters. The shift from high viscosity to low viscosity can be made relatively sudden or relatively gradual. Of course, the actual viscosities at high-shear and low-shear situations can also be adjusted by tweaking other parameters. Typically, these parameters are modified by means of additive packages whose formulations are proprietary and closely protected by their manufacturers.

In order to get a general idea of how the Vogel and Cross equation compare, the properties in Table 3 were input into the Friction OFT model, which is a ring-pack model developed at MIT. This model uses physical principles similar to those utilized for the piston model, so similar trends may be expected. In Fig. E.2, the hydrodynamic and boundary friction losses for various single- and multi-grade oils are plotted. The boundary friction is roughly constant, since it does

not depend on lubricant viscosity. The hydrodynamic friction, on the other hand, increases with viscosity—the same trend predicted for the piston model. Note that much of the benefit of multi-grade lubricants is improved reliability, which is not directly reflected in the friction work calculations. The high-viscosity at low shear rates near TDC and BDC helps preserve the ring and liner surfaces by providing a better cushion.

Thus far, the piston model has been applied to large, stationary natural gas engines that typically use straight-weight oils. However, the advantage of a numerical model is that it can be scaled to any size engine, and it is conceivable that this model could be used for engines that utilize multi-grade oils. In that case, the viscosity values at each crank angle would be governed not by the Vogel equation but by the Cross equation, and more data about oil properties would be needed. This would facilitate a quantitative evaluation of the effects of multi-grade oil properties on piston friction.

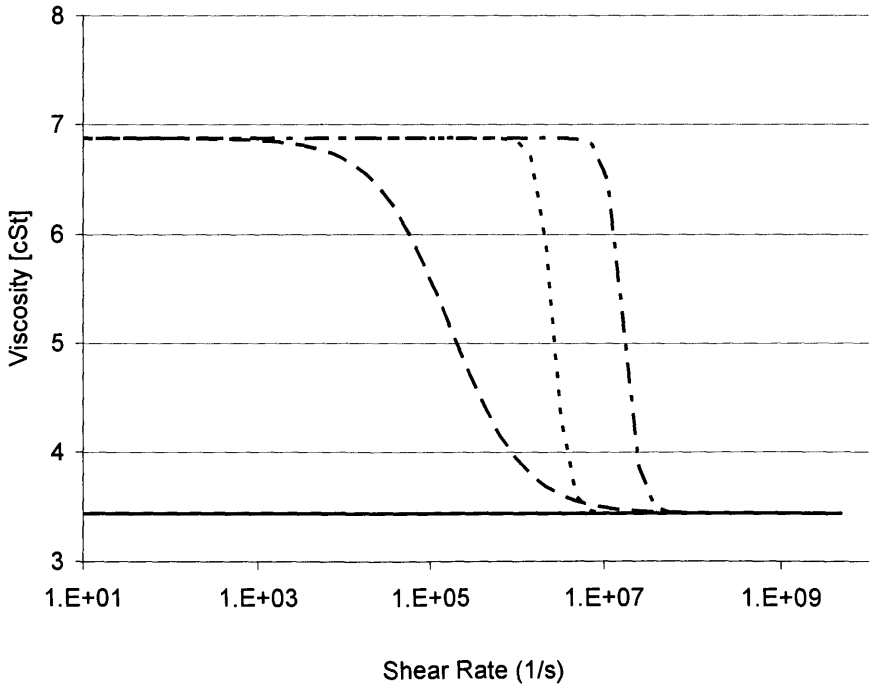

Figure E.1: Comparison of shear-thinning characteristics for three hypothetical multi-grade oils. The transition from high viscosity (at low shear rates) to low viscosity (at high shear rates) can be tuned by adjusting the oil properties.

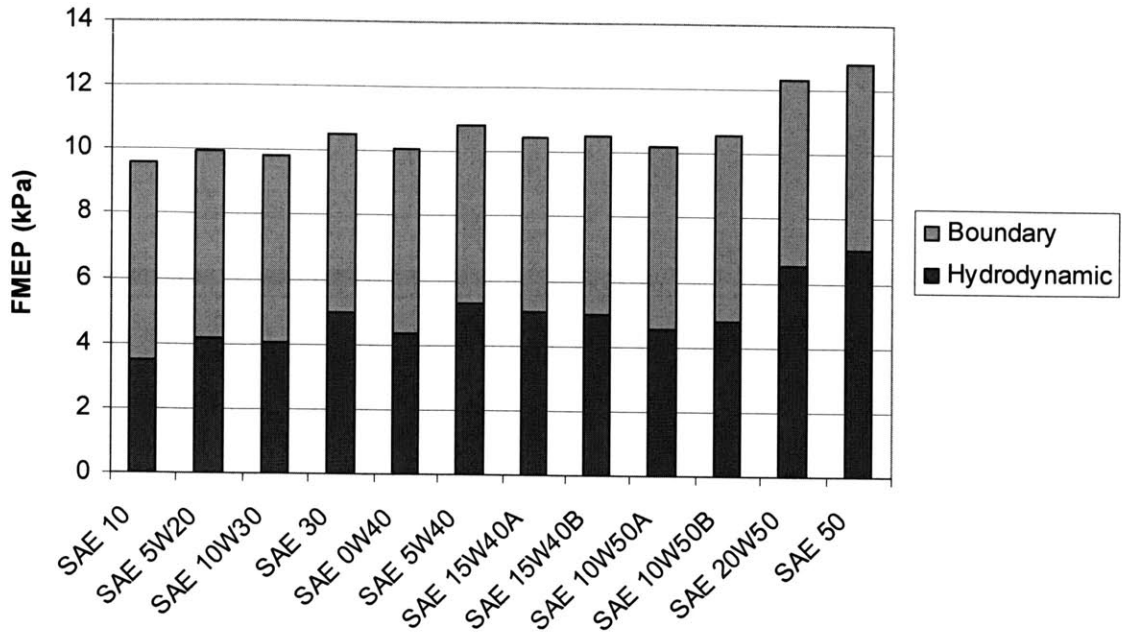

Figure E.2: Net FMEP according to Friction OFT model. Boundary friction is roughly constant, owing to the roughly constant level of contact area and the insensitivity of contact friction to oil viscosity. Note that hydrodynamic friction increases with viscosity.